

# A Geochemical Review of Amphibolite, Granulite, and Eclogite Facies Lithologies: Perspectives on the Deep Continental Crust

Laura G Sammon<sup>1,1</sup> and William F mcdonough<sup>1,1</sup>

<sup>1</sup>University of Maryland

November 30, 2022

## Abstract

Debate abounds regarding the composition of the deep (middle + lower) continental crust. Studies of medium and high grade metamorphic lithologies guide us but encompass mafic (< 52 wt.%) to felsic (> 68 wt.%) compositions. This study presents a global compilation of geochemical data on amphibolite (n = 6500), granulite (n = 4000), and eclogite (n = 200) facies lithologies and quantifies systematic trends, uncertainties, and sources of bias in the deep crust sampling. The continental crust's Daly Gap is well documented in amphibolite and most granulite facies lithologies, with eclogite facies lithologies and granulite facies xenoliths having mostly mafic compositions. Al<sub>2</sub>O<sub>3</sub>, Lu, and Yb vary little from the top to bottom of the crust. In contrast, SiO<sub>2</sub> and incompatible elements show a wider range of abundances. Because of oversampling of mafic lithologies, our predictions are a lower bound on middle crustal composition. The distinction between granulite facies terrains (intermediate SiO<sub>2</sub>, high heat production, high incompatibles) or granulite facies xenoliths (low SiO<sub>2</sub>, low heat production, low incompatibles) as being the best analogs of the deep crust remains disputable. We incorporated both, along with amphibolite facies lithologies, to define a deep crustal composition that approaches 57.6 wt.% SiO<sub>2</sub>. This number, however, represents a compositional middle ground, as seismological studies indicate a general increase in density and seismic velocity with increasing depth. Future studies should analyze more closely the depth dependent trends in deep crustal composition so that we may develop compositional models that are not limited to a three-layer crust.

# JGR Solid Earth

## RESEARCH ARTICLE

10.1029/2021JB022791

### Key Points:

- We synthesize, analyze, and report statistics on ~10,000 whole rock compositions for deep crustal lithologies
- We determine periodic table trends and implications for the composition of the deep continental crust
- We generate compositional models for the middle, lower, combined middle & lower, and bulk crust

### Supporting Information:

Supporting Information may be found in the online version of this article.

### Correspondence to:

L. G. Sammon,  
[lsammon@umd.edu](mailto:lsammon@umd.edu)

### Citation:

Sammon, L. G., & McDonough, W. F. (2021). A geochemical review of amphibolite, granulite, and eclogite facies lithologies: Perspectives on the deep continental crust. *Journal of Geophysical Research: Solid Earth*, 126, e2021JB022791. <https://doi.org/10.1029/2021JB022791>

Received 21 JUL 2021

Accepted 11 NOV 2021

### Author Contributions:

**Conceptualization:** William F. McDonough  
**Data curation:** Laura G. Sammon, William F. McDonough  
**Formal analysis:** Laura G. Sammon  
**Funding acquisition:** William F. McDonough  
**Investigation:** Laura G. Sammon  
**Methodology:** Laura G. Sammon, William F. McDonough  
**Project Administration:** William F. McDonough  
**Supervision:** William F. McDonough  
**Visualization:** Laura G. Sammon  
**Writing – original draft:** Laura G. Sammon  
**Writing – review & editing:** Laura G. Sammon, William F. McDonough

© 2021. American Geophysical Union.  
All Rights Reserved.

# A Geochemical Review of Amphibolite, Granulite, and Eclogite Facies Lithologies: Perspectives on the Deep Continental Crust

Laura G. Sammon<sup>1</sup>  and William F. McDonough<sup>1,2</sup> 

<sup>1</sup>Department of Geology, University of Maryland, College Park, MD, USA, <sup>2</sup>Department of Earth Sciences and Research Center for Neutrino Science, Tohoku University, Sendai, Japan

**Abstract** Debate abounds regarding the composition of the deep (middle + lower) continental crust. Exhumed medium- and high-grade metamorphic rocks, which range in composition from mafic to felsic, provide information about the bulk composition of the deep crust. This study presents a global compilation of geochemical data on amphibolite ( $n = 6,500$ ), granulite ( $n = 4,000$ ), and eclogite ( $n = 200$ ) facies lithologies and quantifies trends, uncertainties, and sources of bias in the deep crust sampling. The continental crust's Daly Gap is well documented in amphibolite and most granulite facies lithologies. Igneous differentiation processes likely control the compositional layering in the crust.  $Al_2O_3$ , Lu, and Yb vary little from top to bottom of the crust. In contrast,  $SiO_2$ , light rare earth elements, Th, and U show a wider range of abundances throughout. Because of oversampling of mafic lithologies, our predictions are a lower bound on middle crustal composition. Additionally, the distinction between granulite facies terrains (intermediate  $SiO_2$ , high heat production, high incompatibles) or granulite facies xenoliths (low  $SiO_2$ , low heat production, low incompatibles) as being the best analogs of the deep crust remains disputable. We have incorporated both rock types, along with amphibolite facies lithologies, to define a deep crustal composition that approaches 57.6 wt.%  $SiO_2$ . This number, however, represents a compositional middle ground; the shallower parts of the deep crust (middle crust) resemble quartz monzonite while the deepest portions (lower crust) more resemble a Ca-rich monzonite. Future studies should analyze more closely the depth dependent trends in deep crustal composition to develop composition models that are not limited to a three-layer crust.

**Plain Language Summary** The composition and origins of the bottom  $\frac{2}{3}$  of the continental crust has been a topic of geologic debate for many years. Because of the inaccessible depths of these middle and lower sections of the continents, we cannot sample them directly. We must rely on rocks brought to the surface through mountain building and magma entrainment processes. Deep crustal rocks delivered via these processes come from a wide variety of depths and encompass many different chemical compositions. This study seeks to understand and better characterize the average composition of the deep crust (typically from 15 to 40 km beneath the surface) and identify the processes that produced the crust's present-day, chemically layered structure.

## 1. Introduction

The composition of the deep continental crust has been the subject of many studies for the past half century because of its importance in crustal evolution and the lack of consensus on its composition. The combined middle and lower continental crust (referred to here as the “deep crust”) are the integrated chemical products of billions of years of crust formation and deformation, yet their inaccessibility (deeper than 10 km) has led to a poorly constrained compositional model for the lower two-thirds of the continent. The deep continental crust can be sampled through tectonically emplaced or eroded exposures of high-grade metamorphic rock (referred to here as “terrains”) or deep crustal xenoliths that are rapidly carried to the surface through volcanic eruptions. The composition of these deep crustal analogs ranges widely, encompassing lithologies from metamorphosed basalt to granite. Varied tectonic regimes and widespread crustal heterogeneity have led to numerous geochemical and geophysical models that help to explain local phenomena, but struggle to produce a coherent global picture. Attempts to resolve the debate are limited by nonunique solutions and poorly quantified uncertainties. Defining the bulk compositional properties of the deep continental crust and describing its depth dependent changes endures as a long-standing challenge. Thus, the deep crustal composition puzzle remains, troublingly, unsolved.

Rudnick (1995) posited the paradox of the continental crust: the continental crust has an andesitic composition, however melts from the mantle are basaltic. In doing so, she identified that the formation of continental crust, as compared to making oceanic crust, must be an open system process involving, to different extents, weathering, intra-crustal melting (leaving behind a dense residue), and delamination as some of the operating processes. Consequently, the geochemical uncertainty associated with deep crust composition has led to competing models for crust formation (Bürgmann & Dresen, 2008; Hacker et al., 2015; Rudnick & Gao, 2014).

In developing their model, Hacker et al. (2015) outlines two processes that they envisage as shaping crustal evolution: delamination and relamination. Delamination occurs when gravitationally unstable material in the deep crust, such as eclogite and other garnet-rich lithologies, separates and flows into the less dense underlying mantle. This process leads to a dense, mafic deep crust as eclogitization occurs but before the lower crust delaminates. In contrast, the process of relamination thrusts subducting sediment under the continental crust, resulting in a more felsic, less dense lower crust. While individual examples can be found to support each of these processes, the difficulty remains in determining the dominant pattern of crust evolution.

The continental crust is conventionally split into upper,  $\pm$  middle, and lower layers, though distinct seismic or petrological/geochemical boundaries are not always evident (Holbrook et al., 1992). Petrological and geochemical studies of the deep continental crust have therefore sought to define its composition through analysis of various high grade metamorphic lithologies. It is difficult to gauge, however, if isolated metamorphic samples are representative of the entire deep crust. Temperature and pressure, and therefore metamorphic grade, increase with increasing depth in the crust, though the geothermal gradient varies by up to a factor of  $\sim 3$  depending on continental crust type and tectonic regime (Christensen & Mooney, 1995). If a pressure of 1 GPa is reached at 35 km (assuming an average crustal density of 2,900 kg/m<sup>3</sup> (Wipperfurth et al., 2020)), the deep crust could plausibly be composed of greenschist, amphibolite, granulite, and/or eclogite facies lithologies. However, amphibolite and granulite facies material dominate what are interpreted as deep crustal cross-sections (such as metamorphosed terrains exhumed in the Ivrea-Verbano Zone, Italy), with minimal evidence for greenschist facies lithologies (Rudnick & Gao, 2014). Eclogite facies lithologies likely contribute to orogenic regions with thickened deep crust (pressures up to 1.5–2 GPa following the same density scheme as above) (Leech, 2001; Lombardo & Rolfo, 2000). For these reasons, this study focuses on amphibolite, granulite, and eclogite facies lithologies as potential major components of the deep crust. We report on an expanded database developed by Rudnick and Presper (1990) and added to by Hacker et al. (2015), including data sourced from [Earthchem.org](https://earthchem.org); we examine the chemical trends among various medium to high grade metamorphic lithologies to understand and better characterize what is the average composition of the deep continental crust and follow this with implications for crustal differentiation and evolution processes.

## 2. The Art and Science of Deep Crustal Modeling

In many ways, predicting the composition of the deep continental crust is as much an art as it is a science, because deep crustal models depend not only on the input data, but also the approach each modeler takes to interpreting said data. The definition of the deep crust depends on the question each researcher is trying to address, and is therefore neither a static nor universal term. These differences can sometimes lead to confusion and produce seemingly contradictory models of the crust when in fact, each model is simply looking at the crust through a different lens.

How many layers should we split the crust into? What is the scale of lateral variations in the crust? The answers differ based on the model. This fundamental question is the crux of the disagreement between popular composition models (e.g., Hacker et al., 2015; Rudnick & Gao, 2014). While some split the crust into two layers (e.g., Hacker et al., 2015), upper and lower, shallow and deep, others split it into three (upper, middle, and lower) or more sections (Christensen & Mooney, 1995; Mooney et al., 1998; Rudnick & Fountain, 1995). Thus, debates about compositional models need to be clear about their specific crustal mass fractions. Much geophysical effort has gone into determining the layering and seismic structure of the continental crust. Such topics are beyond the scope of this study, but we want to bring the concept of model resolution to the readers' attention so that they can appreciate the complexity of the task of modeling deep crust composition and be mindful that we are taking but one approach. Nevertheless, averaging geochemical data on large and diverse sample sets has merits. An average deep crustal composition provides an integrated view of how the crust has evolved through time, informing us of

the dominant crust formation pathways, though unique tectonic regions may still require specialized compositional models. Bulk crust and silicate Earth compositions are also useful when comparing Earth to other planetary bodies, such as Mars or Super Earths. On a more concrete level, crustal corrections are required for geophysical applications, such as tomographic models of the mantle or geoneutrino studies, and an average crustal composition is detailed enough to provide further resolution than the Preliminary Reference Earth Model (Dziewonski & Anderson, 1981) but simple enough to implement without significant detriment to calculation time. As such, we have decided to press forward with a global-scale deep crustal model.

Classically, two approaches have been taken to assess deep crustal composition: sample driven modeling and process driven modeling. Sample-driven models base their conclusions on the premise that deep crustal analogue samples, such as mafic high grade metamorphic xenoliths, are by and large representative of the composition of the deep crust. Empirical analyses are the main source of data for this type of model. This geochemical inverse model takes measured element concentrations from exhumed rocks and derives the conditions under which they formed. A second approach considers physical processes and constraints that build the deep crust and the effects of crust formation and evolution. A variety of mafic and felsic compositions can satisfy the geophysical observables, such as Vp or viscosity (e.g., Hacker et al., 2015; Shinevar et al., 2018). These forward process models consider all possible geochemical solutions, avoiding the potential bias of xenoliths, which may be sampling a restricted portion of the deep crust, or whose chemistry has been influenced by their limited eruption environments. Both approaches have their strengths, by being based on petrological and geochemical observation or by reducing sampling bias, and in the end, both methods are valid.

This study more closely resembles the first approach, using samples to infer deep crustal composition. We are mindful of the potential biases this leads to (refer to Section 3.2). For the sake of comparison to other models, we operate under the assumption of a three-layer crust, though we advocate for embracing the potential for vertical and lateral compositional variation by analyzing the full spectrum of available data. Future studies should move beyond bisecting or trisecting the crust, taking advantage of the quality and resolution of both geochemical and geophysical data currently being produced.

### 3. Data Sets

#### 3.1. Amphibolite, Granulite, and Eclogite

For the rest of this study, “amphibolite”, “granulite”, and “eclogite” will refer to rocks in those metamorphic facies, without imposing constraint on composition. Both amphibolite and granulite facies lithologies range from mafic (<52 wt.% SiO<sub>2</sub>) to felsic (>68 wt.% SiO<sub>2</sub>) in composition, and can have Mg#’s (molar  $\frac{Mg}{Mg + Fe}$ ) that resemble the mantle (Mg# ~89), the upper continental crust (Mg# ~30), or any number in between. Eclogite facies lithologies are less heterogeneous than amphibolite or granulite facies, consisting of >75 vol% of omphacite and garnet and lacking plagioclase (Tsujimori & Mattinson, 2020). Please note that “eclogite” as a metamorphic facies is less restrictive in composition than the largely garnet-omphacite, bi-mineralic rock, eclogite, and can include arclogite samples.

The medium pressure (e.g., 0.2–0.8 GPa) and temperature (e.g., 500–750 °C) equilibrium assemblages of amphibolite facies lithologies presumably reflects the conditions of the middle continental crust. Granulite facies lithologies are widely held to comprise the lower continental crust, with its base being defined seismically by the Moho. Amphibolite facies lithologies are generally sampled through exhumed terrains and are more rarely sampled through xenoliths. Granulite facies lithologies can be sampled via terrains or xenoliths. Granulite facies xenoliths have predominantly mafic to intermediate-mafic (45–55 wt.% SiO<sub>2</sub>) silica content, while granulite facies terrains span the range of mafic to felsic. Granulite facies rocks are distinguished from amphibolite facies rocks by the dehydration of hydrous mineral phases. The water-rich minerals that can occur in amphibolites, such as amphiboles and micas, breakdown into pyroxenes in the granulite stability field due to higher temperatures. Granulite facies metamorphism can initiate at 600 °C, meaning that any granulite facies rocks present in areas where the crust is thin and/or the lower crust is at temperatures < 600 °C are in thermal disequilibrium. Granulite facies lithologies, however, are only expected to undergo retrograde metamorphism under limited circumstances due to the kinetic barrier of rehydration (Semprich & Simon, 2014). Thus, many studies still use metastable granulite as a lower crustal analogue.

The eclogite facies is traditionally bounded by the pressures and temperatures required to transform basaltic mineral assemblages into high pressure clinopyroxene and garnet  $\pm$  rutile  $\pm$  accessory minerals. Though it can be difficult to achieve the pressures required to form eclogite in average continental crustal settings (crustal thicknesses  $<40$  km), eclogite facies materials may be a significant component of modern and paleo-orogenic belts (Leech, 2001; Lombardo & Rolfo, 2000). Eclogite facies lithologies, however, may not be preserved through time even in thicker crust because, unlike granulite, they are more susceptible to retrograde metamorphism (e.g., Abbott & Greenwood, 2001; Carswell & Cuthbert, 1986; Dokukina & Mints, 2019; Krogh et al., 1994). Despite their occurrence being potentially localized to orogenic regions in the crust, eclogite facies lithologies are considered germane to the discussion of deep continental crust because eclogite is commonly found at subduction zones, one of the main tectonic settings where continental crust is generated (Hawkesworth & Kemp, 2006; Rudnick, 1995). We analyze the abundance trends in eclogite-bearing terrains since instances of large, coherent swaths of eclogite facies material are rare, though from here on out we refer to these samples simply as eclogite facies terrains to be consistent with our granulite nomenclature. Eclogitic xenoliths can be crust-sourced (e.g., the Colorado Plateau eclogite facies xenoliths (Helmstaedt & Schulze, 1988)) or brought up from the mantle through kimberlite pipes or Hawaiian eruptions. Oxygen isotopic data have shown that even "mantle sourced" eclogites in kimberlites are likely pieces of crustal material (Jacob, 2004).

### 3.2. Potential Biases

The first step in analyzing a data set is to admit that it is potentially biased. Throughout this paper, we scrutinize the statistical uncertainty of deep crust compositions. Systematic uncertainties, however, are not so easily quantified. This section offers what limited insight we have on the potential for systematic bias in our deep crust sample set. The analyses and conclusions in the rest of this paper are generally founded upon the assumption that the following systematic biases have a limited effect on our data set, and if any datasets do fall prey to bias, we operate under the assumption they can be amended without significantly changing the overall picture of deep crust composition. Should any systematic errors fundamentally shift our understanding of the deep crust, that in and of itself would be worthy of future assays.

In this study, we consider large scale, widespread deep crustal samples in order to identify the dominant global chemical patterns. It has been recognized, however, that different types of crustal regimes (e.g.) display different compositional patterns. Sammon et al. (2021), explores the differences between crustal types and tectonic settings using the geochemical data presented here and constraints from seismic and geophysical data.

Our compendium of deep crustal samples, available in the supplemental information of this paper, consists of published data from various sources, most of which are available on [Earthchem.org](http://Earthchem.org) ([www.earthchem.org](http://www.earthchem.org)). We used a subset of the data available, limiting our calculations and analyses to samples whose major oxide content is reported and totals to  $100 \pm 10\%$ . Because of the numerous opportunities for bias in our data set, we only limited samples by metamorphic grade and major oxide totals. Removing the oxide totals filter does not substantially change the distributions of most elements, but tends to increase the data scatter. The filtered and unfiltered data sheets are available as supplemental information.

#### 3.2.1. Location Bias

The global distribution of medium and high grade metamorphic samples shows little correlation between composition and location (Figures S1 and S2 in Supporting Information S1). In fact, samples of mafic and felsic compositions are often found within the same region. We are, of course, limited to areas where terrains and/or xenoliths have been exposed at Earth's surface, but our data include samples from all seven continents. Amphibolite facies lithologies have been extensively studied in crust of various ages. Granulite facies lithologies are also widely sampled, though the xenoliths are relegated to areas that have experienced uncommon eruptions of mafic, xenolith-bearing magmas. In addition, Archean granulite facies terrains are generally restricted to cratonic regions, as active tectonic environments tend not to preserve Archean-aged rocks. Eclogite facies xenoliths and terrains are our most limited datasets, but  $>200$  samples are still available for study. Many eclogite facies samples are from the western United States, potentially biasing the data set toward the eclogites of the Franciscan Complex and eclogites formed from oceanic crust subduction (Tsuji-mori et al., 2006). South America and Antarctica are not represented in the eclogite facies data set.

### 3.2.2. Buoyancy and Transport Mechanism Bias

The deep crust may not be fully represented by the *analogue* samples that have reached Earth's surface. Medium and high grade metamorphic lithologies that have survived surface transport do not necessarily reflect the full distribution, abundance, or composition of the deep crust. Felsic terrains could be over-represented at the surface due to their lower densities. Buoyancy is a significant dynamical force that may play a critical role in determining what types of metamorphic terrains outcrop at the surface (Gerya et al., 2002; Kelemen & Behn, 2016).

On the other hand, eruption type and location may likewise bias xenolith compositions (Jaupart & Mareschal, 2003), including contaminating them with the basaltic lavas (Rogers & Hawkesworth, 1982; Rudnick & Presper, 1990; Rudnick & Taylor, 1987). Studies have also found that felsic xenoliths often cannot withstand the frequently hot, violent eruptions that transport samples to the surface and tend to be re-assimilated (Halliday et al., 1993; Rudnick & Fountain, 1995). Granulite facies xenoliths in particular could be biased by location and/or eruption method: they tend to be co-located with cratonic crust and they are often carried by kimberlite eruptions and fast-erupting alkali basaltic volcanism (Rudnick & Presper, 1990; Russell et al., 2012). Cratonic xenoliths, which presumably have not experienced recent tectonic activity aside from their transport to Earth's surface, may be sampling the composition of an older deep crust.

### 3.2.3. Preservation and Exposure Bias

We recognize also the potential of sample preservation bias. Recent studies outline different weathering rates for different metamorphic rock compositions (e.g., Ohta & Arai, 2007; Price & Velbel, 2003). Age and weathering rate, along with protolith composition, may affect the current metamorphic sample population.

Metastable conditions in the deep crust are another concern. Granulitic lithologies would not be in thermal equilibrium under most projected geotherms (e.g., Kuszniir & Park, 1987). On the other hand, it has been proposed that felsic granulite facies lithologies will not transform into eclogite facies under high pressures but remain as metastable granulite (Hacker et al., 2010). By contrast, the middle continental crust should be stable in the greenschist facies and the lower crust in amphibolite facies. This lower grade combination is not often observed in exposed cross-sections, which, on average, display high temperature/pressure metamorphism and have a mean pressure of 0.8 GPa (i.e., 25–30 km depth) (Brown & Johnson, 2019). The abundance of amphibolite and granulite facies material in (what we deem to be) deep crustal cross-sections suggests that the deep crust reached peak metamorphic conditions some time in the past and has since cooled off. Additionally, metamorphic terrains may undergo retrogression during the exhumation process. We classify these observations as a “preservation bias” because we are preferentially preserving metastable mineral assemblages.

### 3.2.4. Sample Collection and Naming Bias

Lastly we face the bias that we as scientists impose ourselves: collection and classification bias. Unique localities can be over-sampled for their novelty, and thus, overly abundant in the data set. Common andesitic rocks, with their lack of attractive phenocrysts and dull grayish-pink hue, may unfortunately be glossed over in favor of more attractive samples (apologies to Dr. J. Blundy and colleagues). Oversampling the same locations seems to plague the amphibolite facies data set most, with many nearly identical samples in Japan, Alaska, the western United States, and the Appalachian region of the eastern United States. We look more closely at the consequences of this redundant sampling in Section 8. However, for the main analysis of amphibolite facies lithologies in this paper, we keep all amphibolite facies samples in the datasets so that we can see the full span of available data.

Metamorphic lithologies can be categorized by texture (e.g., schist, gneiss) or pressure-temperature (P-T) grade (e.g., amphibolite, granulite), and incomplete changes in lithology can lead to subjective naming. Unfortunately, >6,000 gneisses, schists, and meta-igneous samples were excluded from this study because they were not accompanied by mineral assemblage information. Metamorphic texture on its own cannot be correlated to precise P-T conditions.

To mitigate the oversampling of individual geologic formations, we averaged all samples of the same facies collected within  $0.2^\circ \times 0.2^\circ$  latitude x longitude of each other. This averaging did not change the median composition of granulite facies xenoliths. The median composition of eclogite facies xenoliths and terrains, and granulite

facies terrains of all ages changed by <4%. For amphibolite facies lithologies, however, the median composition, especially SiO<sub>2</sub>, increased drastically by >10%.

While an unknown amount of bias plagues our data set, over 10,000 samples contribute to our understanding of deep crustal composition. Systematic differences among the different metamorphic lithologies are discussed in the appropriate sections. These differences, where quantifiable, serve as markers for different possible deep crustal compositions. This study focuses on a contextualized overview of compositional aspects; it does not delve deeply into metamorphic processes.

## 4. Major Element Compositions

### 4.1. SiO<sub>2</sub>, MgO, FeO, and the Daly Gap

The abundance of major oxides in deep crustal analogue samples is difficult to summarize with a single value and uncertainty. Elemental distributions are not always well defined by the convenient-to-describe Gaussian, normal, log normal, or gamma distribution functions. Table 1 reports summary statistics for amphibolite, granulite, and eclogite facies lithologies major oxide content, but are by no means the most comprehensive descriptions of these complex distributions. Unless indicated otherwise, we will reference the median  $\pm \frac{1}{2}$  the interquartile ranges because of their resistance to skewness and outliers.

A discussion of the significance of median versus mean should also include the practice of evaluating element ratios. Should one consider the representative element ratio to be represented by a ratio of the means or a mean of the ratios? (Likewise, be represented by a ratio of the medians or a median of the ratios?) There is no simple answer to this question; it has been debated extensively without reconciliation. The fundamental question asks—how representative is one's data set of the geological domain being evaluated? For the deep crust, there are many unknowns including unknown unknowns. Hence our preference is to use median values and a median of the ratio, as these resist the influence of skewness and outliers.

Because the distributions of major oxides tend to be skewed and/or multi-modal, our oxide totals are between 90% and 95% when summing the means or medians. We delve further into assessing the modality of our distributions in Supporting Information S1. Tables S1—S6 in Supporting Information S1 list distribution parameters and summary statistics for all elements. We acknowledge our hubris in attempting to parameterize non-parametric distributions, but we are condemned to using bite-sized descriptions of data in the somewhat Sisyphean task of quantifying the chemical composition of a crust we cannot easily access.

The most noticeable data trend is the bimodal distribution of primitive and evolved samples, illustrated by Figure 1. The phenomenon published by Rudnick and Presper (1990) persists in this data set of over 4,000 granulite facies samples and is also present in over 6,000 amphibolite facies samples. Granulite facies xenoliths are dominantly mafic, having <55 wt.% SiO<sub>2</sub> and ranging from mantle-like Mg#s ~89 to Mg#s of 45–50. Granulite facies terrains encompass both mafic and felsic compositions. The felsic samples follow a Fe-enrichment/Mg-depletion trend, leading to a double-peaked structure, resembling a chair, when plotted in Mg# versus SiO<sub>2</sub> space. There is also an age-dependent trend in composition within the granulite facies terrains data set: older, Archean samples are more evolved than Post-Archean samples. Amphibolite facies lithologies show the same chair-like structure, but with a greater concentration of mafic samples. No distinction is made between amphibolite facies terrains and xenoliths in the data set because of the scarcity of amphibolite facies xenolith data.

The corollary to this bimodality is the “missing” intermediate samples between 53 and 68 wt.% SiO<sub>2</sub>. The well-documented Daly Gap (Daly, 1914) describes an apparent dearth of intermediate composition rocks, and is collectively observed in all 586,000 metamorphic and igneous samples in the *Earthchem.org* database. Thermodynamic instability of intermediate compositions (Daly, 1914; Dufek & Bachmann, 2010) and liquid immiscibility (Charlier et al., 2011; Reubi & Blundy, 2009), among other hypotheses (Jackson et al., 2018; Yamasaki, 2018), have been proposed to explain the gap. These hypotheses primarily revolve around the temperature and timing of melt injections, magmatic buoyancy, and/or the stability range of a melt or crystal slush to produce bimodal, intra-crustal differentiation. While it is possible that these rocks are not representative of the crust, we conclude that this is dubious given its coherence across multiple lithologies.

The systematically mafic composition of granulite facies xenoliths was noted by Rudnick and Presper (1990) along with many other studies thereafter. Among the proposed explanations for the relative abundance mafic

**Table 1**  
*Major Element Compositions*

	Mean	Median	Geo-mean	$\gamma$ -mean	STD	IQR	Geo-STD	$\gamma$ -STD	N (filtered)	N (original)
<b>Amphibolite facies lithologies</b>										
SiO <sub>2</sub>	59.1	57.1	58.4	59.1	9.43	18.2	1.17	9.37	2,240	5,490
TiO <sub>2</sub>	0.83	0.73	0.68	0.83	0.49	0.65	1.92	0.50	2,240	5,490
Al <sub>2</sub> O <sub>3</sub>	14.8	14.8	14.7	14.8	1.57	2.15	1.11	1.58	2,240	5,490
FeO <sub>T</sub>	5.31	5.26	4.33	5.31	2.88	5.03	2.03	3.29	847	2,510
MnO	0.13	0.14	0.11	0.13	0.065	0.12	1.85	0.07	2,220	5,430
MgO	4.13	3.70	2.93	4.13	2.81	5.03	2.57	3.27	2,240	5,490
CaO	5.94	5.69	4.58	5.94	3.61	6.95	2.23	4.13	2,230	5,480
Na <sub>2</sub> O	2.96	2.97	2.78	2.96	0.99	1.46	1.46	1.06	2,230	5,480
K <sub>2</sub> O	1.72	1.32	1.18	1.72	1.33	2.05	2.60	1.42	2,230	5,470
P <sub>2</sub> O <sub>5</sub>	0.15	0.14	0.13	0.15	0.083	0.11	1.84	0.084	2,157	5,284
Mg#	46.4	46.8	45.0	46.4	10.6	15.1	1.28	11.2	2,220	5,430
<b>Granulite facies xenoliths</b>										
SiO <sub>2</sub>	51.6	50.2	51.3	51.6	5.05	4.96	1.10	4.88	147	1,490
TiO <sub>2</sub>	0.98	0.92	0.88	0.98	0.42	0.58	1.62	0.44	144	1,480
Al <sub>2</sub> O <sub>3</sub>	16.2	16.2	16.1	16.2	1.74	2.31	1.11	1.75	147	1,490
FeO <sub>T</sub>	6.76	6.71	6.42	6.76	2.15	2.75	1.39	2.16	81	723
MnO	0.15	0.15	0.14	0.15	0.043	0.056	1.36	0.045	143	1,440
MgO	7.05	7.19	6.60	7.05	2.29	3.14	1.48	2.55	145	1,480
CaO	9.23	9.56	8.83	9.23	2.48	3.27	1.37	2.73	147	1,490
Na <sub>2</sub> O	2.56	2.48	2.44	2.56	0.74	1.14	1.38	0.78	147	1,490
K <sub>2</sub> O	0.78	0.66	0.60	0.78	0.54	0.72	2.10	0.54	147	1,480
P <sub>2</sub> O <sub>5</sub>	0.16	0.15	0.13	0.16	0.10	0.13	2.08	0.11	143	1,434
Mg#	56.9	57.1	56.2	56.9	9.05	12.9	1.18	9.16	145	1,480
<b>Post Archean granulite facies terrains</b>										
SiO <sub>2</sub>	59.3	61.5	58.6	59.3	8.73	16.1	1.16	8.83	145	1,660
TiO <sub>2</sub>	0.87	0.76	0.75	0.87	0.44	0.65	1.78	0.46	122	1,630
Al <sub>2</sub> O <sub>3</sub>	15.8	15.5	15.6	15.8	2.05	2.88	1.14	2.04	122	1,630
FeO <sub>T</sub>	5.75	5.59	5.33	5.75	2.10	3.33	1.50	2.21	81	758
MnO	0.13	0.13	0.12	0.13	0.045	0.071	1.50	0.049	120	1,600
MgO	5.06	4.10	3.79	5.06	3.64	5.06	2.25	3.70	123	1,630
CaO	6.11	5.41	4.83	6.11	3.76	7.17	2.08	4.05	123	1,630
Na <sub>2</sub> O	2.51	2.50	2.33	2.51	0.86	1.32	1.51	0.95	122	1,620
K <sub>2</sub> O	1.87	1.73	1.30	1.87	1.36	2.09	2.66	1.53	155	1,700
P <sub>2</sub> O <sub>5</sub>	0.15	0.12	0.12	0.15	0.10	0.11	2.05	0.10	112	1,454
Mg#	48.0	45.8	46.5	48.0	12.0	15.7	1.28	11.9	119	1,610
<b>Archean granulite facies terrains</b>										
SiO <sub>2</sub>	60.1	61.5	59.5	60.1	8.44	16.9	1.15	8.52	123	1,530
TiO <sub>2</sub>	0.66	0.61	0.58	0.655	0.34	0.42	1.68	0.33	122	1,490
Al <sub>2</sub> O <sub>3</sub>	15.3	14.9	15.2	15.3	2.10	2.36	1.14	2.02	122	1,510
FeO <sub>T</sub>	5.12	4.13	4.06	5.12	3.28	5.08	2.05	3.37	78	902
MnO	0.12	0.10	0.10	0.12	0.061	0.094	1.79	0.063	112	1,440
MgO	4.36	3.72	3.40	4.36	2.88	4.53	2.10	2.96	123	1,520

**Table 1**  
*Continued*

	Mean	Median	Geo-mean	$\gamma$ -mean	STD	IQR	Geo-STD	$\gamma$ -STD	N (filtered)	N (original)
CaO	5.33	4.49	4.25	5.33	3.24	5.65	2.08	3.48	122	1,510
Na <sub>2</sub> O	3.05	3.24	2.83	3.05	1.06	1.63	1.51	1.17	120	1,500
K <sub>2</sub> O	1.50	1.20	1.14	1.50	1.06	1.67	2.18	1.07	125	1,630
P <sub>2</sub> O <sub>5</sub>	0.16	0.16	0.14	0.16	0.082	0.087	1.67	0.080	105	1,426
Mg#	48.3	47.0	47.3	48.3	9.81	12.2	1.22	9.56	122	1,500
Eclogite facies xenoliths										
SiO <sub>2</sub>	46.2	46.2	46.1	46.2	1.91	2.46	1.04	1.93	15	173
TiO <sub>2</sub>	0.62	0.607	0.49	0.68	0.34	0.62	2.15	0.41	15	173
Al <sub>2</sub> O <sub>3</sub>	16.1	15.7	15.9	16.1	2.79	2.76	1.17	2.61	15	173
FeO <sub>T</sub>	8.56	8.74	8.39	8.56	1.64	2.63	1.23	1.72	6	46
MnO	0.19	0.18	0.18	0.19	0.037	0.035	1.20	0.034	15	172
MgO	11.7	11.6	11.3	11.7	3.02	4.34	1.31	3.07	15	173
CaO	11.4	11.3	11.1	11.4	2.49	4.99	1.26	2.55	15	173
Na <sub>2</sub> O	2.06	1.58	1.61	2.06	1.49	1.31	2.06	1.39	15	173
K <sub>2</sub> O	0.38	0.20	0.21	0.38	0.40	0.38	3.09	0.37	14	131
P <sub>2</sub> O <sub>5</sub>	0.065	0.063	0.055	0.065	0.030	0.035	1.97	0.037	12	86
Mg#	51.8	47.9	50.8	51.8	9.90	15.20	1.21	9.71	13	123
Eclogite facies terrains										
SiO <sub>2</sub>	47.5	47.2	47.4	47.5	2.64	5.33	1.06	2.65	14	60
TiO <sub>2</sub>	1.33	1.09	1.14	1.33	0.72	1.23	1.79	0.73	14	60
Al <sub>2</sub> O <sub>3</sub>	14.9	15.0	14.8	14.9	2.14	3.26	1.16	2.16	14	60
FeO <sub>T</sub>	9.06	8.59	8.48	9.06	3.27	6.30	1.44	3.27	11	31
MnO	0.23	0.19	0.21	0.23	0.089	0.12	1.41	0.080	14	60
MgO	8.11	7.98	7.80	8.11	2.42	2.80	1.31	2.25	14	60
CaO	11.1	11.1	10.9	11.1	2.13	3.85	1.22	2.18	14	60
Na <sub>2</sub> O	2.74	2.56	2.36	2.74	1.57	2.25	1.72	1.46	14	59
K <sub>2</sub> O	0.45	0.43	0.31	0.45	0.33	0.69	2.54	0.37	12	57
P <sub>2</sub> O <sub>5</sub>	0.13	0.11	0.097	0.13	0.11	0.12	2.27	0.10	14	57
Mg#	41.7	40.8	40.8	41.7	8.84	9.60	1.24	8.95	14	60

*Note.* STD, standard deviation; IQR, interquartile range; Geo-Mean, geometric mean; Geo-STD, geometric standard deviation (reported in log units);  $\gamma$ , gamma function mean;  $\kappa \cdot \sigma$  (scale parameter \* shape parameter);  $\gamma$  - STD, gamma function standard deviation,  $\sqrt{\kappa * \sigma^2}$

xenoliths are that felsic xenoliths are less likely to survive the eruption process (Halliday et al., 1993; Rudnick & Fountain, 1995) and that xenoliths might sample deeper regions of the crust than terrains (Bohlen & Mezger, 1989; Rudnick & Fountain, 1995). Terrains, on the other hand might be biased toward sampling shallower or more felsic regions because mafic terrains are less buoyant and less likely to reach the surface (Gerya et al., 2008). Studies have suggested that the ages recorded in these high grade metamorphic samples have been affected by open system behavior (Ashwal et al., 1999) or, as more traditionally argued, hotter temperatures in the Archean allowed for greater amounts of delamination of mafic material, leaving the Archean crust enriched in felsic components (Martin, 1986). The raw SiO<sub>2</sub> concentration for Archean-aged granulites has a median abundance of ~64 wt.%. Once samples from the same locales are averaged together, however, granulite facies terrains show no aged-based compositional biases, with Archean samples (61.5 ± 8.5 wt.% SiO<sub>2</sub>) being roughly equal to Post-Archean samples (61.5 ± 8.7 wt.% SiO<sub>2</sub>). Whether or not this is an artifact of data processing or shows oversampling of felsic Archean granulites remains debatable.

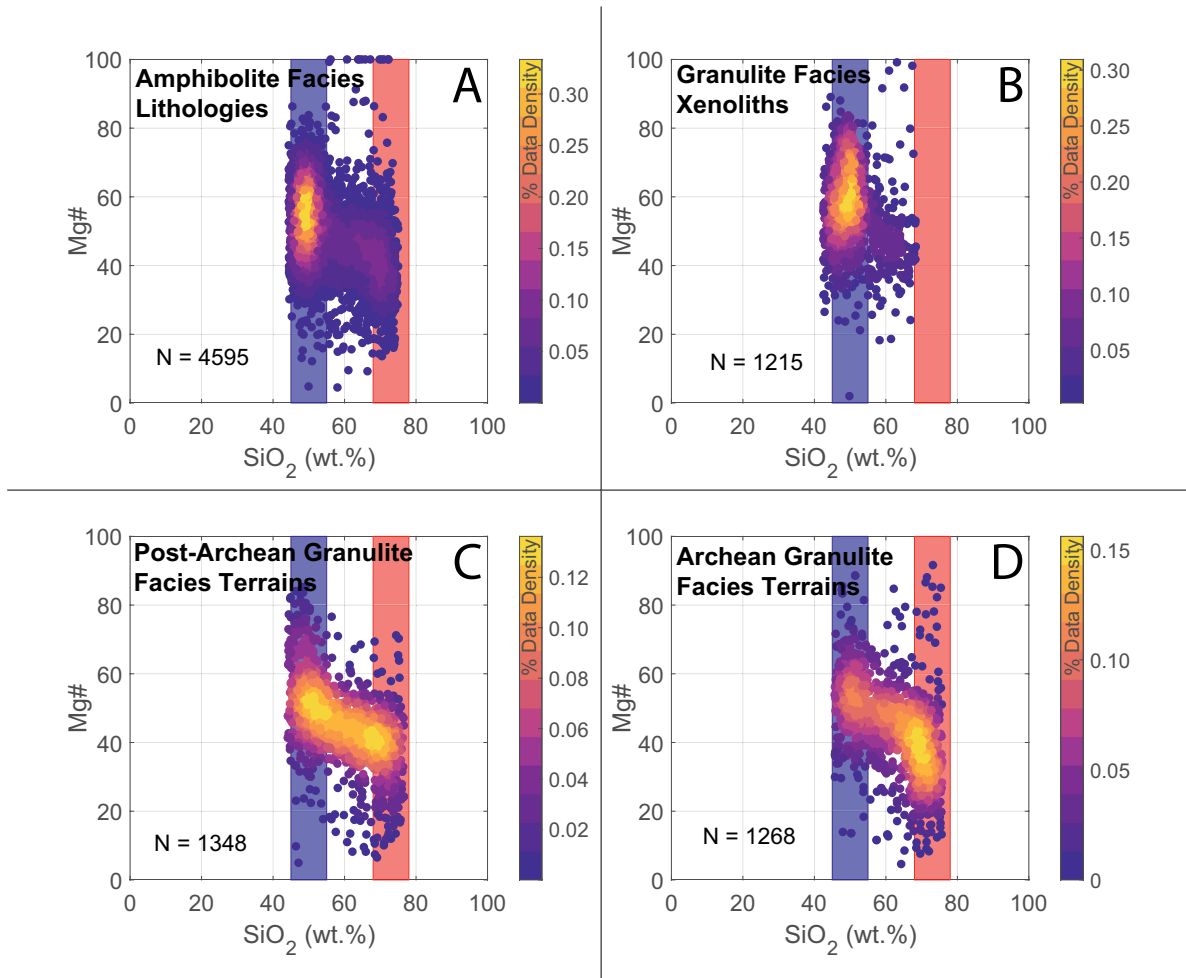


**Figure 1.** Mg# versus SiO<sub>2</sub> for metamorphic facies lithologies of (a) amphibolite, (b) granulite xenoliths, (c) Post-Archean terrains, and (d) Archean terrains. Color indicates relative data point density. Blue and red vertical bands mark the dominant mafic and felsic SiO<sub>2</sub> abundances. Mg# is calculated as molar  $\frac{[Mg]}{[Mg] + [Fe]}$ . The number of samples (N) plotted are reported. All plots show high concentrations of mafic and/or felsic compositions and comparatively few compositions of intermediate SiO<sub>2</sub>.

There is no discernible compositional difference between granulite facies terrains and xenoliths of comparable SiO<sub>2</sub> and Mg# (Figure 2). Most other compositional trends, such as elevated median CaO in granulite facies xenoliths or rare earth element enrichment in terrains (discussed later), correlate to the sample's SiO<sub>2</sub> and MgO content. The composition of granulite facies lithologies seems to have little dependence on location (other than the fact that xenoliths are generally most accessible in regions that have experienced volcanism); if surface transport mechanisms are affecting the composition of these granulite samples, then they are not doing so beyond preferentially selecting for certain SiO<sub>2</sub> content.

The strong preference for mafic compositions in amphibolite facies lithologies is likely biased by mineralogy and geologic naming conventions. Amphibolite facies lithologies unsurprisingly contain amphibole minerals, which generally form in mafic rock compositions. Felsic rocks of similar metamorphic grade seem to be categorized as schists, gneisses, or even metapelites. It is likely that many amphibolite facies samples were excluded from our study because they were given a textural metamorphic grade designation. Thousands of intermediate and felsic gneisses could not be assigned to amphibolite or granulite facies because of insufficient metadata.

The eclogite facies xenoliths and terrains are limited to  $46.2 \pm 1.2$  and  $47.2 \pm 2.2$  wt.% SiO<sub>2</sub>, respectively. This is likely due to the stricter definition of “eclogite”, which can refer to a bi-mineralic rock or require basaltic mineral assemblages to reach high pressure. Eclogite facies lithologies have Mg# of 30–90, with no correlation to location or method of surface transport.

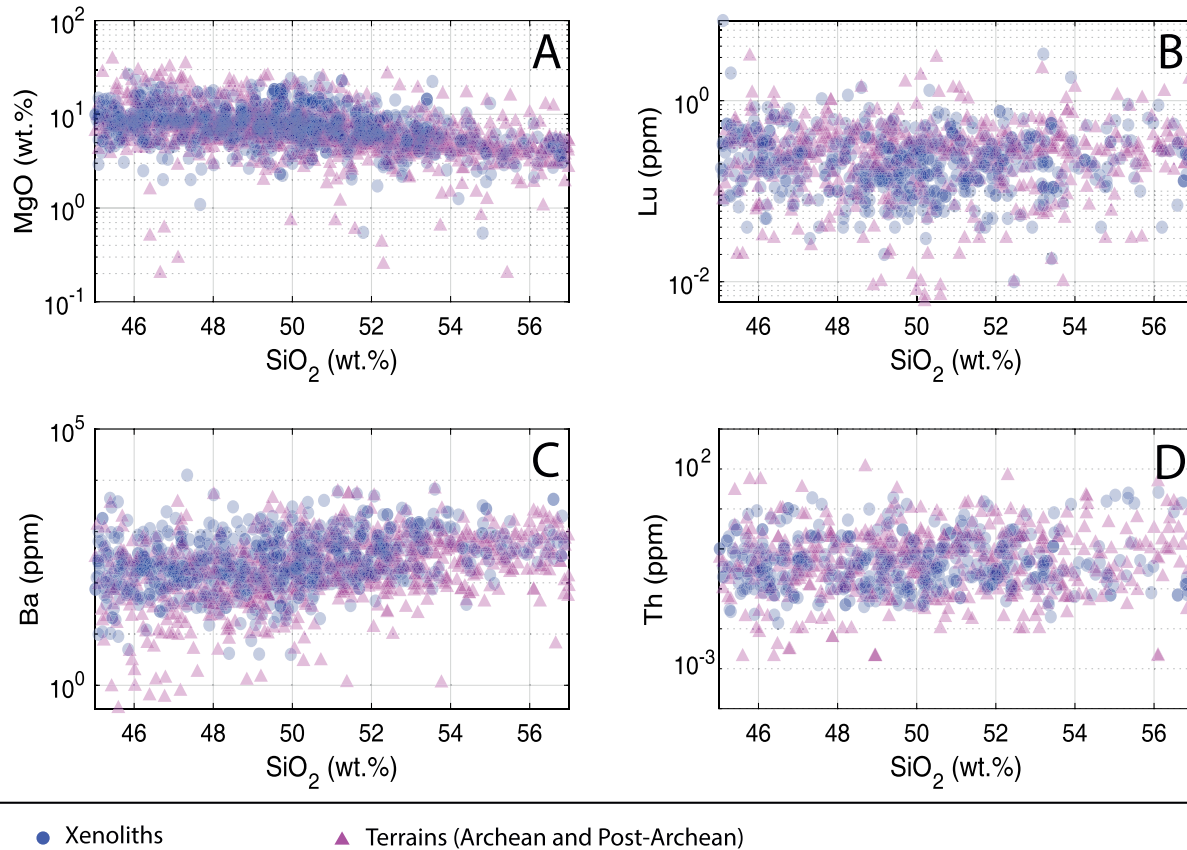


**Figure 2.** Granulite facies xenoliths and terrains of the same  $\text{SiO}_2$  are compositionally indistinguishable in both compatible and incompatible element space. Panels A through D are arranged from most compatible ( $\text{MgO}$ , a major thermodynamic component) to Th (a highly incompatible trace element).  $\text{Mg\#}$ , not shown in these diagrams, is the next major contributor to data scatter that is, composition trends are correlated to how evolved a sample is first in terms of  $\text{SiO}_2$  content, then to  $\text{Mg\#}$ .

#### 4.2. The Constancy of Al and Ga

Notably,  $\text{Al}_2\text{O}_3$  content remains relatively constant (i.e.,  $\sim 12\%$  variation) throughout all samples. Though eclogite facies lithologies have slightly elevated  $\text{Al}_2\text{O}_3$  content compared to the other samples (Table 1), estimates for  $\text{Al}_2\text{O}_3$  only range from 14 to 17 wt.%. The  $\text{Al}_2\text{O}_3$  values of granulite facies lithologies are roughly 5%–15% lower than the commonly accepted lower crustal  $\text{Al}_2\text{O}_3$  values of Rudnick and Gao (2014) though still within the study's given error. Our estimated  $\text{Al}_2\text{O}_3$  content in granulite facies lithologies are more in line with Wedepohl (1995) and Gao et al. (1998) lower crustal values.

Elements of the same group in the periodic table tend to behave similarly. For example, the abundance of Ga tracks with Al and Ge tracks with Si (De Argollo & Schilling, 1978). Comparable to Al, Ga concentrations are nearly constant in amphibolite and granulite facies lithologies: median abundance ranges from 17.3 to 19.5 ppm. Eclogite facies samples again behave differently. Due to the significantly smaller sample sizes of the eclogite lithologies. There is little or no data reported for Ge and so we predict its concentration in the deep crust to be relatively invariable at about 1.3–1.4 ppm, based on chemical trends for igneous rocks (De Argollo & Schilling, 1978).

##### 4.2.1. Understanding Protolith Populations

A comparison of the molar abundances of Al to alkali metals and alkaline earths provides a potential provenance indicator for the origin of deep crustal rocks. Sedimentary rocks typically have  $\text{Al}_2\text{O}_3$  contents of  $\sim 20$  wt.% (Taylor & McLennan, 1985), whereas most igneous rocks vary from 12 to 19 wt.%  $\text{Al}_2\text{O}_3$  (De La Roche et al., 1980). Anorthositic and other plagioclase-rich cumulate rocks, however, can have much higher  $\text{Al}_2\text{O}_3$  contents.

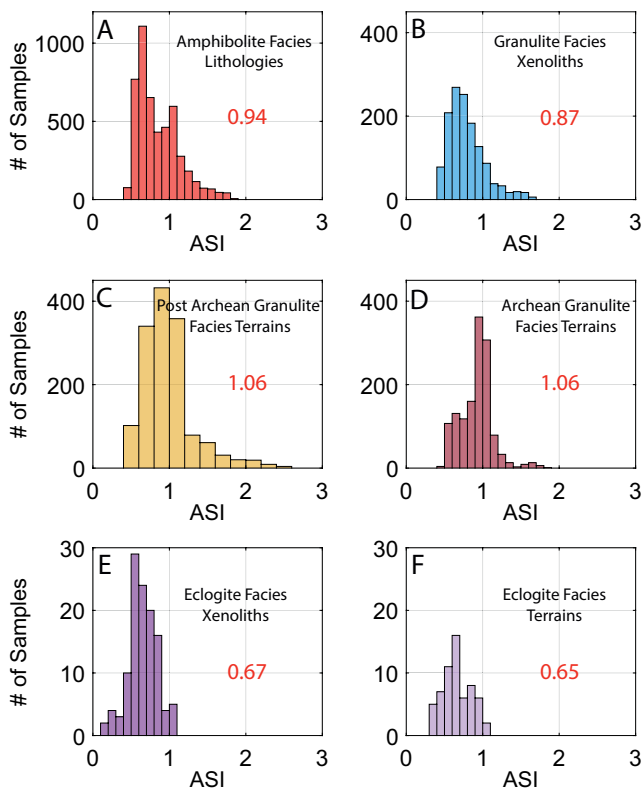


**Figure 3.** Natural log of the aluminum saturation index (ASI), molar  $\text{Al}_2\text{O}_3/(\text{CaO} + \text{Na}_2\text{O} + \text{K}_2\text{O})$ . Red numbers indicate the median value for each sample type. The ASI value is an ambiguous indicator of a rock's protolith; rocks with  $\text{ASI} > 1$  (i.e., peraluminous) can be from igneous or metasedimentary protoliths. More mafic samples have lower ASI values, while granulite facies terrains often have values  $\sim 1$ .

Al content and Aluminum Saturation Index (ASI) have in the past been used to help infer the protolith of deep crustal samples. When a rock's ASI (molar  $\text{Al}_2\text{O}_3/(\text{CaO} + \text{Na}_2\text{O} + \text{K}_2\text{O}) > 1$ , it is classified as peraluminous (Zen, 1988), but with no characterization of its source of origin, so caution is needed. Though sedimentary rocks tend to have higher Al contents (ASI = 1.12, excluding carbonates), Keller et al. (2015) found that common crustal cumulates are also often  $\text{Al}_2\text{O}_3$ -rich. Zen (1988) reported granites having ASI values between 1 and 1.4 and noted that these rocks can be derived from a variety of source lithologies, with the proviso that for large bodies of strongly peraluminous granitic rocks peraluminous sources seem necessary. Chappell et al. (2012) observed that many I (igneous)-type granites are peraluminous and owe their origins to partial melting of more mafic source rocks. They also noted that gradations from peraluminous felsic granites to metaluminous igneous compositions are seen for rock suites that have a shared, closed isotopic system.

Unknowns remain significant regarding the abundance of sedimentary lithologies in the deep crust. Our samples have median ASI values ranging from 0.65 to 1.06, yet the distribution of aluminum indices is wide and sometimes asymmetrical (Figure 3). Amphibolite facies lithologies and granulite facies xenoliths have ASI values comparable to igneous lithologies (Earthchem.org data, median ASI = 0.76), but eclogite facies lithologies have a median ASI values lower than either. The eclogite facies distributions lack the long tail of higher ASI values which will skew their medians somewhat despite its robustness to outliers. If eclogite facies lithologies were not sufficiently sampled to encounter high ASI samples, then it is possible that their actual median ASI value is higher. The change in eclogite ASI distribution shape would lend the appearance of a log-normal trend among the datasets.

It is difficult to distinguish between metaigneous and metasedimentary protoliths for deep crustal lithologies with certainty (e.g., Wilkinson et al., 2009). Hacker et al. (2015) identified 44% Archean and Post-Archean granulite-facies rocks as peraluminous and noted that they may be metasedimentary; going further, they suggested that amphibolite-facies terrains have similar

statistics and that 16% granulite-facies xenoliths that are peraluminous may be metasedimentary. We do not find compelling evidence that the ASI value provides unambiguous indication of what is a metasediment. In fact, as cautioned by Chappell et al. (2012), many peraluminous rocks are igneous. Given that the term peraluminous does not effectively identify what might be a metasediment, we turned to a machine learning algorithm to predict a metamorphic protolith from major element chemistry (Hasterok, Gard, Bishop, et al., 2019). This method, however, also produced unclear results. The algorithm showed low confidence in whether the protoliths were igneous or sedimentary, with ratings close to 0 instead of  $-1$  (confidently igneous) or  $1$  (confidently sedimentary). It is also nearly impossible to distinguish between a restitic metasediments and a mafic igneous rock in the deep crust Keller et al. (2015). Since is no reliable geochemical indicator to distinguish the two, this is an area that requires further research. A broader view of factors must be considered to determine the formation and evolution processes of the deep crust.

## 5. Minor and Trace Element Composition

Here we discuss key geochemical trends seen in incompatible elements; other observations are not covered here for the sake of brevity. The rest of the data is addressed in more detail in Supporting Information S1, which reviews our findings for fluid mobile elements, high field strength elements, transition metals, and other important groups of elements. Regardless of surface transport mechanism (eruption as xenoliths or tectonic emplacement as terrains), there are no differences in trace element content between granulites of similar  $\text{SiO}_2$  content. Therefore, granulite facies xenoliths and terrains can be treated as one lithology when discussing silica-correlated

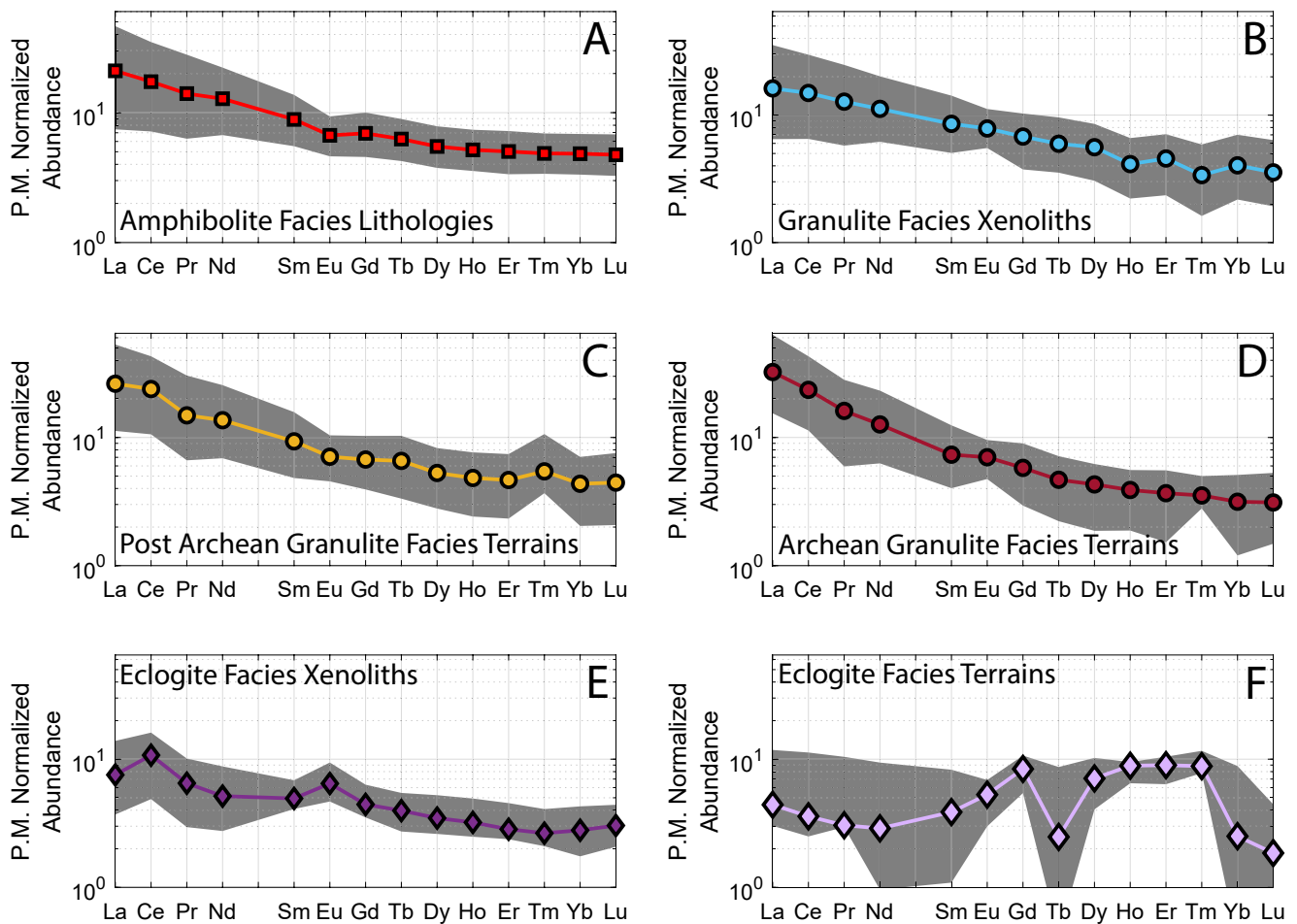


**Figure 4.** Rare earth element (REE) median values. The gray shaded bands represent the first and third quartile values for each REE.

compositional trends. Eclogite facies xenoliths and terrains have fewer data points, so it remains unclear whether or not they should be given the same treatment.

### 5.1. Rare Earth Elements

Figures 4 and 5 illustrate that the rare earth element patterns of all of the samples are congruent, having greater variation in the light rare earths (LREE) and than in the heavy rare earth elements (HREE). The amphibolite and granulite data show LREE enrichments and their variability is comparable to that shown by Rudnick and Gao (2014), with granulite facies terrains having the highest median concentrations of La through Nd. The greatest abundance of La and Ce is not seen in the most hydrated samples (amphibolites) but in the most evolved samples (granulite facies terrains). Eclogite facies lithologies are relatively depleted in LREE compared to amphibolites, yet they are more enriched than granulite facies xenoliths. Therefore, igneous processes—rather than metamorphic changes or chemical weathering—control the relative enrichment in LREEs seen in granulite facies terrains. In other words, the elevated LREEs signatures were inherited from the felsic granulites' protoliths rather than the result of a metamorphic change. The standard deviation of the REE distributions narrows from La to Lu. Eclogite facies samples show no relative enrichments in HREEs. HREE enrichment is typical in garnet-bearing igneous rocks, but the protoliths of these eclogites were basaltic. Because these eclogites did not inherit elevated HREEs from their protoliths, the metamorphic garnets do not cause the bulk rock composition to have an enriched HREE signature.

Amphibolite facies lithologies and granulite facies xenoliths span similar ranges of La/Yb,  $8.16 \pm 6.5$  and  $7.52 \pm 3.2$ , respectively. Archean granulite facies terrains have a much higher median value (La/Yb =  $16.0 \pm 10.2$ )

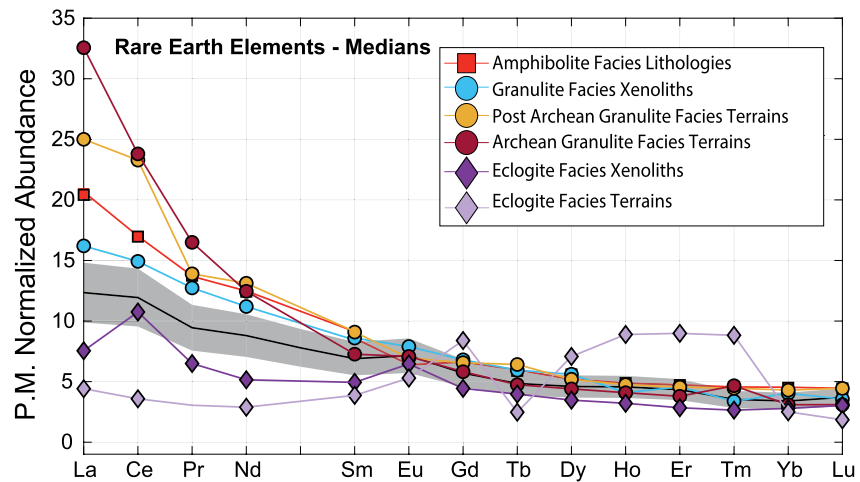


**Figure 5.** While the most variation is seen in the light rare earth elements, the heavy rare earth elements are tightly knit at  $\sim 5\times$  primitive mantle. Note the scale is linear. The black line and gray shaded region surrounding it is the Rudnick and Gao (2014) lower crustal composition  $\pm 15\%$ .

than Post-Archean terrains ( $\text{La/Yb} = 10.1 \pm 4.50$ ) despite having similar  $\text{SiO}_2$  content, yet  $\text{La/Yb}$  and is correlated to  $\text{SiO}_2$  and forms the same chair-like structure when in natural log space as  $\text{SiO}_2$  versus  $\text{Mg\#}$ . The bimodal structure suggests that the Daly Gap affects  $\text{La/Yb}$ , and that the ratio reflects the original igneous processes that formed the rock rather than metamorphism or weathering.

Flatter REE patterns (lower  $\text{La/Yb}$  ratios), common among the eclogite facies xenoliths and eclogite-bearing terrains, do not seem to be relegated to specific regions. It is possible that eclogite-bearing terrains are biased by alteration and subduction processes despite how closely they resemble xenoliths because of our limited data set (e.g., Tsujimori et al., 2006). As mentioned earlier, many of our eclogite facies terrains samples originate from areas that have evidence of significant subduction, such as the western United States. Eclogite-bearing terrains from the Caledonides in Norway (e.g., Rockow et al., 1997; Svensen et al., 2001) also show REE variation even within the same formation. Sampling exposures of eclogite terrains in regions that have not been subjected to significant amounts of subduction would provide more clarity—if such terrains exist. The apparent enrichment in Gd, Dy, Ho, Er, and Tm in eclogite terrains is due to our limited data set, with those elements having only 1–5 datapoints each.

On average, the crust shows a systematic vertical concentration gradient in REE abundances (i.e.,  $\text{UC} \rightarrow \text{MC} \rightarrow \text{LC}$ , showing  $\text{La } 36 \pm 7.2 \rightarrow 18 \pm 12.8 \rightarrow 12 \pm 6.5$ ;  $\text{Yb } 3.1 \pm 0.33 \rightarrow 2.2 \pm 0.75 \rightarrow 1.7 \pm 0.81$  ppm), with a mildly fractionated downward decrease in the LREE (factor of 3) and HREE (factor of 2). Likewise,  $\text{Eu/Eu}^*$  changes from a 30% negative anomaly in the upper crust (Gaschnig et al., 2016) to essentially no anomaly in the lower crust. These compositional gradient are most likely products of intracrustal differentiation, with granite magmas moving upward and residuals being stored in the lower crust or lost to the mantle via gravitational processes.

## 5.2. Heat Producing Elements

Heat producing elements (HPEs: K, Th and U) are of particular interest because they are crucial to understanding Earth's radioactive heat budget (these three elements produce 99.5% on the radiogenic heat) through time as well as the temperature and strength of the crust. Rudnick and Gao (2014) estimate the continents host 35%–40% of the Earth's budget of HPE. Constraining Earth's HPE abundances (especially the abundance of the refractory lithophiles, e.g., U and Th) also constrains  $\sim 26$  other elements (McDonough & Sun, 1995) that are in conserved, chondritic ratios relative to U and Th.

### 5.2.1. Th, U, and K

The behavior HPE can often be understood through comparisons of elemental ratios. About 80% of the Earth's total heat production comes from Th and U and thus the Th/U ratio is key. Wipperfurth et al. (2018) recently reviewed Th/U values for  $\sim 150,000$  crustal rocks and sediments and found that the median values for igneous and metamorphic rocks were close to the bulk Earth's value of 3.8. We find that amphibolites have a median Th/U

of 3.7, whereas granulite terrains appear to have lost U (see below) relative Th (median Th/U for Archean and Post-Archean granulite terrains are 7.3 and 6.6, respectively). In contrast, the median Th/U of granulite xenoliths (3.4) appears to be normal (i.e., no U loss or proportional U and Th loss). There is little correlation between K content and K/U, with median K/U values for all metamorphic lithologies ranging upwards of one to three times that of upper continental crust. We observe K/U values from 10,000 to 100,000 with uncertainties on the order of 60%. Whether K behaves as a trace element or thermodynamic component (i.e., mineral) controls the K abundance in our samples. That is, K abundance is high if K-feldspar is present in the system, whereas K is low if K-feldspar is not present. The K/Th value is relatively constant in deep crustal lithologies and similar to that of the upper crust (Alessio et al., 2018; Rudnick & Gao, 2014), implying K/U fractionation is due to U loss, not K loss, and in agreement with the earlier finding of Rudnick and Presper (1990).

A question that remains is, how long ago did this uranium loss occur in the granulite terrains? To address this issue we combined the two separate measures of Th/U. The isotopic ratio of  $^{232}\text{Th}/^{238}\text{U}$  value is referred to as  $\kappa$  ( $\kappa \sim \text{Th}/\text{U} \times 1.033$ ), while the time-integrated Pb isotopic ratio ( $^{208}\text{Pb}^*/^{206}\text{Pb}^*$ , the decay products of  $^{232}\text{Th}/^{238}\text{U}$ ) is  $\kappa_{pb}$ , which serves as a proxy for Th/U. [ $\kappa_{pb}$  values are calculated from the measured lead isotopic composition of the sample minus its primordial lead contribution; see details in Wipperfurth et al. (2018).] The  $\kappa_{pb}$  provides a measure of the time-integrated Th/U value and is resistant to recent resetting. The average (and median)  $\kappa_{pb}$  for the amphibolites, granulite xenoliths, and Archean and Post-Archean granulite terrains is  $4.1 \pm 0.1$  ( $4.0 \pm 0.1$ ;  $n = 165, 357, 33, \text{ and } 4$ , respectively), while eclogite xenoliths are 5.5 (5.8;  $n = 21$ ) and no data for eclogite terrains; see Table S3 in Supporting Information S1 for further details. The ~70% difference between Th/U and  $\kappa_{pb}$  values for granulite facies terrains is consistent with a relatively recent (<450 Ma) uranium loss. On average it appears that exhumation or surficial weathering processes (oxidized  $\text{U}^{6+}$  is much more fluid mobile than  $\text{U}^{4+}$  or  $\text{Th}^{4+}$ ) result in the loss of U from the granulite facies terrains relative to Th and less so due to dehydration metamorphism.

In general, U and Th show positive correlations with  $\text{SiO}_2$ . Mean and median U and Th values increase with increasing  $\text{SiO}_2$  abundance for amphibolite and granulite facies rocks. While the relationship between  $\text{SiO}_2$  and U or Th is log-normal within uncertainties, the concentration of U and Th could potentially also be derived from  $\text{SiO}_2$  through a probability analysis (e.g., Gard et al., 2019; Hasterok, Gard, Cox, et al., 2019).

Deep crustal heat production is but a fraction of upper crustal heat production. The median heat production in the deep crustal lithologies ranges from 0.04 to 0.41 nW/kg (roughly 0.1–1.2  $\mu\text{W}/\text{m}^3$ , assuming a density of 2,900  $\text{kg}/\text{m}^3$ ). Post Archean granulite facies terrains have the highest heat production to  $0.4 \pm 0.5$  nW/kg ( $\sim 1.2$   $\mu\text{W}/\text{m}^3$ ). How we calculate our heat production is significant: the *mean of the averages* does not equal the *average of the means*. Using the median  $\text{K}_2\text{O}$ , Th, and U abundances, we calculate heat production for Post-Archean and Archean granulite facies terrains to be 0.14 and 0.15 nW/kg (0.41 and 0.42  $\mu\text{W}/\text{m}^3$ ), respectively. The answer lies in the shape of the distributions, which are neither normal nor log-normal. In this case, our simplified statistics are sub par descriptors of the datasets. Yet, we see that median deep crustal heat production should be minimal unless there is significant incorporation of granulite facies terrain material.

## 6. Distributions That Trend, Periodically

The periodic table is a wonderful tool to use when analyzing elemental trends because of its structure and organization. It shows that elements of similar valence states and radii behave predictably and highlights anomalies caused by specific minerals or sampling methods. We expect to see more skewed distributions for elements that change abundance with depth, since our data set includes samples from a range of depths (Bohlen & Mezger, 1989). The difference between mean and median is one metric for quickly assessing the shape of non-normal distributions. McDonough (1990) found that major and compatible trace elements have similar average and median values, whereas median values are systematically lower than average values for the incompatible trace elements (e.g., LREE, K, Rb), with differences between average and median values increasing with increasing incompatibility. Figures 6 and 7 are color coded to show the % difference between mean and median for amphibolite and granulite facies lithologies. The same methodology can be applied to eclogite facies lithologies, but the distributions are more discontinuous, and trends are less clear due to having an order of magnitude fewer samples. Even in the amphibolite and granulite data sets, elements with relatively few data points (such as the highly siderophile elements) appear highly skewed.

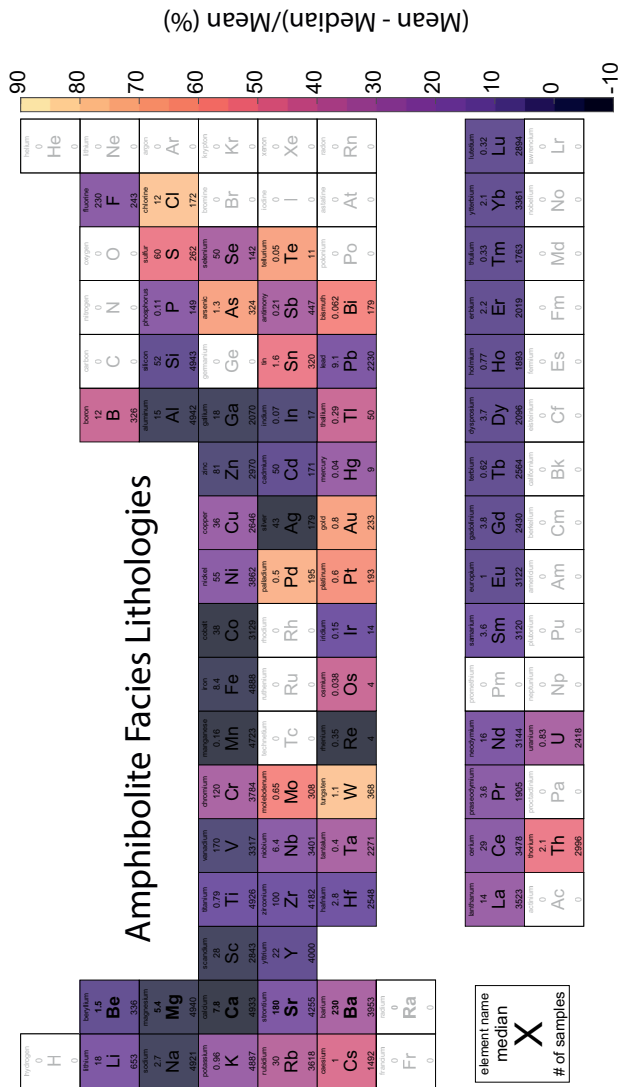


**Figure 6.** Median composition of amphibolite facies rocks. The elements color correlates to the percent difference between the mean and median for elemental distributions for amphibolites. The  $\Delta_{\text{mean}-\text{median}}$  is an indicator of the symmetry of the distribution. Elements that are grayed out have insufficient data. The number of available samples is indicated at the bottom of each element box; the median concentration is given above the element label. Median concentrations are given in wt.% oxide for Na, Mg, Al, Si, K, Ca, Ti, Mn, and Fe. All other elements are reported in ppm. Similar trends emerge among elements of the same family and among the lathanides. Heavier, larger elements vary more in amphibolite facies lithologies than in granulite facies lithologies.

Al and Ga are unimodal, with little variation in their abundances compared to other elements, and Na is relatively constant, with some possible bimodality. The mean and median values for Si are similar because of its bimodal distribution, but we do not find conclusive evidence for bimodality in other oxides. Fe, Mg, and Ca show some degree of multi-modality. Most of other elements in the table are unimodal. The rare earth elements exhibit consistent patterns between amphibolite and granulite facies lithologies, though amphibolites have greater differences between mean and medium in the light rare earth elements. The homogeneity of the rare earth element distributions underscores their predictable behavior, with the greatest skewness occurring in the LREE which tapers off to a steady  $\sim 10\%$  difference between mean and median toward the heavy rare earths.

Both Th and U have highly skewed distributions that verge on log-normal for both amphibolite and granulite facies lithologies. The distributions of U and Th in granulite facies terrains are indistinguishable from both a gamma and a log-normal distribution (using a Wilcoxon rank sum test of median values). The distributions of U and Th in granulite facies xenoliths and amphibolite facies lithologies, however are more accurately described by log-normal distributions. That is to say, the misfit between either the Th or U distribution and log-normal distributions with the same  $\mu$  and  $\sigma$  is negligible according to the (admittedly simplistic) statistical test mentioned above. On the other hand, the misfit between Th or U and the corresponding gamma distributions with the same shape and rate parameters is significant according to the same statistical test. Th and U are expected to be skewed because their abundance changes rapidly as a function of depth (e.g., Huang et al., 2013; Rudnick & Fountain, 1995; Rudnick & Gao, 2014).

### 6.1. Fluid Mobility of K, Rb, and Cs

The transition from amphibolite to granulite facies can be considered, for the major elements, an isochemical dehydration reaction, but this is not the case for the most fluid mobile elements: K, Rb, and Cs. Consistent with the observations of Rudnick & Presper (1990),  $K_2O/Rb$  ratios in amphibolite and granulite facies lithologies are negatively correlated with  $K_2O$  content, especially at  $K_2O < 1.2$  wt.%, indicating Rb depletion relative to  $K_2O$ . We restrict our analysis of  $K_2O/Rb$  to compositions to rock with  $>55$  wt.%  $SiO_2$ ; unmetamorphosed basalts have highly variable  $K_2O/Rb$ , making it difficult to evaluate their Rb depletions (Rudnick & Presper, 1990).  $K_2O/Rb$  values reach a maximum at about 1 in most of the metamorphic datasets. Although we omit them, mafic lithologies follow the same trend, though lower  $K_2O$  values are reached. As suggested by various studies, this trend likely reflects a mineralogical control on the partitioning of Rb and K between minerals and a fluid phase (e.g., Fowler, 1986; Rudnick et al., 1985). Low concentrations of  $K_2O$  and Rb, and high  $K_2O/Rb$  ratios, may reflect igneous processes rather than metamorphic processes (Van Calsteren et al., 1986). However, several mafic granulite facies and amphibolite facies lithologies have high K/Rb ratios compared to basalts, which suggests that they have experienced some Rb depletion during metamorphism (Stosch et al., 1986). The similarities between the amphibolite and granulite facies K/Rb are striking, because high  $K_2O/Rb$  was thought to be the providence of dehydration metamorphism. Partial dehydration of amphibolite facies lithologies might lead to high  $K_2O/Rb$  ratios while still leaving behind enough hydrous mineral assemblages to classify the rock as amphibolite. Future studies should explore the quantification of dehydration as it relates to  $K_2O/Rb$  ratios. Alternatively, metamorphosing gabbro to the amphibolite facies can produce uneven increases in K and Rb (Field & Elliott, 1974), leading to lower  $K_2O/Rb$  ratios. Low  $K_2O/Rb$  ratios in amphibolites could also be inherited from the retrograde metamorphism of granulite with low  $K_2O/Rb$  (Field & Clough, 1976).



**Table 2**

Median Major Oxide Compositions for Our Sample Sets, Mid Ocean Ridge Basalts (MORB, Gale et al. (2013)), Ocean Island Basalts (OIB, MacDonald and Katsura (1964)), Oceanic Plateau Basalts<sup>a</sup>, and Arc Tholeiites<sup>b</sup>

	Amph. Lith.	Gran. Xen.	PA gran. Ter.	A gran. Ter.	Ecg. Xen.	Ecg. Ter.	MORB	OIB	Oceanic plateau	Arc tholeiite
SiO <sub>2</sub>	62.2	53.3	63.18	65.4	48.0	50.1	50.7	50.1	49.5	49.9
TiO <sub>2</sub>	0.79	0.98	0.78	0.65	0.63	1.16	1.69	2.53	1.28	0.69
Al <sub>2</sub> O <sub>3</sub>	16.1	17.2	15.9	15.8	16.3	15.9	14.8	14.1	13.6	16.1
FeO <sub>T</sub>	5.73	7.12	5.74	4.39	9.09	9.11	10.5	11.4	11.0	10.2
MnO	0.15	0.16	0.13	0.11	0.18	0.20	0.18	0.16	0.19	0.17
MgO	4.03	7.63	4.21	3.96	12.1	8.47	7.61	8.53	8.71	8.12
CaO	6.20	10.2	5.56	4.77	11.8	11.8	11.4	10.4	11.4	11.8
Na <sub>2</sub> O	3.23	2.63	2.57	3.45	1.64	2.72	2.80	2.16	2.23	1.82
K <sub>2</sub> O	1.44	0.70	1.78	1.28	0.21	0.45	0.16	0.38	0.31	0.30
P <sub>2</sub> O <sub>5</sub>	0.15	0.16	0.12	0.17	0.07	0.11	0.18	0.25	0.19	0.11
Mg#	46.8	57.1	45.8	47.0	47.9	40.8	-	-	-	-
Mg# Calc.	55.6	65.6	56.7	61.6	70.3	62.4	56.4	57.2	58.6	58.8

<sup>a</sup>From published Ontong-Java Plateau basalts, database set in Supporting Information S1. <sup>b</sup>Combination of values from Jakeš and White (1971) and Kuno (1966).

the lower crust, whereas granulite facies xenoliths appear to dominate the bottom of the lower crust (Rudnick & Gao, 2014).

Though amphibolite facies lithologies are held to represent the middle crust, the median SiO<sub>2</sub> for amphibolite lithologies is ~10% lower than existing estimates. This makes our bulk continental crustal model more mafic in the middle crust, leaving a potential mid-crustal deficit in many incompatible elements. A mafic bias in our amphibolite facies lithologies may exist and seems to stem from:

1. biasedly assigning medium grade, mafic metamorphic samples to “amphibolite” facies (due to the abundant mode % of amphiboles) but not assigning medium grade, felsic metamorphics to amphibolite facies; and
2. the oversampling of mafic amphibolite facies locations

Figure 10 orders elements left to right from the most to least abundant in the continental crust, relative to a BSE model. In doing so, we highlight the enrichments of Cs, Rb, Ba, Pb, U, Th, K, W, and La in the continental

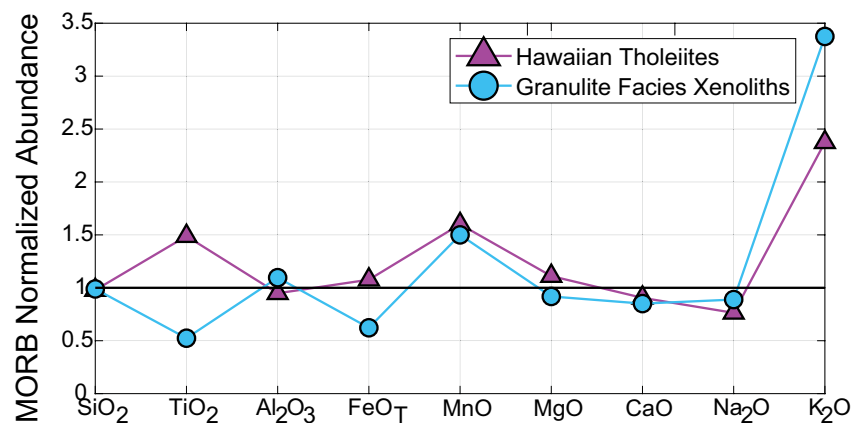


**Figure 8.** Granulite facies xenoliths and Hawaiian tholeiites (MacDonald & Katsura, 1964) (typical ocean island basalt) have similar major element compositions that resemble mid ocean ridge basalts (Gale et al., 2013).

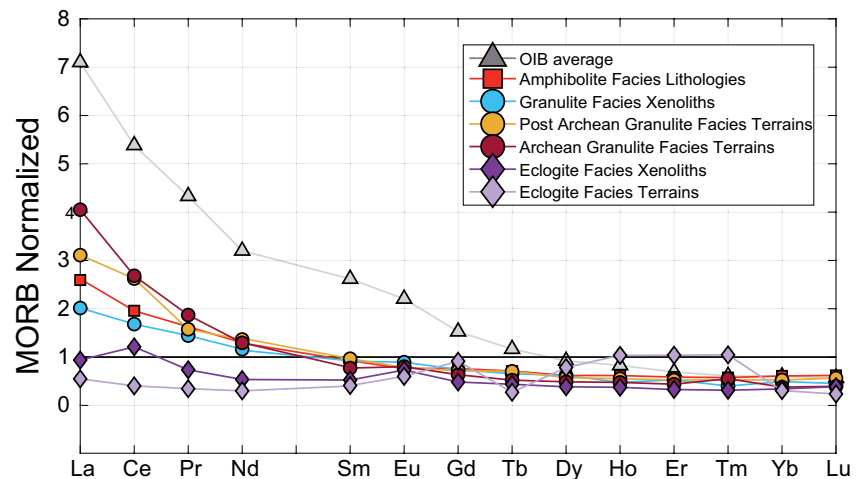


**Figure 9.** Rare earth element concentrations for granulite and amphibolite facies lithologies fall between mid ocean ridge basalt (MORB) (Gale et al., 2013) and ocean island basalt (OIB) (Arevalo & McDonough, 2010) abundances. The shape of their rare earth elements patterns, however, resemble OIB more so than MORB. Amphibolite, granulite, eclogite, and OIB rare earth element patterns converge toward the heavy rare earths. Note, scale is linear.

crust and identify the crust as an important host for these elements in the BSE, despite its insignificant mass contribution (0.55% of the BSE mass). Assuming a BSE composition (McDonough & Sun, 1995; Palme & O'Neill, 2014), the estimated crustal contribution represents 15%–50% of Earth's total budget of these elements sequestered in the continental crust. Importantly, ~35% of the HPEs are stored in the crust and not available for driving mantle convection.

The continental crust is often viewed as the complementary reservoir of the Depleted Mantle, particularly for the incompatible elements. In Figure 10 we compare the composition of the continental crust with that of the average MORB, a representation for the upper portion of the oceanic crust. A crude comparison of the composition of the Depleted Mantle (DM) can be taken as  $\sim \frac{1}{10}$  the value of MORB. If the upper mantle (mantle above the 670 km seismic discontinuity; 26% of the mass of the BSE), often considered the Depleted Mantle, was uniformly depleted to create the continents, then it cannot be the complement to the continental crust. Elements whose crustal mass contribution exceeds 26% (i.e., Cs, Rb, Ba, Pb, U, Th, K, and W) documents that the lower mantle is required to produce the composition of the continental crust. Therefore, the part of the BSE referred to as the Depleted Mantle extends considerably into the lower mantle (nearly half a mantle mass is necessary to account for all of the Ba, Rb & Cs in the continental crust). The implications of this finding demand that all or most of the mantle has been involved, to some extent, in the production of the continents.

Apparent non-complementary relationships are found for K, Sr, and Li. The average MORB (Gale et al., 2013) pattern (Figure 10) shows marked depletion in the primitive mantle normalized abundance for K, Sr, and Li relative to adjacent elements. The relative incompatibility of these elements during mantle melting are  $K \sim U$ ,  $Sr \sim Pr-Nd$ , and  $Li \sim Dy$  (Sun & McDonough, 1989). The K/U values of continental crust and MORB are complementary relative to that of the BSE (Arevalo et al., 2009; Farcy et al., 2020), consistent with these patterns (Figure 10). The marked depletion in Sr seen in the MORB pattern is due to these basalts having experienced considerable plagioclase fractionation. However, as Tang et al. (2017) noted, primitive MORBs with  $\geq 10\text{wt.}\%$  MgO, those yet to experience plagioclase fractionation, do not show any depletion in Sr. Finally, the depletion in Li is somewhat more challenging to explain. Lithium's position (established by crustal abundances) suggests its relative incompatibility is enhanced due, most likely, to a combination of melting and weathering processes. That said, however, the continental crust, which hosts only ~6% of the BSE's Li budget, cannot account for the marked depletion seen in the MORB pattern. (Moving the MORB Li data point over to the heavy REE still does not account for its depletion.) We offer no explanation for this enigmatic observation.

The composition of the lowest continental crust cannot be determined through geochemical analyses alone. The wide range of granulite  $\text{SiO}_2$  compositions is the major confounding factor. If mafic granulites represent the lowest portion of the crust, basaltic injection or underplating from the mantle could serve as a major contributor

**Table 3**  
*Recommended Continental Crust Composition*

	Upper crust	Middle crust	Lower crust	Deep crust	Bulk crust
SiO <sub>2</sub>	68.0	62.2	53.3	57.6	61.1
TiO <sub>2</sub>	0.66	0.80	0.98	0.89	0.81
Al <sub>2</sub> O <sub>3</sub>	15.1	16.1	17.2	16.66	16.1
FeO <sub>T</sub>	5.21	5.73	7.12	6.44	6.02
MnO	0.10	0.15	0.16	0.15	0.14
MgO	2.29	4.03	7.63	5.87	4.66
CaO	2.75	6.20	10.15	8.21	6.36
Na <sub>2</sub> O	2.63	3.23	2.63	2.93	2.82
K <sub>2</sub> O	3.11	1.44	0.70	1.06	1.75
P <sub>2</sub> O <sub>5</sub>	0.17	0.15	0.16	0.16	0.16
Li	26.8	15.0	6.89	10.9	16.0
Be	2.18	1.44	0.48	0.96	1.35
B	10.6	9.00	-	-	-
N	51.1	-	-	-	-
F	343	399	-	-	-
S	382	22.0	140	81	178
Cl	181	29.3	151	90.5	120
Sc	13.3	21.0	28.0	24.5	20.9
V	88.1	134	186	160	137
Cr	77.2	81.0	168	125	109
Co	15.2	29.9	46.8	38.4	30.9
Ni	39.2	39.7	100	70.1	60.1
Cu	26.3	30.0	37.8	33.9	31.5
Zn	69.3	78.0	81.1	79.6	76.2
Ga	17.8	18.0	17.3	17.6	17.7
Ge	1.53	-	-	-	-
As	2.92	1.30	-	-	-
Se	0.06	0.05	-	-	-
Br	0.98	-	-	-	-
Rb	92.8	43.8	10.6	27.1	48.3
Sr <sup>a</sup>	320	201	465	334	329
Y	25.7	22.5	19.0	20.7	22.3
Zr	203	123	83.3	103	135
Nb	12.1	7.20	7.00	7.10	8.73
Mo <sup>a</sup>	1.12	0.52	1.90	1.21	1.18
Ru	0.24	-	-	-	-
Rh	-	-	-	-	-
Pd	0.00080	0.00085	0.0055	0.0032	0.0021
Ag <sup>a</sup>	0.033	0.048	-	-	-
Cd	0.097	0.060	-	-	-
In	0.058	0.071	-	-	-
Sn	2.23	1.60	1.58	1.59	1.80

**Table 3**  
*Continued*

	Upper crust	Middle crust	Lower crust	Deep crust	Bulk crust
Sb	0.39	0.20	-	-	-
Te	-	0.050	-	-	-
I	0.86	-	-	-	-
Cs	4.18	1.19	0.390	0.787	1.88
Ba	665	330	393	362	460
La	33.3	18.1	11.6	14.8	20.8
Ce	67.0	36.5	27.0	31.7	43.1
Pr	7.65	4.68	3.48	4.08	5.23
Nd	29.4	18.3	14.7	16.5	20.7
Sm	5.38	4.10	3.57	3.83	4.33
Eu	1.15	1.09	1.29	1.19	1.18
Gd	4.79	3.91	3.77	3.84	4.15
Tb	0.78	0.66	0.57	0.62	0.67
Dy	4.55	3.91	3.60	3.75	4.01
Ho	0.95	0.82	0.64	0.73	0.80
Er	2.67	2.29	1.89	2.09	2.28
Tm	0.38	0.35	0.25	0.30	0.33
Yb	2.44	2.19	1.70	1.94	2.10
Lu	0.37	0.33	0.25	0.287	0.32
Hf	5.73	3.42	2.05	2.73	3.70
Ta	0.90	0.54	0.60	0.57	0.68
W <sup>a,b</sup>	1.59	0.44	0.31	0.37	0.77
Re <sup>a</sup>	0.00022	-	-	-	-
Os <sup>a</sup>	0.000042	-	0.000021	-	-
Ir <sup>a</sup>	0.000027	0.000015	0.000029	0.000022	0.000016
Pt <sup>a</sup>	0.00062	0.00065	0.00025	0.00016	0.00013
Au	0.00094	0.00080	-	-	-
Hg	0.034	0.030	-	-	-
Tl	0.81	0.50	-	-	-
Pb	16.5	11.7	4.50	8.08	10.8
Bi	0.19	0.070	-	-	-
Th	10.6	3.68	0.77	2.21	4.90
U	2.64	1.00	0.25	0.62	1.27
Eu/Eu <sup>c</sup>	0.69	0.83	1.07	0.95	0.848
Heat prod. (nW/kg)	0.62	0.24	0.064	0.15	0.303
Heat prod. ( $\mu$ W/m <sup>3</sup> )	1.81	0.68	0.19	0.43	0.878
Nb/Ta	13.4	13.3	11.7	12.5	12.9
Zr/Hf	35.5	36.0	40.6	37.7	36.6
Th/U	4.00	3.68	3.09	3.56	3.85
K/U	10,500	12,800	25,100	15,200	12,300
La/Yb	13.7	8.27	6.82	7.63	9.89

**Table 3**  
Continued

	Upper crust	Middle crust	Lower crust	Deep crust	Bulk crust
Rb/Cs	22.2	36.8	27.2	34.4	25.7
K/Rb	278	272	547	325	301
La/Ta	36.9	33.5	19.4	26.1	0.71

Note. Oxides reported in wt.%. All other abundances reported in ppm.

<sup>a</sup>Denotes Upper crustal values from sources other than Gaschnig et al. (2016). Please see text for sources of <sup>a</sup> abundances. <sup>b</sup>W values from Archean granulite facies terrains ( $n = 3$ ) excluded as outliers. <sup>c</sup>Denotes elements for which  $N < 6$  for middle and/or lower crust.

to crust formation. However, basaltic underplating does not solve the compositional paradox of the crust: that the crust is, on average, andesitic in composition while primary mantle melts are mafic. Alternatively, if the lower crust is restitic, it is the remnant of intra-crustal melting, which produced more felsic/andesitic melts that ascended upwards (see Daly Gap discussion for mechanisms). Intra-crustal differentiation could occur because of changes from crustal thickening, either by compression or by adding intracrustal basaltic layer on top of each other. Density sorting and lower crustal foundering/delamination can remove denser mafic material from the bottom of the crust, recycling it back into the mantle and increasing the overall crustal  $\text{SiO}_2$  to andesitic. Of course, whether the continental crust has significant portions of andesitic material or is simply a mixture of basalts (gabbros) and rhyolites (granites) is one of the prevailing Daly Gap mysteries.

If instead the lowermost portion of the crust is more intermediate in composition, it points to the relamination of upper crustal material due to density differences between subducting sediment and the mantle. Still, these metasediments could devolatilize and melt within the lower crust, once again causing the base of the continental crust to be a more mafic restite. Assuming the more felsic metasediments remain un-differentiated, though, leads to considerable questions in crustal dynamics: how much upper crustal material is being recycled into the lower crust at subduction zones?; how fast does this material accumulate?; how dispersed or localized is the more felsic material?; and how old (or young) is the lower crust? Ultimately, the task of determining the proportion of felsic sedimentary material in the deep crust requires geophysical input.

The composition of the deep crust has been tested with seismic velocity data before (Christensen & Moon, 1995; Rudnick & Fountain, 1995; Sammon et al., 2021). Seismic velocities and densities are controlled by mineral forming, major elements (e.g.,  $\text{SiO}_2$  and CaO), not the trace, highly incompatible ones. However, these latter elements correlate to a sample's degree of differentiation (i.e.,  $\text{SiO}_2$  content); therefore, incompatible element abundances can still be derived from major element concentrations. Table 4 compares the continent's expected velocities and densities, computed by *Perple\_X* via Gibbs free energy minimization, for the middle (MC) and lower (LC) crust based on different geophysical and geochemical models. Our MC model has  $V_p = 6.8$  km/s,  $V_{\text{S}} = 4.0$  km/s, and density of  $2,980$  kg/m<sup>3</sup>, values higher than other models. A middle crust calculated from Rudnick and Gao (2014)'s average composition also has a high density (Brocher, 2005) when compared to the  $V_p$  and surface wave predictions of CRUST 1.0 (Laske et al., 2013) and LITHO 1.0 (Pasyanos et al., 2014). These inconsistencies between geochemical and geophysical predictions extend into the deep crust, again with all but the lowest density and  $V_p$  geochemical estimates (Hacker et al., 2015) exceeding seismic expectations. Though these global averaged seismic models are not infallible, a reconciliation is still required between geochemically based and geophysically based models for Earth's deep crust. We explore further these ideas in our accompanying paper (Sammon et al., 2021).

## 9. Conclusion

The deep continental crust will remain a topic of intense debate for years to come due to its inaccessibility. Amphibolite, granulite, and eclogite facies metamorphic terrains and xenoliths serve as windows to middle and lower continental crust. Compositional variability even within these facies underscores the potential for deep crustal heterogeneity, though certain elements and patterns anchor our understanding of the chemistry of the crust. The Daly Gap, evident in amphibolite facies lithologies and granulite facies terrains, dominates the relative abundance of  $\text{SiO}_2$  in the deep crust, especially its lowermost portions. The more homogeneous mineralogy of eclogite

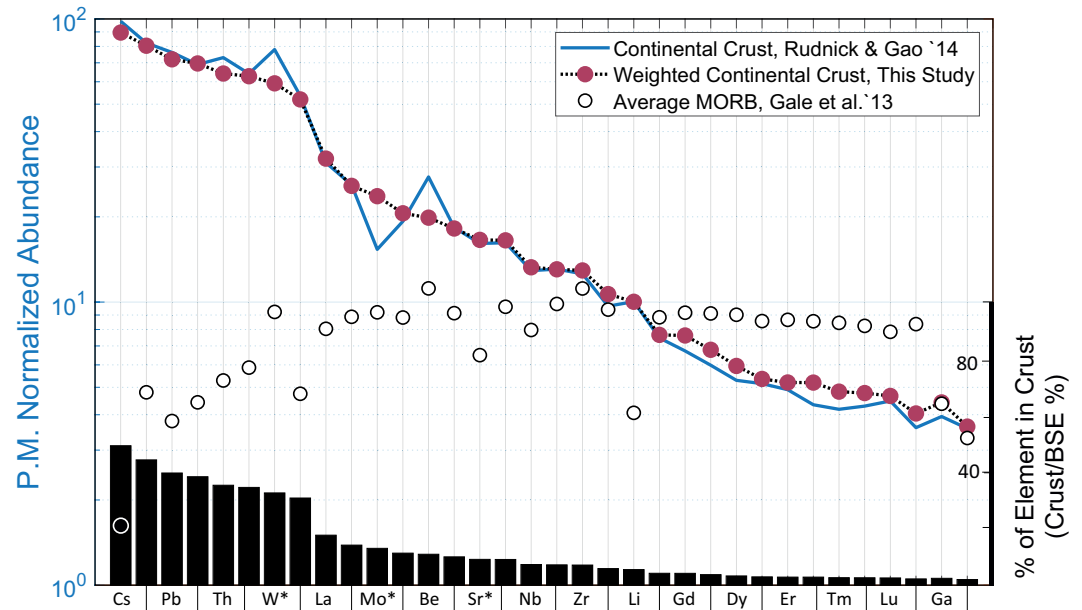


**Figure 10.** Weighted proportions of amphibolite and granulite facies lithologies were combined with upper crustal composition (see text) to generate a model for the bulk Continental crust. Element abundances are normalized to the primitive mantle composition (PM, aka bulk silicate Earth (BSE)) (McDonough & Sun, 1995) (with W from Arevalo & McDonough, 2008). Elements are ordered from left to right by their relative enrichment in the continental crust. This ordering approximately reflects an element's incompatibility (greatest to least, left to right) during mantle melting. Colored circles show our bulk continental crust model while empty circles plots average mid ocean ridge basalt (Gale et al., 2013). Black bars follow the right-hand y-axis scale and show the % of each element sequestered in the continental crust relative to that in the BSE.

**Table 4**  
Comparison of Deep Crustal Physical Properties

Model # of samples	Vp (km/s)	Vs(km/s)	Vp/Vs	Poiss.	Density (kg/m <sup>3</sup> )
Our MC <sup>a</sup>	6.84	4.04	1.69	0.233	2,980
RG MC <sup>a</sup>	6.74	3.97	1.70	0.235	2,940
Low Vp MC <sup>b</sup>	6.57	3.80	1.73	0.235	2,720
CRUST 1.0 MC	6.47	3.70	1.75	0.257	2,830
LITHO 1.0 MC	6.51	3.75	1.74	0.252	2,840
Our LC <sup>**</sup>	7.05	4.13	1.71	0.239	3,090
RG LC <sup>**</sup>	7.00	4.01	1.74	0.255	3,050
Low Vp LC <sup>b</sup>	6.80	3.92	1.74	0.235	2,920
CRUST 1.0 LC	7.04	4.01	1.76	0.261	3,010
LITHO 1.0 LC	7.05	4.00	1.76	0.263	2,990
MORB (LC) <sup>**</sup>	7.40	4.23	1.75	0.258	3,260
OIB (LC) <sup>**</sup>	7.46	4.28	1.74	0.255	3,330

Note. "RG" = Rudnick and Gao (2014).

<sup>a</sup>LC Conditions—500 C, 0.85 GPa. <sup>b</sup>Table 4 Middle Crust Vp 6.5–6.6; Lower Crust 6.7–6.9 (Hacker et al., 2015) MC Conditions—300 C, 0.4 GPa.

facies lithologies distinguishes them from amphibolite or granulite facies lithologies, though all three could plausibly contribute to previous deep crustal compositional estimates. Constraining the proportion of mafic to felsic material in the deep crust will in turn constrain its trace element content and distribution, because its enrichment or depletion in these elements is most heavily influenced by differentiation processes.

Thankfully, all is not lost when using these samples to parse out the composition of the deep crust. The amount of Al<sub>2</sub>O<sub>3</sub> is similar among all of the samples, as are the HREE. We find that the concentrations of Er, Tm, Yb, and Lu in particular show little variation among samples of different metamorphic grades. The controlling factor in incompatible element abundance among our deep crustal lithologies is how differentiated the material is, not metamorphic grade. This means that igneous processes and protolith composition rather than metamorphic processes dictate the chemical signatures of the deep crust.

Although the deep continental crust has been studied at length, many elements still lack sufficient concentration data (such as the highly siderophile elements). Future studies will be challenged to reduce the size of the uncertainty on element concentrations, and since instrumental precision is not the main source of uncertainty, inquiry into the processes that alter elemental abundances in different samples will have to be identified and explained. As it stands, there is also a density discrepancy between highly cited geochemical models (e.g., Rudnick and Gao (2014) vs. Hacker et al. (2015)) and

common geophysical crust models, with geochemical samples suggesting a deep crust that has higher overall density than what is seismically observed. Ultimately, the future of deep crustal modeling will depend on the integration of multiple types of datasets, such as geochemical and seismological measurements and gravity analyses.

## Data Availability Statement

Geochemical data were provided by [Earthchem.org](http://www.EarthChem.org/) (<http://www.EarthChem.org/>) and can be found in the supplemental information or at <https://doi.org/10.5281/zenodo.5113835>.

## Acknowledgments

L. G. Sammon would like to acknowledge Caerwyn Hartten for her assistance in curating the metamorphic datasets. L. G. Sammon and W. F. McDonough gratefully acknowledge the NSF for support (grants EAR1650365 and EAR2050374). We would also like to thank Derrick Hasterok, Tatsuki Tsujomori, and anonymous other reviewers for the insight, suggestions, and encouragement on this study.

## References

- Abbott, R., & Greenwood, J. (2001). Retrograde metamorphism of eclogite in the southern appalachian mountains, USA—a case involving seamount subduction? *Journal of Metamorphic Geology*, *19*(4), 433–443. <https://doi.org/10.1046/j.0263-4929.2001.00321.x>
- Alessio, K. L., Hand, M., Kelsey, D. E., Williams, M. A., Morrissey, L. J., & Barovich, K. (2018). Conservation of deep crustal heat production. *Geology*, *46*(4), 335–338. <https://doi.org/10.1130/g39970.1>
- Arevalo, R., & McDonough, W. F. (2008). Tungsten geochemistry and implications for understanding the earth's interior. *Earth and Planetary Science Letters*, *272*(3–4), 656–665. <https://doi.org/10.1016/j.epsl.2008.05.031>
- Arevalo, R., & McDonough, W. F. (2010). Chemical variations and regional diversity observed in MORB. *Chemical Geology*, *271*(1), 70–85. <https://doi.org/10.1016/j.chemgeo.2009.12.013>
- Arevalo, R., McDonough, W. F., & Luong, M. (2009). The K/U ratio of the silicate earth: Insights into mantle composition, structure and thermal evolution. *Earth and Planetary Science Letters*, *278*(3–4), 361–369. <https://doi.org/10.1016/j.epsl.2008.12.023>
- Ashwal, L. D., Tucker, R. D., & Zinner, E. K. (1999). Slow cooling of deep crustal granulites and pb-loss in zircon. *Geochimica et Cosmochimica Acta*, *63*(18), 2839–2851. [https://doi.org/10.1016/s0016-7037\(99\)00166-0](https://doi.org/10.1016/s0016-7037(99)00166-0)
- Bohlen, S. R., & Mezger, K. (1989). Origin of granulite terranes and the formation of the lowermost continental crust. *Science*, *244*(4902), 326–329. <https://doi.org/10.1126/science.244.4902.326>
- Brocher, T. M. (2005). Empirical relations between elastic wavespeeds and density in the Earth's crust. *Bulletin of the Seismological Society of America*, *95*(6), 2081–2092. <https://doi.org/10.1785/0120050077>
- Brown, M., & Johnson, T. (2019). Time's arrow, time's cycle: Granulite metamorphism and geodynamics. *Mineralogical Magazine*, *83*(3), 323–338. <https://doi.org/10.1180/mgm.2019.19>
- Bürgmann, R., & Dresen, G. (2008). Rheology of the lower crust and upper mantle: Evidence from rock mechanics, geodesy, and field observations. *Annual Review of Earth and Planetary Sciences*, *36*, 531–567. <https://doi.org/10.1146/annurev.earth.36.031207.124326>
- Carswell, D., & Cuthbert, S. (1986). Eclogite facies metamorphism in the lower continental crust. *Geological Society, London, Special Publications*, *24*(1), 193–209. <https://doi.org/10.1144/gsl.sp.1986.024.01.18>
- Chappell, B. W., Bryant, C. J., & Wyborn, D. (2012). Peraluminous i-type granites. *Lithos*, *153*, 142–153. <https://doi.org/10.1016/j.lithos.2012.07.008>
- Charlier, B., Namur, O., Toplis, M. J., Schiano, P., Cluzel, N., Higgins, M. D., & Auwera, J. V. (2011). Large-scale silicate liquid immiscibility during differentiation of tholeiitic basalt to granite and the origin of the daly gap. *Geology*, *39*(10), 907–910. <https://doi.org/10.1130/g32091.1>
- Chen, K., Rudnick, R. L., Wang, Z., Tang, M., Gaschnig, R. M., Zou, Z., & Liu, Y. (2020). How mafic was the archaic upper continental crust? Insights from cu and ag in ancient glacial diamictites. *Geochimica et Cosmochimica Acta*, *278*, 16–29. <https://doi.org/10.1016/j.gca.2019.08.002>
- Chen, K., Walker, R. J., Rudnick, R. L., Gao, S., Gaschnig, R. M., Puchtel, I. S., & Hu, Z.-C. (2016). Platinum-group element abundances and re-os isotopic systematics of the upper continental crust through time: Evidence from glacial diamictites. *Geochimica et Cosmochimica Acta*, *191*, 1–16. <https://doi.org/10.1016/j.gca.2016.07.004>
- Christensen, N. I., & Mooney, W. D. (1995). Seismic velocity structure and composition of the continental crust: A global view. *Journal of Geophysical Research: Solid Earth*, *100*(B6), 9761–9788. <https://doi.org/10.1029/95JB00259>
- Daly, R. (1914). Igneous rocks and their origin. *Preliminary Note on Alkaline Rhyolites from Tokati, Hokkaido*, *319*, 20.
- De Argollo, R., & Schilling, J.-G. (1978). Ge/si and ga/al fractionation in hawaiian volcanic rocks. *Geochimica et Cosmochimica Acta*, *42*(6), 623–630. [https://doi.org/10.1016/0016-7037\(78\)90007-8](https://doi.org/10.1016/0016-7037(78)90007-8)
- De La Roche, d. H., Leterrier, J. t., Grandclaude, P., & Marchal, M. (1980). A classification of volcanic and plutonic rocks using r1r2-diagram and major-element analyses—Its relationships with current nomenclature. *Chemical Geology*, *29*(1–4), 183–210. [https://doi.org/10.1016/0009-2541\(80\)90020-0](https://doi.org/10.1016/0009-2541(80)90020-0)
- Dokukina, K., & Mints, M. (2019). Subduction of the mesoarchaic spreading ridge and related metamorphism, magmatism and deformation by the example of the gridino eclogitized mafic dyke swarm, the belomorian eclogite province, eastern fennoscandian shield. *Journal of Geodynamics*, *123*, 1–37. <https://doi.org/10.1016/j.jog.2018.11.003>
- Dufek, J., & Bachmann, O. (2010). Quantum magmatism: Magmatic compositional gaps generated by melt-crystal dynamics. *Geology*, *38*(8), 687–690. <https://doi.org/10.1130/g30831.1>
- Dziewonski, A. M., & Anderson, D. L. (1981). Preliminary reference earth model. *Physics of the Earth and Planetary Interiors*, *25*(4), 297–356. [https://doi.org/10.1016/0031-9201\(81\)90046-7](https://doi.org/10.1016/0031-9201(81)90046-7)
- Farcy, B., Arevalo, R., & McDonough, W. F. (2020). K/U of the morb source and silicate earth. *Journal of Geophysical Research: Solid Earth*, *125*(12), e2020JB020245. <https://doi.org/10.1029/2020jb020245>
- Field, D., & Clough, P. W. L. (1976). K/Rb ratios and metasomatism in metabasites from a precambrian amphibolite–granulite transition zone. *Journal of the Geological Society*, *132*(3), 277–288. <https://doi.org/10.1144/gsjgs.132.3.0277>
- Field, D., & Elliott, R. B. (1974). The chemistry of gabbro/amphibolite transitions in south norway. *Contributions to Mineralogy and Petrology*, *47*(1), 63–76. <https://doi.org/10.1007/bf00418557>
- Fowler, M. B. (1986). Large-ion lithophile element characteristics of an amphibolite facies to granulite facies transition at gruinard bay, north-west scotland. *Journal of Metamorphic Geology*, *4*(3), 345–359. <https://doi.org/10.1111/j.1525-1314.1986.tb00355.x>
- Gale, A., Laubier, M., Escrig, S., & Langmuir, C. H. (2013). Constraints on melting processes and plume-ridge interaction from comprehensive study of the famous and north famous segments, mid-atlantic ridge. *Earth and Planetary Science Letters*, *365*, 209–220. <https://doi.org/10.1016/j.epsl.2013.01.022>

- Gao, S., Zhang, B.-R., Jin, Z.-M., Kern, H., Luo, T.-C., & Zhao, Z.-D. (1998). How mafic is the lower continental crust? *Earth and Planetary Science Letters*, *161*(1–4), 101–117. [https://doi.org/10.1016/S0012-821X\(98\)00140-X](https://doi.org/10.1016/S0012-821X(98)00140-X)
- Gard, M., Hasterok, D., Hand, M., & Cox, G. (2019). Variations in continental heat production from 4 ga to the present: Evidence from geochemical data. *Lithos*, *342*, 391–406. <https://doi.org/10.1016/j.lithos.2019.05.034>
- Gaschnig, R. M., Rudnick, R. L., McDonough, W. F., Kaufman, A. J., Valley, J. W., Hu, Z., & Beck, M. L. (2016). Compositional evolution of the upper continental crust through time, as constrained by ancient glacial diamictites. *Geochimica et Cosmochimica Acta*, *186*, 316–343. <https://doi.org/10.1016/j.gca.2016.03.020>
- Gerya, T. V., Perchuk, L. L., & Burg, J.-P. (2008). Transient hot channels: Perpetrating and regurgitating ultrahigh-pressure, high-temperature crust–mantle associations in collision belts. *Lithos*, *103*(1–2), 236–256. <https://doi.org/10.1016/j.lithos.2007.09.017>
- Gerya, T. V., Perchuk, L. L., Maresch, W. V., Willner, A. P., Reenen, D. D. V., & Smit, C. A. (2002). Thermal regime and gravitational instability of multi-layered continental crust: Implications for the buoyant exhumation of high-grade metamorphic rocks. *European Journal of Mineralogy*, *14*(4), 687–699. <https://doi.org/10.1127/0935-1221/2002/0014-0687>
- Hacker, B. R., Andersen, T. B., Johnston, S., Kylander-Clark, A. R., Peterman, E. M., Walsh, E. O., & Young, D. (2010). High-temperature deformation during continental-margin subduction & exhumation: The ultrahigh-pressure western gneiss region of Norway. *Tectonophysics*, *480*(1–4), 149–171. <https://doi.org/10.1016/j.tecto.2009.08.012>
- Hacker, B. R., Kelemen, P. B., & Behn, M. D. (2015). Continental lower crust. *Annual Review of Earth and Planetary Sciences*, *43*(1), 167–205. <https://doi.org/10.1146/annurev-earth-050212-124117>
- Halliday, A. N., Dickin, A. P., Hunter, R. N., Davies, G. R., Dempster, T. J., Hamilton, P. J., & Upton, B. G. J. (1993). Formation and composition of the lower continental crust: Evidence from Scottish xenolith suites. *Journal of Geophysical Research*, *98*(B1), 581–607. <https://doi.org/10.1029/92JB02276>
- Hasterok, D., Gard, M., Bishop, C. M. B., & Kelsey, D. (2019). Chemical identification of metamorphic protoliths using machine learning methods. *Computers & Geosciences*, *132*, 56–68. <https://doi.org/10.1016/j.cageo.2019.07.004>
- Hasterok, D., Gard, M., Cox, G., & Hand, M. (2019). A 4 ga record of granitic heat production: Implications for geodynamic evolution and crustal composition of the early earth. *Precambrian Research*, *331*, 105375. <https://doi.org/10.1016/j.precamres.2019.105375>
- Hawkesworth, C. J., & Kemp, A. (2006). Evolution of the continental crust. *Nature*, *443*(7113), 811–817. <https://doi.org/10.1038/nature05191>
- Helmstaedt, H., & Schulze, D. (1988). Eclogite-facies ultramafic xenoliths from Colorado plateau diatreme breccias: Comparison with eclogites in crustal environments, evaluation of the subduction hypothesis, and implications for eclogite xenoliths from diamondiferous kimberlites. In *Eclogites and eclogite-facies rocks* (pp. 387–450).
- Holbrook, W. S., Mooney, W. D., & Christensen, N. I. (1992). The seismic velocity structure of the deep continental crust. *Continental lower crust*, *23*, 1–43.
- Huang, Y., Chubakov, V., Mantovani, F., Rudnick, R. L., & McDonough, W. F. (2013). A reference Earth model for the heat-producing elements and associated geoneutrino flux. *Geochemistry, Geophysics, Geosystems*, *14*(6), 2003–2029. <https://doi.org/10.1002/ggge.20129>
- Jackson, M. D., Blundy, J., & Sparks, R. S. J. (2018). Chemical differentiation, cold storage and remobilization of magma in the earth's crust. *Nature*, *564*(7736), 405–409. <https://doi.org/10.1038/s41586-018-0746-2>
- Jacob, D. (2004). Nature and origin of eclogite xenoliths from kimberlites. *Lithos*, *77*(1–4), 295–316. <https://doi.org/10.1016/j.lithos.2004.03.038>
- Jakeš, P., & White, A. (1971). Composition of island arcs and continental growth. *Earth and Planetary Science Letters*, *12*(2), 224–230.
- Jaupart, C., & Mareschal, J. C. (2003). Constraints on heat production from heat flow data, treatise on geochemistry. In R. Rudnick (Ed.), *The crust*. (Vol. 3). Elsevier Science.
- Kelemen, P. B., & Behn, M. D. (2016). Formation of lower continental crust by relamination of buoyant arc lavas and plutons. *Nature Geoscience*, *9*(3), 197–205. <https://doi.org/10.1038/ngeo2662>
- Keller, C. B., Schoene, B., Barboni, M., Samperton, K. M., & Husson, J. M. (2015). Volcanic–plutonic parity and the differentiation of the continental crust. *Nature*, *523*(7560), 301–307. <https://doi.org/10.1038/nature14584>
- Krogh, E., Oh, C., & Liou, J. (1994). Polyphase and anticlockwise p–t evolution for Franciscan eclogites and blueschists from Jenner, California, USA. *Journal of Metamorphic Geology*, *12*(2), 121–134. <https://doi.org/10.1111/j.1525-1314.1994.tb00008.x>
- Kuno, H. (1966). Lateral variation of basalt magma type across continental margins and island arcs. *Bulletin Volcanologique*, *29*(1), 195–222. <https://doi.org/10.1007/bf02597153>
- Kusznir, N. J., & Park, R. G. (1987). The extensional strength of the continental lithosphere: Its dependence on geothermal gradient, and crustal composition and thickness. *Geological Society, London, Special Publications*, *28*(1), 35–52. <https://doi.org/10.1144/gsl.sp.1987.028.01.04>
- Laske, G., Masters, G., Ma, Z., & Pasyanos, M. (2013). Update on crust1.0 — a 1-degree global model of earth's crust. *Geophysical Research Abstracts*, *15*, 2658.
- Leech, M. L. (2001). Arrested orogenic development: Eclogitization, delamination, and tectonic collapse. *Earth and Planetary Science Letters*, *185*(1), 149–159. [https://doi.org/10.1016/S0012-821X\(00\)00374-5](https://doi.org/10.1016/S0012-821X(00)00374-5)
- Lombardo, B., & Rolfo, F. (2000). Two contrasting eclogite types in the Himalayas: Implications for the Himalayan orogeny. *Journal of Geodynamics*, *30*(1), 37–60. [https://doi.org/10.1016/S0264-3707\(99\)00026-5](https://doi.org/10.1016/S0264-3707(99)00026-5)
- MacDonald, G. A., & Katsura, T. (1964). Chemical composition of Hawaiian lavas. *Journal of Petrology*, *5*(1), 82–133. <https://doi.org/10.1093/ptrology/5.1.82>
- Martin, H. (1986). Effect of steeper Archean geothermal gradient on geochemistry of subduction-zone magmas. *Geology*, *14*(9), 753–756. [https://doi.org/10.1130/0091-7613\(1986\)14<753:eosagg>2.0.co;2](https://doi.org/10.1130/0091-7613(1986)14<753:eosagg>2.0.co;2)
- McDonough, W. F. (1990). Constraints on the composition of the continental lithospheric mantle. *Earth and Planetary Science Letters*, *101*(1), 1–18. [https://doi.org/10.1016/0012-821X\(90\)90119-I](https://doi.org/10.1016/0012-821X(90)90119-I)
- McDonough, W. F. (1991). Partial melting of subducted oceanic crust and isolation of its residual eclogitic lithology. *Philosophical Transactions of the Royal Society of London, Series A: Physical and Engineering Sciences*, *335*(1638), 407–418.
- McDonough, W. F., & Sun, S.-s. (1995). The composition of the Earth. *Chemical Geology*, *120*(3), 223–253. [https://doi.org/10.1016/0009-2541\(94\)00140-4](https://doi.org/10.1016/0009-2541(94)00140-4)
- Mooney, W. D., Laske, G., & Masters, T. G. (1998). CRUST 5.1: A global crustal model at 5° x 5°. *Journal of Geophysical Research*, *103*(B1), 727–747. <https://doi.org/10.1029/97JB02122>
- Ohta, T., & Arai, H. (2007). Statistical empirical index of chemical weathering in igneous rocks: A new tool for evaluating the degree of weathering. *Chemical Geology*, *240*(3–4), 280–297. <https://doi.org/10.1016/j.chemgeo.2007.02.017>
- Palme, H., & O'Neill, H. S. C. (2014). Cosmochemical estimates of mantle composition. In H. D. Holland, & K. K. Turekian (Eds.), *Treatise on geochemistry* (2nd ed., Vol. 3, pp. 1–39). Elsevier. <https://doi.org/10.1016/B978-0-08-095975-7.00201-1>
- Pasyanos, M. E., Masters, T. G., Laske, G., & Ma, Z. (2014). LITHO1.0: An updated crust and lithospheric model of the Earth. *Journal of Geophysical Research: Solid Earth*, *119*(3), 2153–2173. <https://doi.org/10.1002/2013JB010626>

- Price, J. R., & Velbel, M. A. (2003). Chemical weathering indices applied to weathering profiles developed on heterogeneous felsic metamorphic parent rocks. *Chemical Geology*, 202(3–4), 397–416. <https://doi.org/10.1016/j.chemgeo.2002.11.001>
- Reubi, O., & Blundy, J. (2009). A dearth of intermediate melts at subduction zone volcanoes and the petrogenesis of arc andesites. *Nature*, 461(7268), 1269–1273. <https://doi.org/10.1038/nature08510>
- Rockow, K. M., Haskin, L. A., Jollif, B., & Fountain, D. M. (1997). Constraints on element mobility associated with the conversion of granulite to eclogite along fractures in an anorthositic complex on holsnøy, norway. *Journal of Metamorphic Geology*, 15(3), 401–418. <https://doi.org/10.1111/j.1525-1314.1997.00028.x>
- Rogers, N., & Hawkesworth, C. J. (1982). Proterozoic age and cumulate origin for granulite xenoliths, lesotho. *Nature*, 299(5882), 409–413. <https://doi.org/10.1038/299409a0>
- Rudnick, R. L. (1995). Making continental crust. *Nature*, 378(6557), 571–578. <https://doi.org/10.1038/378571a0>
- Rudnick, R. L., Barth, M., Horn, I., & McDonough, W. F. (2000). Rutile-bearing refractory eclogites: Missing link between continents and depleted mantle. *Science*, 287(5451), 278–281. <https://doi.org/10.1126/science.287.5451.278>
- Rudnick, R. L., & Fountain, D. M. (1995). Nature and composition of the continental crust: A lower crustal perspective. *Reviews of Geophysics*, 33(3), 267–309. <https://doi.org/10.1029/95RG01302>
- Rudnick, R. L., & Gao, S. (2014). Composition of the Continental Crust. In *Treatise on geochemistry* (pp. 1–51). Elsevier. <https://doi.org/10.1016/B978-0-08-095975-7.00301-6>
- Rudnick, R. L., McLennan, S. M., & Taylor, S. R. (1985). Large ion lithophile elements in rocks from high-pressure granulite facies terrains. *Geochimica et Cosmochimica Acta*, 49(7), 1645–1655. [https://doi.org/10.1016/0016-7037\(85\)90268-6](https://doi.org/10.1016/0016-7037(85)90268-6)
- Rudnick, R. L., & Presper, T. (1990). Geochemistry of intermediate-/to high-pressure granulites. In *Granulites and crustal evolution* (pp. 523–550). Springer. [https://doi.org/10.1007/978-94-009-2055-2\\_27](https://doi.org/10.1007/978-94-009-2055-2_27)
- Rudnick, R. L., & Taylor, S. R. (1987). The composition and petrogenesis of the lower crust: A xenolith study. *Journal of Geophysical Research*, 92(B13), 13981–14005. <https://doi.org/10.1029/jb092ib13p13981>
- Russell, J. K., Porritt, L. A., Lavallée, Y., & Dingwell, D. B. (2012). Kimberlite ascent by assimilation-fuelled buoyancy. *Nature*, 481(7381), 352–356. <https://doi.org/10.1038/nature10740>
- Sammon, L. G., McDonough, W. F., & Mooney, W. D. (2021). The composition of the deep continental crust inferred from geochemical and geophysical data. *Earth and Space Science Open Archive*.
- Semprich, J., & Simon, N. S. C. (2014). Inhibited eclogitization and consequences for geophysical rock properties and delamination models: Constraints from cratonic lower crustal xenoliths. *Gondwana Research*, 25(2), 668–684. <https://doi.org/10.1016/j.gr.2012.08.018>
- Shinevar, W. J., Behn, M. D., Hirth, G., & Jagoutz, O. (2018). Inferring crustal viscosity from seismic velocity: Application to the lower crust of Southern California. *Earth and Planetary Science Letters*, 494, 83–91. <https://doi.org/10.1016/j.epsl.2018.04.055>
- Stosch, H.-G., Lugmair, G. W., & Seck, H. A. (1986). Geochemistry of granulite-facies lower crustal xenoliths: Implications for the geological history of the lower continental crust below the eifel, west Germany. *Geological Society, London, Special Publications*, 24(1), 309–317. <https://doi.org/10.1144/gsl.sp.1986.024.01.27>
- Sun, S.-s., & McDonough, W. F. (1989). Chemical and isotopic systematics of oceanic basalts: Implications for mantle composition and processes. *Geological Society, London, Special Publications*, 42(1), 313–345. <https://doi.org/10.1144/GSL.SP.1989.042.01.19>
- Svensen, H., Jamtveit, B., Banks, D. A., & Austrheim, H. (2001). Halogen contents of eclogite facies fluid inclusions and minerals: Caledonides, western Norway. *Journal of Metamorphic Geology*, 19(2), 165–178. <https://doi.org/10.1046/j.0263-4929.2000.00301.x>
- Tang, M., McDonough, W. F., & Ash, R. D. (2017). Europium and strontium anomalies in the morb source mantle. *Geochimica et Cosmochimica Acta*, 197, 132–141. <https://doi.org/10.1016/j.gca.2016.10.025>
- Taylor, S. R., & McLennan, S. M. (1985). *The continental crust: Its composition and evolution*: Blackwell Scientific Pub.
- Tsujimori, T., & Mattinson, C. (2020). *Eclogites in different tectonic settings* (S. Elias, & D. Alderton (Eds.)). Elsevier.
- Tsujimori, T., Sisson, V. B., Liou, J. G., Harlow, G. E., & Sorensen, S. S. (2006). Very-low-temperature record of the subduction process: A review of worldwide lawsonite eclogites. *Lithos*, 92(3–4), 609–624. <https://doi.org/10.1016/j.lithos.2006.03.054>
- Van Calsteren, P., Harris, N., Hawkesworth, C., Menzies, M., & Rogers, N. (1986). Xenoliths from southern Africa: A perspective on the lower crust. *Geological Society, London, Special Publications*, 24(1), 351–362. <https://doi.org/10.1144/gsl.sp.1986.024.01.30>
- Wedepohl, K. H. (1995). The composition of the continental crust. *Geochimica et Cosmochimica Acta*, 59(7), 1217–1232. [https://doi.org/10.1016/0016-7037\(95\)00038-2](https://doi.org/10.1016/0016-7037(95)00038-2)
- Wilkinson, B. H., McElroy, B. J., Kesler, S. E., Peters, S. E., & Rothman, E. D. (2009). Global geologic maps are tectonic speedometers—Rates of rock cycling from area-age frequencies. *The Geological Society of America Bulletin*, 121(5–6), 760–779. <https://doi.org/10.1130/b26457.1>
- Wipperfurth, S. A., Guo, M., Šrámek, O., & McDonough, W. F. (2018). Earth's chondritic Th/U: Negligible fractionation during accretion, core formation, and crust–mantle differentiation. *Earth and Planetary Science Letters*, 498, 196–202. <https://doi.org/10.1016/j.epsl.2018.06.029>
- Wipperfurth, S. A., Šrámek, O., & McDonough, W. F. (2020). Reference models for lithospheric geoneutrino signal. *Journal of Geophysical Research: Solid Earth*, 125(2), e2019JB018433. <https://doi.org/10.1029/2019jb018433>
- Yamasaki, T. (2018). The role of bimodal magmatism in seafloor massive sulfide (sms) ore-forming systems at the middle okinawa trough, Japan. *Ocean Science Journal*, 53(2), 413–436. <https://doi.org/10.1007/s12601-018-0031-1>
- Zen, E.-A. (1988). Phase relations of peraluminous granitic rocks and their petrogenetic implications. *Annual Review of Earth and Planetary Sciences*, 16(1), 21–51. <https://doi.org/10.1146/annurev.ea.16.050188.000321>

## References From the Supporting Information

- Arndt, N. (1994). Archean komatiites. *Archean crustal evolution*, 10, 11–44. [https://doi.org/10.1016/s0166-2635\(08\)70219-6](https://doi.org/10.1016/s0166-2635(08)70219-6)
- Banks, D. A., Green, R., Cliff, R., & Yardley, B. W. D. (2000). Chlorine isotopes in fluid inclusions: Determination of the origins of salinity in magmatic fluids. *Geochimica et Cosmochimica Acta*, 64(10), 1785–1789. [https://doi.org/10.1016/s0016-7037\(99\)00407-x](https://doi.org/10.1016/s0016-7037(99)00407-x)
- Barnes, S.-J. (2016). *Chalcophile elements* (W. M. White (Ed.)). Springer International Publishing.
- Barnhart, K. R., Mahan, K. H., Blackburn, T. J., Bowring, S. A., & Dudas, F. O. (2012). Deep crustal xenoliths from central montana, usa: Implications for the timing and mechanisms of high-velocity lower crust formation. *Geosphere*, 8(6), 1408–1428. <https://doi.org/10.1130/ges00765.1>
- Bellini, G., Ianni, A., Ludhova, L., Mantovani, F., & McDonough, W. F. (2013). Geo-neutrinos. *Progress in Particle and Nuclear Physics*, 73, 1–34. <https://doi.org/10.1016/j.pnpnp.2013.07.001>
- Hartigan, J. A., & Hartigan, P. M. (1985). The dip test of unimodality. *Annals of Statistics*, 13(1), 70–84. <https://doi.org/10.1214/aos/1176346577>

- Jenner, F. E. (2017). Cumulate causes for the low contents of sulfide-loving elements in the continental crust. *Nature Geoscience*, *10*(7), 524–529. <https://doi.org/10.1038/ngeo2965>
- Kusebauch, C., John, T., Barnes, J. D., Klügel, A., & Austrheim, H. O. (2015). Halogen element and stable chlorine isotope fractionation caused by fluid–rock interaction (bamble sector, se Norway). *Journal of Petrology*, *56*(2), 299–324. <https://doi.org/10.1093/petrology/egv001>
- Markl, G., Musashi, M., & Bucher, K. (1997). Chlorine stable isotope composition of granulites from Lofoten, Norway: Implications for the cl isotopic composition and for the source of cl enrichment in the lower crust. *Earth and Planetary Science Letters*, *150*(1–2), 95–102. [https://doi.org/10.1016/s0012-821x\(97\)00084-8](https://doi.org/10.1016/s0012-821x(97)00084-8)
- Polat, A., Hofmann, A., & Rosing, M. T. (2002). Boninite-like volcanic rocks in the 3.7–3.8 ga isua greenstone belt, west greenland: Geochemical evidence for intra-oceanic subduction zone processes in the early earth. *Chemical Geology*, *184*(3–4), 231–254. [https://doi.org/10.1016/s0009-2541\(01\)00363-1](https://doi.org/10.1016/s0009-2541(01)00363-1)
- Sighinolfi, G. P. (1971). Investigations into deep crustal levels: Fractionating effects and geochemical trends related to high-grade metamorphism. *Geochimica et Cosmochimica Acta*, *35*(10), 1005–1021. [https://doi.org/10.1016/0016-7037\(71\)90018-4](https://doi.org/10.1016/0016-7037(71)90018-4)

# Supporting Information for "A Geochemical Review of Amphibolite, Granulite, and Eclogite Facies Lithologies: Perspectives on the Deep Continental Crust"

Laura G. Sammon<sup>1</sup>, William F. McDonough<sup>1,2</sup>

<sup>1</sup>Department of Geology, University of Maryland, College Park, MD 20742, USA

<sup>2</sup>Department of Earth Sciences and Research Center for Neutrino Science, Tohoku University, Sendai 980-8578, Japan

## Contents of this file

1. Multi-modality in Oxides, Further Discussion
2. Eu anomalies
3. Various elemental trends
4. Figures S1 to S2, sample locations
5. Figures S3 to S9, additional major and trace element data

## Additional Supporting Information (Files uploaded separately)

1. Geochemical datasets (totals outside of  $100 \pm 10$  % not included)
2. Pb isotope and  $\kappa_{Pb}$  data
3. Extended tables for minor and trace elements, various element ratios, and  $\kappa_{Pb}$

## 1. Multi-modality in Oxides, Further Discussion

Many major oxides show biasing towards either mafic or felsic compositions. This means that the predictors of the oxide's central value is neither mafic or felsic, but a mixture of two or more modes from the ensemble data. One of many tests for unimodality or multimodality in a distribution is the Hartigan's Dip Test (Hartigan & Hartigan, 1985). We applied this statistical test to our datasets in an attempt to quantify the presence of multimodal trends, namely the Daly Gap. Table ST13 lists the results. Oxides with values closer to 1 are more likely to have a unimodal distribution. A challenge we find is in determining where to put the cutoff for unimodal vs. bimodal (multimodal) distribution. For example,  $\text{SiO}_2$  has Dip Test value that reflects its bimodality. In other datasets, however, such as  $\text{FeO}_T$ , the gap is less clear. Visual assessments of bimodality in the dataset are heavily influenced by the binning of data (e.g. Fig. S3) and lead to ambiguous results. Each dataset was randomly sampled 10,000 times to minimize differences in results solely because one set had more data points than another.

$\text{FeO}_T$  and MnO appear to be bimodal in all of the granulite facies lithologies, including granulite facies xenoliths. Their Dip Test values are likely affected by the discontinuous pattern of  $\text{FeO}_T$  abundances and a few outliers in MnO concentrations. While Post Archean granulite facies terrains do likely show evidence of the Daly Gap in their  $\text{FeO}_T$  distributions, it is once again difficult to say conclusively whether bimodality is actually evident in Archean granulite facies terrains'  $\text{FeO}_T$ . MnO is once again plagued by outliers both in granulite and amphibolite facies lithologies.

K<sub>2</sub>O content is highly variable, spanning at least six orders of magnitude for each dataset. K<sub>2</sub>O distributions in granulite and eclogite facies xenoliths approach log-normal, but granulite facies terrains and amphibolites are skewed towards low K<sub>2</sub>O values. The abundance of K<sub>2</sub>O depends on the crystallization of K-feldspars (Rudnick & Presper, 1990). If K-feldspar is present, K behaves like a major element. If K-feldspar does not crystallize, K behaves like a trace element.

Multimodality in the other oxides is also open to debate. MgO stands out as potentially bimodal in amphibolite facies lithologies but is heavily influenced by the number of data bins. When the number of bins is increased, we see a secondary peak developing towards low MgO concentrations (Figure S3). We run into the same trouble when looking at Na<sub>2</sub>O and CaO; whether or not they appear bimodal depends on the data binning. CaO seems to be the most likely candidate for multi-modality when binned according to Sturge's Law but becomes more unimodal as the number of bins increases. All Dip Test values for eclogite facies lithologies are elevated compared to amphibolite and granulite facies lithologies because of eclogite's fewer numbers and increased variability.

## 2. Eu Anomalies

All amphibolite, granulite, and eclogite facies lithologies have similar median Eu anomalies ( $\frac{Eu}{\sqrt{Sm_N * Gd_N}}$ ). While granulite facies lithologies tend to show more variation in Eu anomalies (Figure S4), the median Eu/Eu\* values for all of our groups fall between 0.89 and 1.2. The distributions of Eu/Eu\*, shown in Figure S4, are skewed towards the right, moreso for granulite facies than for other facies, favoring Eu/Eu\* values around 1 but reaching as high as 2-3. These values of Eu/Eu\* < 1 (which translate to negative median Eu anomalies) are in line with previous estimates for the middle and lower crust

and could indicate voluminous crustal recycling (Tang et al., 2017). The lack of strong, positive Eu anomalies in the deep crust counters the argument that the deep (or lower) crust is complementary to the upper crust, which also has a negative Eu anomaly (Taylor & McLennan, 1985).

### **3. Element Trends**

#### **3.1. Fluid Mobile Elements**

##### **3.1.1. K, Rb, and Cs**

The transition from amphibolite to granulite facies can be considered, for the major elements, an isochemical dehydration reaction, but this is not the case for the most fluid mobile elements: K, Rb, and Cs. Consistent with the observations of (Rudnick & Presper, 1990),  $K_2O/Rb$  ratios in amphibolite and granulite facies lithologies are negatively correlated with  $K_2O$  content, especially at  $K_2O < 1.2$  wt.%, indicating Rb depletion relative to  $K_2O$ . We restrict our analysis of  $K_2O/Rb$  to compositions to rock with  $> 55$  wt.%  $SiO_2$  because the  $K_2O/Rb$  ratios of unmetamorphosed basalts are highly variable, making it difficult to evaluate Rb depletion in mafic lithologies (Rudnick & Presper, 1990).  $K_2O/Rb$  ratios reach a maximum at about 1 in most of the metamorphic datasets. Although we omit them, mafic lithologies follow the same trend, though lower  $K_2O$  values are reached. As suggested by various studies, this trend likely reflects a mineralogical control on the partitioning of Rb and K between minerals and a fluid phase (e.g., Rudnick et al., 1985; Fowler, 1986). Low concentrations of  $K_2O$  and Rb, and high  $K_2O/Rb$  ratios, may reflect igneous processes rather than metamorphic processes (Van Calsteren et al., 1986). However, several mafic granulite facies and amphibolite facies lithologies have high  $K/Rb$  ratios compared to basalts, which suggests that they have experienced some Rb depletion

during metamorphism (Stosch et al., 1986; Rudnick & Taylor, 1987). The similarities between the amphibolite and granulite facies K/Rb are striking, because high  $K_2O/Rb$  was thought to be the providence of dehydration metamorphism. Partial dehydration of amphibolite facies lithologies might lead to high  $K_2O/Rb$  ratios while still leaving behind enough hydrous mineral assemblages to classify the rock as amphibolite. Future studies should explore the quantification of dehydration as it relates to  $K_2O/Rb$  ratios. Alternatively, metamorphosing gabbro to the amphibolite facies can produce uneven increases in K and Rb (Field & Elliott, 1974), leading to lower  $K_2O/Rb$  ratios. Low  $K_2O/Rb$  ratios in amphibolites could also be inherited from the retrograde metamorphism of granulite with low  $K_2O/Rb$  (Field & Clough, 1976).

### **3.1.2. La/Th and Th/U**

Granulite facies lithologies and eclogite facies terrains show greater Th and U depletion than amphibolite facies lithologies or eclogite facies xenoliths. While the granulite and amphibolite facies lithologies show comparable amounts of U loss, indicated by elevated Th/U and low La/Th values, the granulite facies lithologies can reach almost an order of magnitude greater La/Th values with low Th/U, indicating a loss of both U and Th. U can be depleted through loss of water due to its redox sensitivity ( $U^{6+}$  is fluid mobile;  $U^{4+}$  is not), though both U and Th depletions typically indicate a lack of U and Th-bearing accessory phases (Rudnick et al., 1985; Fowler, 1986). Archean granulite facies terrains reach higher levels of U depletion than Post-Archean terrains, a curious observation since many Archean terrains contain monazite, a Th and U-bearing accessory phase (Rudnick & Presper, 1990). Eclogite facies lithologies on the whole have Th/U ratios around 2 and a wider range (0.1 to 20) in La/Th.

### 3.1.3. Alkalis and Alkaline Earth Metals, in General

The alkali and alkaline earth metals are, generally, large ion lithophiles due to their low charges and high ionic radii. The abundance of these fluid mobile elements becomes more variable as ionic radius increases, with Rb and Cs having the greatest variability and greatest fluid mobility. Samples that lack K-feldspar typically display depletions in K, Rb, and Cs while Na and Ca remain rather remarkably invariable outside of their felsic and mafic modes. Ba is also quite variable with relative uncertainties ranging from 100 to 200% (similar to Rb, Cs, and La, though Ba is more normally distributed than those three). Many of the amphibolite and granulite facies lithologies are also metaluminous, though our samples span the range of peraluminous to peralkaline.

As alluded to in Section 3.1.3, the alkali metals show considerable variability. K, Rb, and Cs increase in skewness as their ionic radius increases, with Cs being the largest and most labile. Rb is also incompatible and fluid mobile. We suspect much of the variation in K stems from the presence or absence of K-feldspar. Lithium also shows a moderate to high level of variability in amphibolite and granulite facies, which could be the result of Li's fluid mobility. Ba and Sr, also incompatible and fluid mobile elements, vary more than their smaller radii counterparts, Mg and Ca, but not nearly as much as the alkalis.

### 3.2. High Field-Strength Elements

Eclogite facies lithologies display the most fractionation of the generally insoluble high field strength elements (HFSEs). Of the HFSEs, Ta and Mo display the largest spread and highest uncertainties for most of our lithologies. There is not enough data to plot Mo or Ta for eclogite facies lithologies. Once more Mo data are reported, paired spikes in both Mo and Nb content in eclogites could indicate that Mo and Nb, which have

similar ionic radii, are both being retained in rutile (Rudnick et al., 2000). With 64 data points, granulite facies xenoliths' elevated Mo is more of a conundrum. High abundances of rutile are not expected for granulite facies xenoliths (Rudnick & Presper, 1990), and the xenoliths do not have a complementary Nb spike. Since titanite (sphene), ilmenite, and magnetite typically host the greatest abundance of Mo in crustal rocks (Greaney et al., 2018), along with rutile, it is possible that these minerals exist in higher abundances in granulite facies xenoliths and/or the deep crust than previously thought.

The data also show variable depletions in Ta compared to (Rudnick & Gao, 2014)'s value. Nb/Ta values also exceed previous lower crustal estimates (Rudnick & Gao, 2014), mimicking more the middle crust's ratio, suggesting that the deep crust might have a super-chondritic Nb/Ta ratio. Plotting Nb vs. Ta (Figure S8) yields a linear log-log plot for amphibolite, granulite, and eclogite facies lithologies. In many cases, we do not have high resolution measurements for Ta concentrations at the sub-ppm level, evidenced by the diagonal lines of data on the Nb vs. Nb/Ta plots (ratios dominated solely by changing Nb) and horizontal array of dots on the Ta vs. Nb/Ta plots. Concentrations which have been rounded to the nearest 100 ppb or ppm when reported. Eclogite facies xenoliths and terrains have notably different Nb/Ta ratios:  $15.6 \pm 1.9$  and  $22.4 \pm 10.2$ , respectively. Studies have hypothesized that Nb can be sequestered by rutile in eclogite formation, but Ta is not expected to increase (Rudnick et al., 2000). Eclogitic material in down-going crustal slabs could be a complementary reservoir to the apparent Nb depletion in the rest of the observable bulk silicate Earth.

### 3.3. Transition Metals

Transition metal data exists in more abundance for amphibolite facies lithologies than for granulite or eclogite. Trends in the first row transition elements are discussed in depth in Section 6 of the main text, but we wanted to briefly mention them in context with the other elements here. The dearth of data on moderately and highly siderophile elements is because they exist in such low abundances in the silicate portion of Earth that only recently have we been able to obtain high precision measurements.

Ti, Zr, and Hf have similar variability, with more mafic lithologies having lower absolute concentrations of Zr. Eclogite facies lithologies have the lowest concentrations of all three elements, a curious finding considering that eclogite facies lithologies tend to have an abundance of rutile ( $\text{FeTiO}_2$ ). Though they track similarly, what controls the abundance of Ti family elements is unclear.

The Cr family, on the other hand, shows much greater variability, perhaps due to Cr concentrating in garnets, spinels, chromite, or even olivine. Olivine fractionation in the source melt could also explain the variations also seen in Ni (Arndt, 1994) among amphibolite and granulite facies lithologies. However, Mo's slightly chalcophile behavior (e.g., Barnes, 2016) could be lending the Cr-family a more discontinuous and variable look than, for example, the Sc, Ti, or Mn families. The Ni and Cu display more variable abundances as well, especially in amphibolite facies lithologies. Their behavior could be attributed to S-affinity and/or the presence of Ni- or Cu-bearing accessory mineral phases (e.g., olivine, diopside). Weathering has been shown to (e.g., Arndt, 1994; Polat et al., 2002), making it more likely that the spread of Cr and Ni abundances is controlled by igneous factors.

A stepped increase in variability is visible from the top to the bottom of the V family for both amphibolite and granulite facies lithologies. This trend, notable in other parts of the periodic table is discussed in Section 6 of the main text. Of course, limited sample numbers may be causing the fluctuation in third-row transition metal abundances. More data is always welcomed to better constrain the abundances and behaviors of the transition metals.

Not much can be said about the elements towards the bottom and right of the periodic table for granulite facies lithologies due to a lack of data, though we can devise a few hypotheses to explain the increased spread in abundances of heavier elements compared to their lighter counterparts. Especially in heavy elements that do not lack for data, such as Ta, Pb, Th, and U, the continuous but wide distribution of data could be caused by the vertical fractionation of these elements within the continental crust. Vertical fractionation of elements within the crust has been discussed in depth for decades (e.g., Sighinolfi, 1971; Taylor & McLennan, 1985; Rudnick & Gao, 2014). One means for testing this hypothesis is comparing trace element abundance to inferred maximum pressure conditions - the higher the pressure, the deeper from within the crust the sample originated. Sadly, most of our data does not have precise pressures and/or temperatures associated with it, though some studies have explored these composition-pressure relationships with quantitative methods (e.g., Bohlen & Mezger, 1989; Rudnick & Jackson, 1995; Barnhart et al., 2012).

Cr, Ni, and Cu break the homogeneity of the first row transition elements. Cr and the two other elements it shares a family with, Mo and W, are more variable than any other transition metals, though we must consider that Mo and W have fewer analyses than many of the others (89 and 42 data points, respectively, compared to the 1000's of analyses

done on first row transition elements and Y, Zr, Nb, Hf, and Ta). The Cr family takes on an abnormal valence electron structure ( $4s^13d^5$ ). This causes Cr to have a range of valence states, though it commonly exists in a 3+ valence state as a substitution in garnet (uvarovite,  $Ca_3Cr_2(SiO_4)_3$ ). Mo and W are high field strength elements with high valences and large radii, which make it harder for them to substitute into common minerals and may contribute to their variability. Mo is typically hosted in Ti-oxides though displays much more variation than Ti.

The Ni and Cu families might also be special cases, not because of their valence structure, but because of their metal and sulfide affinity. The variability in S content may cause fluctuations chalcophile-siderophile elements (CSEs), including Ni and Cu. Of the other CSE's, Zn, a moderately chalcophile element (Jenner, 2017), is much more normally distributed than either Ni or Cu. There are too few measurements on Au and Ag to determine whether their apparent variation is caused by CSE (Jenner, 2017) behavior or if they are under-sampled. The Cu and Ni distributions have far more outliers than any other first row transition metals. Cross-referencing the original data sources show that > 1100 amphibolite and > 900 granulite measurements come from samples with 0.01 - 0.1 wt.% Cu or Ni. The spread in Cu and Ni compositions could be due to cumulate formation and recycling processes, whereby CSE's can be partitioned by magnetite-induced sulfide fractionation in lower crustal settings. While we expect enrichment in CSE's in these lower crustal cumulates, delamination of such material could also cause depletion and contribute to the bulk crust's low Cu concentrations.

### 3.4. Halogens

Limited data is available for the halogens in these medium and high grade metamorphic lithology datasets. F and Cl are the only elements measured for amphibolite and granulite facies lithologies. No halide data is available for eclogite facies lithologies in our dataset. Halides can be transported in fluids or incorporated into select mineral phases, such as Cl-rich biotite and amphibole, apatite, and fluorite (Kusebauch et al., 2015). High solubility in water means these elements are often mobilized by fluid fluxing and can often be found as chemical weathering and alteration byproducts in granulites, despite granulites being nominally anhydrous (e.g., Markl et al., 1997; Banks et al., 2000; Kusebauch et al., 2015). Stable Cl isotopes have been studied in granulites to track mantle participation in silicate Earth's Cl cycle and fluid infiltration processes (Markl et al., 1997). However, the volatility of halogens and their incompatibility in many melt systems has resulted in relatively low halide abundances in the deep crust outside of fluid processes.

#### 4. Supplementary Tables

Table S1: Amphibolite Facies Lithologies

	Mean	Median	Geometric Mean	$\gamma$ Mean	STD	IQR	Geo STD	$\gamma$ STD	N (filtered)	N (original)
Li	17.9	15.0	14.8	17.9	10.7	14.5	1.89	10.6	455	727
Be	1.57	1.44	1.21	1.57	1.02	1.10	2.22	1.08	212	374
B	14.0	9.00	8.44	14.0	14.5	15.6	2.81	13.1	184	362
N	-	-	-	-	-	-	-	-	0	0
F	435	399	60	435	351	512	48.2	746	180	269
S	41.2	22.0	25.2	41.2	46.1	44.0	2.6	38.2	93	292
Cl	51.0	29.3	1.2	51.0	62.2	86.7	83.3	114	81	196
Sc	23.1	21.0	18.3	23.1	13.6	24.4	2.11	15.2	1360	3160
V	152	134	104	152	108	192	2.71	125	1840	3690
Cr	119	81.0	63.5	119	121	151	3.57	124	1820	4200
Co	30.1	29.9	22.2	30.1	19.1	33.1	2.42	22.4	1420	3480
Ni	51.8	39.7	31.2	51.8	47.1	62.0	3.08	49.0	1810	4290
Cu	41.3	30.0	25.8	41.3	36.4	49.5	2.89	37.6	1290	2970
Zn	80.7	78.0	73.0	80.7	34.6	49.5	1.60	35.7	1550	3310
Ga	18.1	18.0	17.7	18.1	3.66	4.32	1.23	3.69	1120	2320
Ge	-	-	-	-	-	-	-	-	0	0.0
As	2.9	1.3	1.4	2.9	4.2	2.4	3.1	3.2	200	368
Se	77.5	53.0	57.1	77.5	63.9	69.0	2.2	57.8	136	158
Br	-	-	-	-	-	-	-	-	0	0
Rb	59.1	43.8	35.1	59.1	51.8	80.0	3.16	56.5	1910	4030
Sr	245	201	201	245	151	204	1.91	149	2100	4730
Y	24.3	22.5	21.9	24.3	11.0	15.0	1.60	11.0	1970	4460
Zr	133	123	115	133	69.5	97.0	1.77	70.9	2070	4650
Nb	8.61	7.20	6.90	8.61	5.47	7.93	2.02	5.55	1790	3790
Mo	1.29	0.520	0.670	1.29	1.56	1.48	3.10	1.37	208	354
Ru	-	-	-	-	-	-	-	-	0	0
Rh	0.0	0.0	0.0	0.0	0.0	0.0	0.0	0.0	0	0
Pd	1.71	0.85	0.89	1.71	2.20	1.70	3.09	1.81	118	218
Ag	47.7	48.0	34.2	47.7	22.1	25.0	3.4	37.1	150	200
Cd	66.2	60.0	49.1	66.2	36.4	58.0	3.0	49.0	146	192
In	0.0712	0.0712	0.0712	-	0.0	0.0	1.0	-	1	28
Sn	3.08	1.60	1.85	3.08	3.58	2.75	2.67	2.90	215	377
Sb	0.30	0.20	0.21	0.30	0.27	0.32	2.38	0.25	253	497
Te	0.08	0.05	0.05	0.08	0.11	0.05	2.76	0.08	8	14
I	-	-	-	-	-	-	-	-	0	0
Cs	1.8	1.2	1.1	1.8	1.8	2.0	2.9	1.7	752	1680
Ba	399	330	268	399	306	486	2.7	337	2030	4400
La	22.3	18.1	15.8	22.3	16.7	25.5	2.5	17.5	1820	3920
Ce	44.4	36.5	33.1	44.4	31.8	46.4	2.3	32.7	1790	3870
Pr	5.6	4.7	4.3	5.6	3.8	5.4	2.1	3.9	1110	2120
Nd	21.6	18.3	17.7	21.6	13.5	18.0	1.9	13.3	1710	3500
Sm	4.6	4.1	4.0	4.6	2.4	3.0	1.7	2.3	1630	3470
Eu	1.1	1.1	1.0	1.1	0.5	0.6	1.5	0.5	1640	3470
Gd	4.4	3.9	3.9	4.4	2.1	2.7	1.6	2.1	1390	2700
Tb	0.7	0.7	0.7	0.7	0.3	0.4	1.6	0.3	1250	2860
Dy	4.3	3.9	3.8	4.3	2.0	2.8	1.6	2.0	1150	2330
Ho	0.9	0.8	0.8	0.9	0.4	0.6	1.6	0.4	1050	2100
Er	2.5	2.3	2.2	2.5	1.2	1.7	1.7	1.2	1150	2250
Tm	0.4	0.4	0.3	0.4	0.2	0.2	1.6	0.2	821	1960
Yb	2.4	2.2	2.1	2.4	1.1	1.5	1.7	1.1	1740	3740
Lu	0.4	0.3	0.3	0.4	0.2	0.2	1.7	0.2	1550	3240
Hf	3.9	3.4	3.3	3.9	2.3	3.1	1.9	2.3	1320	2830
Ta	0.7	0.5	0.5	0.7	0.5	0.7	2.3	0.5	1120	2540
W	1.0	0.4	0.5	1.0	2.0	0.8	2.9	1.1	182	454
Re	-	-	-	-	-	-	-	-	0	6
Os	-	-	-	-	-	-	-	-	0	6
Ir	0.2	0.2	0.2	0.2	0.1	0.1	1.8	0.1	6	19
Pt	1.7	0.7	0.9	1.7	2.0	1.9	3.1	1.8	120	217
Au	2.0	0.8	1.0	2.0	2.7	1.9	3.0	2.2	160	271
Hg	0.0	0.0	0.0	0.0	0.0	0.0	2.2	0.0	4	12
Tl	0.6	0.5	0.3	0.6	0.5	0.8	3.9	0.6	20	60
Pb	13.2	11.7	10.5	13.2	8.3	11.5	2.1	8.6	1260	2490
Bi	0.1	0.1	0.1	0.1	0.1	0.1	2.2	0.1	143	200
Th	5.6	3.7	3.0	5.6	5.4	8.2	3.6	5.9	1600	3330
U	1.4	1.0	0.9	1.4	1.1	1.5	2.6	1.1	1390	2700

Table S2: Granulite Facies Xenoliths

	Mean	Median	Geometric Mean	$\gamma$ Mean	STD	IQR	Geo STD	$\gamma$ STD	N (filtered)	N (original)
Li	11.8	6.9	9.2	11.8	10.5	6.5	1.9	8.0	12	154
Be	0.5	0.5	0.5	0.5	0.0	0.0	1.1	0.0	2	20
B	-	-	-	-	-	-	-	-	0	0
N	-	-	-	-	-	-	-	-	0	0
F	-	-	-	-	-	-	-	-	0	35
S	143	140	89.8	143.0	110.8	220.6	2.85	129.8	4	67
Cl	151.0	151.0	151.0	-	0.0	0.0	1.0	-	1	28
Sc	28.0	28.0	26.5	28.0	9.0	11.9	1.4	9.1	97	863
V	186.0	186.0	166.0	186.0	79.4	100.0	1.7	88.1	92	1030
Cr	210.0	168.0	165.0	210.0	145.0	162.0	2.1	140.0	120	1140
Co	48.9	46.8	46.5	48.9	15.1	23.5	1.4	15.5	87	759
Ni	103.0	100.0	91.6	103.0	46.7	65.0	1.7	48.3	100	1080
Cu	43.4	37.8	36.0	43.4	27.4	33.1	1.9	25.9	72	774
Zn	77.6	81.1	73.0	77.6	25.2	43.3	1.4	26.9	72	751
Ga	17.1	17.3	16.8	17.1	3.1	4.6	1.2	3.2	48	391
Ge	-	-	-	-	-	-	-	-	0	0
As	-	-	-	-	-	-	-	-	0	0
Se	-	-	-	-	-	-	-	-	0	0
Br	-	-	-	-	-	-	-	-	0	0
Rb	15.5	10.6	10.0	15.5	13.0	20.2	2.8	13.6	112	1180
Sr	482.0	465.0	437.0	482.0	207.0	315.0	1.6	210.0	121	1280
Y	19.9	19.0	17.3	19.9	9.9	16.6	1.8	10.5	102	1030
Zr	91.3	83.3	70.5	91.3	58.9	88.7	2.2	63.1	105	1060
Nb	8.8	7.0	7.0	8.8	5.8	7.7	2.0	5.8	99	888
Mo	2.3	1.9	2.1	2.3	1.2	0.8	1.6	1.1	6	62
Ru	-	-	-	-	-	-	-	-	0	0
Rh	0.0	0.0	0.0	0.0	0.0	0.0	0.0	0.0	0	0
Pd	5.54	5.54	5.54	-	0.00	0.00	1.00	-	1	5
Ag	-	-	-	-	-	-	-	-	0	0
Cd	-	-	-	-	-	-	-	-	0	0
In	-	-	-	-	-	-	-	-	0	0
Sn	1.70	1.58	1.62	1.70	0.52	0.96	1.39	0.54	9	77
Sb	-	-	-	-	-	-	-	-	0	39
Te	-	-	-	-	-	-	-	-	0	0
I	-	-	-	-	-	-	-	-	0	0
Cs	0.752	0.390	0.316	0.752	0.960	0.871	4.280	0.901	44	340
Ba	470	393	358	470	330	428	2	334	107	1120
La	14.1	11.6	11.5	14.1	8.6	12.9	2.0	8.7	118	1080
Ce	30.0	27.0	25.0	30.0	17.2	27.4	1.9	17.6	119	1090
Pr	3.6	3.5	3.0	3.6	2.1	3.3	2.0	2.2	63	535
Nd	15.8	14.7	13.7	15.8	8.0	12.3	1.8	8.4	115	1080
Sm	3.8	3.6	3.4	3.8	1.7	2.3	1.6	1.7	114	1070
Eu	1.2	1.3	1.2	1.2	0.4	0.6	1.4	0.4	108	983
Gd	3.8	3.8	3.4	3.8	1.7	2.4	1.7	1.8	79	705
Tb	0.6	0.6	0.5	0.6	0.3	0.3	1.6	0.3	93	778
Dy	3.7	3.6	3.2	3.7	1.8	3.0	1.8	2.0	73	656
Ho	0.7	0.6	0.6	0.7	0.3	0.6	1.7	0.3	63	538
Er	2.0	1.9	1.7	2.0	1.1	1.9	1.9	1.2	71	645
Tm	0.3	0.3	0.2	0.3	0.2	0.3	2.0	0.2	41	344
Yb	1.9	1.7	1.6	1.9	1.0	1.6	1.7	1.0	109	973
Lu	0.3	0.2	0.2	0.3	0.2	0.3	1.7	0.1	99	815
Hf	2.5	2.1	2.0	2.5	1.6	1.3	1.8	1.4	82	680
Ta	0.8	0.6	0.6	0.8	0.5	0.7	2.1	0.5	62	444
W	2.4	1.9	1.8	2.4	1.7	2.6	2.2	1.7	4	30
Re	-	-	-	-	-	-	-	-	0	1
Os	0.2	0.2	0.2	-	0.0	0.0	1.0	-	1	4
Ir	0.3	0.3	0.3	-	0.0	0.0	1.0	-	1	5
Pt	2.5	2.5	2.5	-	0.0	0.0	1.0	-	1	6
Au	-	-	-	-	-	-	-	-	0	3
Hg	-	-	-	-	-	-	-	-	0	0
Tl	-	-	-	-	-	-	-	-	0	0
Pb	5.6	4.5	4.6	5.6	3.6	4.9	2.0	3.5	77	690
Bi	-	-	-	-	-	-	-	-	0	0
Th	1.8	0.8	0.9	1.8	2.4	1.5	3.0	1.9	94	750
U	0.4	0.2	0.3	0.4	0.5	0.3	2.5	0.4	77	604

Table S3: Post-Archean Granulite Terrains

	Mean	Median	Geometric Mean	$\gamma$ Mean	STD	IQR	Geo STD	$\gamma$ STD	N (filtered)	N (original)
Li	7.9	7.2	7.3	7.9	3.2	4.7	1.5	3.1	6	74
Be	2.0	1.6	1.9	2.0	0.7	1.1	1.4	0.6	3	36
B	-	-	-	-	-	-	-	-	0	0
N	-	-	-	-	-	-	-	-	0	0
F	-	-	-	-	-	-	-	-	3	9
S	300.0	300.0	300.0	-	-	-	-	-	1	10
Cl	100.0	100.0	100.0	-	0.0	0.0	1.0	-	2	6
Sc	25.4	25.6	22.7	25.4	10.5	14.3	1.7	11.9	50	635
V	163.0	157.0	145.0	163.0	68.9	90.9	1.7	78.9	54	1030
Cr	198.0	132.0	126.0	198.0	209.0	183.0	2.6	176.0	81	1130
Co	32.3	31.8	27.8	32.3	16.5	21.6	1.8	17.2	41	677
Ni	80.4	59.0	55.7	80.4	78.4	64.8	2.3	65.5	82	1110
Cu	34.2	29.0	28.2	34.2	20.4	27.7	1.9	20.6	45	748
Zn	81.1	77.7	76.4	81.1	29.4	37.6	1.4	27.7	67	949
Ga	18.6	18.0	18.4	18.6	2.8	3.9	1.2	2.8	38	774
Ge	-	-	-	-	-	-	-	-	0	0
As	-	-	-	-	-	-	-	-	0	0
Se	-	-	-	-	-	-	-	-	0	0
Br	-	-	-	-	-	-	-	-	0	0
Rb	65.2	59.0	42.6	65.2	48.1	79.0	3.0	56.9	127	1340
Sr	280.0	267.0	240.0	280.0	144.0	190.0	1.8	152.0	134	1420
Y	28.7	24.2	24.9	28.7	15.8	17.3	1.7	14.9	67	1170
Zr	166.0	136.0	127.0	166.0	114.0	147.0	2.2	118.0	90	1330
Nb	9.9	9.5	7.7	9.9	6.2	7.9	2.3	6.9	63	948
Mo	2.4	3.2	1.8	2.4	1.3	2.1	2.3	1.7	3	37
Ru	-	-	-	-	-	-	-	-	0	0
Rh	0.0	0.0	0.0	0.0	0.0	0.0	0.0	0.0	0	0
Pd	-	-	-	-	-	-	-	-	0	0
Ag	-	-	-	-	-	-	-	-	0	0
Cd	-	-	-	-	-	-	-	-	0	0
In	-	-	-	-	-	-	-	-	0	0
Sn	3.6	2.9	3.0	3.6	2.6	2.7	1.8	2.3	5	223
Sb	0.1	0.1	0.0	0.1	0.1	0.1	2.9	0.1	6	60
Te	-	-	-	-	-	-	-	-	0	0
I	-	-	-	-	-	-	-	-	0	0
Cs	1.7	0.7	0.6	1.7	2.0	2.5	6.0	2.3	24	530
Ba	470.0	461.0	360.0	470.0	280.0	447.0	2.4	330.0	83	1260
La	26.8	24.5	20.9	26.8	16.7	24.4	2.2	18.3	63	1050
Ce	55.6	50.5	45.0	55.6	33.3	42.5	2.0	35.0	62	1060
Pr	6.0	6.1	4.3	6.0	3.9	5.4	2.7	4.7	27	588
Nd	25.9	24.8	21.6	25.9	15.3	17.1	1.9	15.1	57	878
Sm	5.2	4.9	4.5	5.2	2.8	3.0	1.8	2.8	55	842
Eu	1.3	1.4	1.2	1.3	0.4	0.7	1.4	0.4	53	836
Gd	4.9	4.4	4.3	4.9	2.6	2.3	1.7	2.4	42	683
Tb	0.9	0.7	0.8	0.9	0.5	0.5	1.8	0.5	44	759
Dy	4.3	3.7	3.9	4.3	2.0	2.4	1.6	1.9	32	634
Ho	0.9	0.8	0.8	0.9	0.4	0.6	1.6	0.4	31	607
Er	2.5	2.1	2.3	2.5	1.2	1.3	1.6	1.2	33	642
Tm	0.5	0.4	0.4	0.5	0.2	0.4	1.6	0.2	13	67
Yb	2.5	2.0	2.2	2.5	1.3	1.5	1.7	1.3	61	862
Lu	0.4	0.4	0.3	0.4	0.2	0.2	1.7	0.2	48	802
Hf	4.1	4.1	3.3	4.1	2.3	3.0	2.0	2.5	41	666
Ta	0.7	0.5	0.5	0.7	0.5	0.7	2.4	0.5	29	578
W	-	-	-	-	-	-	-	-	0	29
Re	-	-	-	-	-	-	-	-	0	0
Os	-	-	-	-	-	-	-	-	0	0
Ir	-	-	-	-	-	-	-	-	0	0
Pt	-	-	-	-	-	-	-	-	0	0
Au	-	-	-	-	-	-	-	-	0	0
Hg	-	-	-	-	-	-	-	-	0	0
Tl	-	-	-	-	-	-	-	-	0	18
Pb	13.2	11.7	10.4	13.2	8.2	12.1	2.1	8.7	35	728
Bi	-	-	-	-	-	-	-	-	0	14
Th	9.9	5.4	4.2	9.9	10.2	16.2	4.9	11.7	90	816
U	1.0	0.8	0.7	1.0	0.9	1.0	2.8	0.9	83	732

Units: Pd,W, Re, Os, Ir, Pt, and Au are in ppb. All other elements are in ppm.

Table S4: Archean Granulite Terrains

	Mean	Median	Geometric Mean	$\gamma$ Mean	STD	IQR	Geo STD	$\gamma$ STD	N (filtered)	N (original)
Li	15.3	16.3	14.4	15.3	4.6	7.6	1.4	5.0	4	84
Be	-	-	-	-	-	-	-	-	0	0
B	-	-	-	-	-	-	-	-	0	0
N	-	-	-	-	-	-	-	-	0	0
F	-	-	-	-	-	-	-	-	0	1
S	1772	1772.0	698	1772	2303	3260	4.9	2190	2	5
Cl	90.0	90.0	90.0	-	0.0	0.0	1.0	-	1	6
Sc	16.6	16.1	13.1	16.6	9.8	13.9	2.2	11.0	33	468
V	119.0	115.0	102.0	119.0	62.0	81.0	1.8	64.0	48	1000
Cr	146.0	117.0	104.0	146.0	108.0	170.0	2.4	114.0	67	1060
Co	41.3	35.7	33.6	41.3	25.4	38.1	1.9	25.7	35	604
Ni	72.4	55.0	54.9	72.4	52.1	76.7	2.2	51.7	69	1090
Cu	28.5	24.7	22.4	28.5	17.5	30.3	2.1	18.9	32	736
Zn	66.0	65.9	61.9	66.0	22.0	32.6	1.5	23.6	40	875
Ga	20.2	19.5	19.9	20.2	3.7	4.9	1.2	3.6	27	703
Ge	-	-	-	-	-	-	-	-	0	0
As	30.0	30.0	30.0	-	0.0	0.0	1.0	-	1	11
Se	-	-	-	-	-	-	-	-	0	6
Br	-	-	-	-	-	-	-	-	0	0
Rb	44.2	37.0	23.9	44.2	39.9	63.2	3.7	45.5	89	1340
Sr	307.0	295.0	237.0	307.0	185.0	333.0	2.2	212.0	87	1360
Y	18.4	17.8	15.8	18.4	9.4	13.0	1.8	9.9	70	1130
Zr	155.0	137.0	135.0	155.0	86.4	75.7	1.7	79.8	84	1270
Nb	9.2	7.3	7.5	9.2	6.6	5.7	1.9	5.7	66	973
Mo	-	-	-	-	-	-	-	-	0	2
Ru	-	-	-	-	-	-	-	-	0	0
Rh	0.0	0.0	0.0	0.0	0.0	0.0	0.0	0.0	0	0
Pd	-	-	-	-	-	-	-	-	0	3
Ag	-	-	-	-	-	-	-	-	0	0
Cd	-	-	-	-	-	-	-	-	0	0
In	-	-	-	-	-	-	-	-	0	0
Sn	2.6	2.5	2.5	2.6	0.7	1.2	1.4	0.8	23	95
Sb	-	-	-	-	-	-	-	-	0	6
Te	-	-	-	-	-	-	-	-	0	0
I	-	-	-	-	-	-	-	-	0	0
Cs	1.8	0.9	0.8	1.8	2.2	2.4	4.2	2.1	38	229
Ba	561.0	559.0	459.0	561.0	316.0	425.0	2.0	346.0	69	1220
La	27.3	20.0	21.8	27.3	20.6	24.5	1.9	17.6	66	993
Ce	49.8	40.0	41.6	49.8	33.8	34.5	1.8	28.9	65	987
Pr	5.0	4.4	4.4	5.0	2.6	2.7	1.7	2.4	39	376
Nd	18.1	16.4	15.8	18.1	9.2	8.6	1.7	9.3	64	594
Sm	3.6	3.3	3.3	3.6	1.5	2.3	1.5	1.5	55	661
Eu	1.1	1.1	1.1	1.1	0.3	0.5	1.4	0.33	53	641
Gd	3.5	3.3	3.2	3.5	1.5	2.2	1.6	1.56	45	455
Tb	0.5	0.5	0.5	0.5	0.2	0.3	1.6	0.22	50	571
Dy	3.3	3.0	3.0	3.3	1.2	1.9	1.5	1.28	39	481
Ho	0.6	0.6	0.6	0.6	0.3	0.4	1.7	0.30	40	417
Er	1.8	1.7	1.5	1.8	0.8	0.9	1.8	0.93	42	484
Tm	0.3	0.3	0.3	0.3	0.1	0.1	1.2	0.05	9	86
Yb	1.6	1.6	1.4	1.6	0.8	1.3	1.9	0.91	53	630
Lu	0.3	0.3	0.2	0.3	0.1	0.1	1.8	0.13	35	524
Hf	3.2	3.1	3.0	3.2	0.9	1.4	1.4	0.95	44	377
Ta	0.7	0.4	0.4	0.7	0.9	0.3	2.5	0.61	26	258
W	6.7	6.7	6.7	-	0.0	0.0	1.0	-	1	7
Re	-	-	-	-	-	-	-	-	0	0
Os	-	-	-	-	-	-	-	-	0	0
Ir	-	-	-	-	-	-	-	-	0	7
Pt	-	-	-	-	-	-	-	-	0	3
Au	-	-	-	-	-	-	-	-	0	6
Hg	-	-	-	-	-	-	-	-	0	0
Tl	-	-	-	-	-	-	-	-	0	0
Pb	10.0	8.0	8.8	10.0	5.4	5.4	1.6	4.77	61	758
Bi	-	-	-	-	-	-	-	-	0	0
Th	7.4	2.7	2.9	7.4	14.6	5.2	3.7	9.21	73	772
U	1.2	0.5	0.6	1.2	1.7	1.4	3.3	1.28	66	562

Units: Pd,W, Re, Os, Ir, Pt, and Au are in ppb. All other elements are in ppm.

Table S5: Eclogite Facies Xenoliths

	Mean	Median	Geometric Mean	$\gamma$ Mean	STD	IQR	Geo STD	$\gamma$ STD	N (filtered)	N (original)
Li	28.7	28.7	28.7	-	0.0	0.0	1.0	-	1	8
Be	-	-	-	-	-	-	-	-	0	0
B	-	-	-	-	-	-	-	-	0	0
N	-	-	-	-	-	-	-	-	0	0
F	-	-	-	-	-	-	-	-	0	4
S	-	-	-	-	-	-	-	-	0	0
Cl	-	-	-	-	-	-	-	-	0	4
Sc	56.2	57.0	55.6	56.2	7.5	13.8	1.15	7.6	3	33
V	320	274	314	320	62.4	120	1.21	61.0	5	60
Cr	626	764	552	626	278	554	1.70	308	5	60
Co	62.7	65.2	61.6	62.7	11.4	20.5	1.21	11.9	4	35
Ni	182	157	174	182	53.5	110	1.34	53.2	5	60
Cu	55.2	55.2	55.1	55.2	4.13	8.26	1.08	4.1	2	31
Zn	72.3	68.9	70.9	72.3	14.3	25.5	1.21	14.0	4	58
Ga	11.4	11.4	11.4	-	0.0	0.0	1.00	-	1	46
Ge	-	-	-	-	-	-	-	-	0	0
As	-	-	-	-	-	-	-	-	0	0
Se	-	-	-	-	-	-	-	-	0	0
Br	-	-	-	-	-	-	-	-	0	0
Rb	7.4	7.1	5.4	7.4	4.9	11.0	2.4	5.6	5	41
Sr	165.0	178.0	157.0	165.0	53.5	72.0	1.4	52.0	7	67
Y	19.6	20.7	19.1	19.6	4.1	7.2	1.2	4.2	7	66
Zr	40.1	41.1	34.4	40.1	20.6	29.3	1.8	21.7	6	65
Nb	10.4	6.3	5.1	10.4	9.9	19.2	3.9	11.3	6	58
Mo	-	-	-	-	-	-	-	-	0	2
Ru	-	-	-	-	-	-	-	-	0	0
Rh	-	-	-	-	-	-	-	-	0	0
Pd	-	-	-	-	-	-	-	-	0	18
Ag	-	-	-	-	-	-	-	-	0	0
Cd	-	-	-	-	-	-	-	-	0	0
In	-	-	-	-	-	-	-	-	0	0
Sn	-	-	-	-	-	-	-	-	0	2
Sb	-	-	-	-	-	-	-	-	0	2
Te	-	-	-	-	-	-	-	-	0	0
I	-	-	-	-	-	-	-	-	0	0
Cs	-	-	-	-	-	-	-	-	0	6
Ba	370.0	239.0	242.0	370.0	350.0	382.0	2.6	323.0	7	67
La	5.6	6.0	4.3	5.6	3.5	6.0	2.2	3.9	7	62
Ce	16.5	13.9	12.3	16.5	10.9	20.7	2.3	12.3	7	62
Pr	2.2	1.9	1.9	2.2	1.3	1.9	1.9	1.3	4	30
Nd	9.7	7.9	7.9	9.7	6.2	9.5	1.9	6.0	6	37
Sm	2.6	2.3	2.5	2.6	1.1	1.0	1.4	1.0	5	34
Eu	1.0	0.8	1.0	1.0	0.2	0.4	1.3	0.2	5	34
Gd	2.8	2.4	2.7	2.8	0.8	1.1	1.3	0.8	4	30
Tb	0.4	0.4	0.4	0.4	0.1	0.1	1.2	0.1	5	34
Dy	3.0	3.0	2.9	3.0	0.5	0.9	1.2	0.5	4	30
Ho	0.6	0.6	0.6	0.6	0.1	0.2	1.2	0.1	4	30
Er	1.6	1.7	1.6	1.6	0.2	0.3	1.2	0.2	4	30
Tm	0.3	0.3	0.3	0.3	0.0	0.0	1.1	0.0	2	27
Yb	2.1	1.9	2.0	2.1	0.8	1.3	1.5	0.8	5	34
Lu	0.3	0.3	0.3	0.3	0.1	0.1	1.3	0.1	4	32
Hf	1.5	1.4	1.3	1.5	0.7	1.2	1.6	0.7	4	31
Ta	0.6	0.7	0.6	0.6	0.1	0.1	1.1	0.1	3	29
W	-	-	-	-	-	-	-	-	0	0
Re	-	-	-	-	-	-	-	-	0	0
Os	-	-	-	-	-	-	-	-	0	0
Ir	-	-	-	-	-	-	-	-	0	18
Pt	-	-	-	-	-	-	-	-	0	18
Au	-	-	-	-	-	-	-	-	0	18
Hg	-	-	-	-	-	-	-	-	0	0
Tl	-	-	-	-	-	-	-	-	0	0
Pb	2.9	2.9	2.3	2.9	1.7	3.3	2.0	1.8	4	38
Bi	-	-	-	-	-	-	-	-	0	0
Th	0.4	0.3	0.4	0.4	0.2	0.3	1.7	0.2	5	55
U	0.2	0.2	0.2	0.2	0.2	0.3	1.9	0.1	4	54

Units: Pd,W, Re, Os, Ir, Pt, and Au are in ppb. All other elements are in ppm.

Table S6: Eclogite Facies Terrains

	Mean	Median	Geometric Mean	$\gamma$ Mean	STD	IQR	Geo STD	$\gamma$ STD	N (filtered)	N (original)
Li	-	-	-	-	-	-	-	-	0	2
Be	-	-	-	-	-	-	-	-	0	0
B	-	-	-	-	-	-	-	-	0	0
N	-	-	-	-	-	-	-	-	0	0
F	-	-	-	-	-	-	-	-	0	2
S	-	-	-	-	-	-	-	-	0	0
Cl	-	-	-	-	-	-	-	-	0	1
Sc	37.9	30.3	31.0	37.9	23.2	41.4	1.9	23.4	3	33
V	239.0	244.0	224.0	239.0	75.4	86.5	1.5	84.3	5	14
Cr	167.0	187.0	140.0	167.0	76.6	127.0	2.0	98.2	8	39
Co	38.0	38.1	36.2	38.0	11.5	13.2	1.4	11.7	7	38
Ni	83.7	86.0	77.9	83.7	27.0	35.8	1.5	31.1	8	37
Cu	26.8	17.8	21.7	26.8	18.6	26.5	1.9	17.0	6	13
Zn	108.0	105.0	106.0	108.0	19.8	36.5	1.2	19.7	4	30
Ga	20.3	19.0	19.7	20.3	5.0	9.0	1.3	4.9	3	9
Ge	-	-	-	-	-	-	-	-	0	0
As	-	-	-	-	-	-	-	-	0	23
Se	-	-	-	-	-	-	-	-	0	0
Br	-	-	-	-	-	-	-	-	0	0
Rb	7.6	4.4	5.5	7.6	6.0	10.2	2.2	5.8	3	35
Sr	207.0	183.0	165.0	207.0	118.0	208.0	2.1	134.0	9	45
Y	27.6	26.2	24.8	27.6	12.0	22.0	1.6	12.3	6	13
Zr	89.2	107.0	81.4	89.2	33.1	60.3	1.6	37.6	7	36
Nb	6.5	5.4	6.1	6.5	2.5	4.3	1.4	2.4	3	7
Mo	-	-	-	-	-	-	-	-	0	2
Ru	-	-	-	-	-	-	-	-	0	0
Rh	-	-	-	-	-	-	-	-	0	0
Pd	-	-	-	-	-	-	-	-	0	0
Ag	-	-	-	-	-	-	-	-	0	0
Cd	-	-	-	-	-	-	-	-	0	0
In	-	-	-	-	-	-	-	-	0	0
Sn	-	-	-	-	-	-	-	-	0	2
Sb	-	-	-	-	-	-	-	-	0	25
Te	-	-	-	-	-	-	-	-	0	0
I	-	-	-	-	-	-	-	-	0	0
Cs	0.1	0.1	0.1	-	0.0	0.0	1.0	-	1	26
Ba	212.0	135.0	136.0	212.0	188.0	319.0	2.7	189.0	9	39
La	7.9	6.4	6.3	7.9	5.3	9.4	2.0	5.2	4	35
Ce	15.6	14.8	12.9	15.6	8.8	16.9	1.9	9.3	4	35
Pr	0.8	0.8	0.8	-	0.0	0.0	1.0	-	1	4
Nd	6.7	5.8	6.3	6.7	2.5	3.5	1.4	2.3	4	36
Sm	2.5	2.0	2.4	2.5	1.0	1.4	1.4	0.9	4	36
Eu	1.0	1.0	1.0	1.0	0.1	0.1	1.1	0.1	3	34
Gd	5.0	5.0	5.0	5.0	0.2	0.5	1.1	0.2	2	8
Tb	0.7	0.8	0.7	0.7	0.2	0.4	1.4	0.2	3	34
Dy	6.3	6.3	6.3	-	0.0	0.0	1.0	-	1	4
Ho	1.3	1.3	1.3	1.3	0.1	0.1	1.0	0.1	2	8
Er	3.8	3.8	3.8	3.8	0.2	0.3	1.0	0.2	2	8
Tm	0.5	0.5	0.5	-	0.0	0.0	1.0	-	1	6
Yb	3.4	3.8	3.0	3.4	1.5	2.5	1.7	1.6	6	40
Lu	0.2	0.2	0.2	-	0.0	0.0	1.0	-	1	31
Hf	1.8	1.8	1.8	-	0.0	0.0	1.0	-	1	32
Ta	0.1	0.1	0.1	-	0.0	0.0	1.0	-	1	29
W	-	-	-	-	-	-	-	-	0	0
Re	-	-	-	-	-	-	-	-	0	0
Os	-	-	-	-	-	-	-	-	0	0
Ir	-	-	-	-	-	-	-	-	0	0
Pt	-	-	-	-	-	-	-	-	0	0
Au	-	-	-	-	-	-	-	-	0	0
Hg	-	-	-	-	-	-	-	-	0	0
Tl	-	-	-	-	-	-	-	-	0	0
Pb	2.3	2.3	2.2	2.3	0.7	1.4	1.4	0.7	2	8
Bi	-	-	-	-	-	-	-	-	0	0
Th	0.2	0.2	0.2	0.2	0.1	0.3	2.1	0.1	2	32
U	0.1	0.1	0.1	-	0.0	0.0	1.0	-	1	32

Units: Pd,W, Re, Os, Ir, Pt, and Au are in ppb. All other elements are in ppm.

**Element Ratios and Heat Production**

**Table S7.** Amphibolite Facies Lithologies

	Mean	Median	Geo Mean	$\gamma$ Mean	STD	IQR	Geo STD	$\gamma$ STD	N(filtered)	N(original)
La/Yb	11.6	8.16	7.15	11.6	10.9	13.40	2.88	10.7	1740	3740
Nb/Ta	14.4	14.1	12.6	14.4	5.99	6.33	1.99	7.37	719	1360
Zr/Hf	35.5	35.6	35.0	35.5	6.08	7.70	1.20	6.27	1320	2820
Rb/Cs	48.5	34.0	31.4	48.5	45.4	41.90	2.80	42.7	753	1580
K/Rb	331	294	299	331	160	183.00	1.56	147	1900	3960
La/Th	6.62	5.02	5.30	6.62	4.75	5.42	1.93	4.27	1590	3200
Th/U	4.20	3.65	3.35	4.20	2.67	3.10	2.08	2.73	1380	2600
K/U	15900	12100	11300	15900	13000	14200.00	2.42	12600	1380	2600
Eu/Eu*	0.859	0.884	0.826	0.859	0.229	0.32	1.34	0.241	1372	2674
$k/Pb$	3.89	3.86	3.84	3.89	0.646	0.48	1.17	0.621	-	165
Heat Prod. (nW/kg)	0.470	0.278	0.240	0.470	1.99	0.46	3.16	0.503	490	1467
Heat Prod. (mW/m <sup>3</sup> )	1.36	0.81	0.70	1.36						

**Table S8.** Granulite Facies Xenoliths

	Mean	Median	Geo Mean	$\gamma$ Mean	STD	IQR	Geo STD	$\gamma$ STD	N(filtered)	N(original)
La/Yb	8.71	7.52	7.29	8.71	5.33	6.37	1.83	5.05	103	957
Nb/Ta	18.0	18.6	15.3	18	7.54	9.1	2.14	9.98	41	424
Zr/Hf	39.9	36.3	36.4	39.9	17.8	11.5	1.56	16.9	62	669
Rb/Cs	73.4	40.6	37.2	73.4	84.1	52	3.83	79	39	317
K/Rb	788	643	653	788	491	685	1.86	470	104	1140
La/Th	27.0	17.1	18.0	27.0	25.0	25.8	2.51	23.0	89	683
Th/U	3.79	3.39	3.05	3.79	2.47	2.67	2.03	2.42	67	571
K/U	46300	36900	32300	46300	36100	43000	2.66	37400	72	571
Eu/Eu*	1.28	1.09	1.21	1.28	0.479	0.38	1.38	0.425	79	703
$\kappa_{Pb}$	4.17	4.04	4.14	4.17	0.520	0.24	1.11	0.464	-	357
Heat Prod.	0.147	0.0716	0.0861	0.147	0.187	0.11	2.68	0.142	62	79
Heat Prod. (mW/m <sup>3</sup> )	0.43	0.21	0.25	0.43						

**Table S9.** Post Archean Granulite Facies Terrains

	Mean	Median	Geo Mean	$\gamma$ Mean	STD	IQR	Geo STD	$\gamma$ STD	N(filtered)	N(original)
La/Yb	11.7	10.1	8.54	11.7	7.75	8.96	2.77	8.84	41	658
Nb/Ta	14.7	13.9	9.46	14.7	10.4	8.57	4.00	13.0	22	416
Zr/Hf	35.9	35.7	35.1	35.9	7.2	11	1.24	7.46	29	479
Rb/Cs	100	44.6	44.8	100	159	81.4	3.50	116	18	386
K/Rb	423	291	346	423	335	265	1.78	259	109	1090
La/Th	23.7	11.2	12.3	23.7	30.2	18	3.05	25.0	36	777
Th/U	10.1	6.58	6.50	10.1	9.91	10	2.61	8.90	73	564
K/U	37500	31000	27500	37500	32900	32200	2.22	28300	73	564
Eu/Eu*	1.02	1.03	0.94	1.02	0.411	0.46	1.48	0.395	40	673
$\kappa_{Pb}$	3.99	4.00	3.99	3.99	0.159	0.19	1.04	0.158	-	33
Heat Prod.	0.514	0.407	0.267	0.514	0.490	0.62	4.41	0.544	70	91
Heat Prod. (mW/m <sup>3</sup> )	1.49	1.18	0.77	1.49						

..

**Table S10.** Archean Granulite Facies Terrains

	Mean	Median	Geo Mean	$\gamma$ Mean	STD	IQR	Geo STD	$\gamma$ STD	N(filtered)	N(original)
La/Yb	25.4	16	18.2	25.4	20.3	31.1	2.33	19.8	45	572
Nb/Ta	17.5	16.3	16.4	17.5	6.24	6.92	1.45	6.26	16	218
Zr/Hf	35.4	35.8	34.7	35.4	7.21	9.54	1.22	7.00	39	341
Rb/Cs	86.0	61.0	44.7	86.0	94.0	93.7	3.61	90.9	30	196
K/Rb	640	433	506	640	477	515	1.95	424	81	1250
La/Th	13.4	7.32	7.8	13.4	16.1	14.2	2.88	13.1	47	728
Th/U	9.17	7.26	6.58	9.17	7.00	9.37	2.39	7.13	60	527
K/U	38100	29300	22900	38100	31900	44900	3.30	36100	60	527
Eu/Eu*	1.16	1.09	1.11	1.16	0.331	0.46	1.34	0.330	44	451
$\kappa_{Pb}$	4.16	4.11	4.16	4.16	0.164	0.23	1.03	0.141	-	4
Heat Prod.	0.558	0.179	0.207	0.558	1.04	0.36	3.73	0.708	54	70
Heat Prod. (mW/m <sup>3</sup> )	1.62	0.52	0.60	1.62						

**Table S11.** Eclogite Facies Xenoliths

	Mean	Median	Geo Mean	$\gamma$ Mean	STD	IQR	Geo STD	$\gamma$ STD	STD N(filtered)	N(original)
La/Yb	6.53	4.69	4.87	6.53	5.16	7.37	2.14	4.8	7	34
Nb/Ta	16.70	17.5	7.89	16.7	10.1	16	6.43	18.8	5	29
Zr/Hf	30.20	31.7	28.4	30.2	9.24	13.5	1.47	10.6	5	31
Rb/Cs	26.60	26.6	18.5	26.6	19.1	38.3	2.48	21.6	2	6
K/Rb	542	503	458	542	287	476	1.85	306	7	41
La/Th	9.22	9.56	8.77	9.22	2.66	4.61	1.4	2.91	6	31
Th/U	2.18	2.17	2.03	2.18	0.798	1.47	1.45	0.798	5	29
K/U	16100	5190	7040	16100	17400	25600	4.29	18800	5	29
Eu/Eu*	1.01	0.968	1.01	1.01	0.095	0.14	1.09	0.0926	4	30
$k_{Pb}$	5.48	5.75	5.44	5.48	0.668	1.01	1.13	0.668	-	21
Heat Prod.	0.0792	0.0433	0.0585	0.0792	0.0771	0.07	2.08	0.0590	3	5
Heat Prod. (mW/m <sup>3</sup> )	0.23	0.13	0.17	0.23						

..

**Table S12.** Eclogite Facies Terrains

	Mean	Median	Geo Mean	$\gamma$ Mean	STD	IQR	Geo STD	$\gamma$ STD	N(filtered)	N(original)
La/Yb	7.46	5.48	3.96	7.46	6.9	10.4	3.69	7.77	5	40
Nb/Ta	29.40	29.4	29.4	-	0	0	1	-	1	25
Zr/Hf	27.20	27.2	20.6	27.2	17.7	35.4	2.18	19.4	2	32
Rb/Cs	53.30	53.3	52.7	53.3	7.52	15	1.15	7.55	2	23
K/Rb	693	526	564	693	498	435	1.84	431	5	35
La/Th	60.50	60.5	31.7	60.5	51.5	103	3.53	63.6	2	19
Th/U	2.73	2.56	2.7	2.73	0.424	0.746	1.16	0.415	3	26
K/U	68000	44300	24700	68000	65600	117000	6.04	87100	3	26
Eu/Eu*	0.875	0.875	0.875	0.875	0.0182	0.036	1.02	0.0182	2	8
$\kappa_{Pb}$	-	-	-	-	-	-	-	-	-	0
Heat Prod.	0.0647	0.0437	0.0539	0.0647	0.0489	0.0681	1.81	0.0380	1	3
Heat Prod. (mW/m <sup>3</sup> )	0.19	0.13	0.16	0.19						

## 5. Supplementary Figures

## References

- Arndt, N. (1994). Archean komatiites. *Archean crustal evolution*, 10, 11–44.
- Banks, D., Green, R., Cliff, R., & Yardley, B. (2000). Chlorine isotopes in fluid inclusions: determination of the origins of salinity in magmatic fluids. *Geochimica et Cosmochimica Acta*, 64(10), 1785–1789.
- Barnes, S.-J. (2016). Chalcophile elements.
- Barnhart, K. R., Mahan, K. H., Blackburn, T. J., Bowring, S. A., & Dudas, F. O. (2012). Deep crustal xenoliths from central montana, usa: Implications for the timing and mechanisms of high-velocity lower crust formation. *Geosphere*, 8(6), 1408–1428.
- Bohlen, S., & Mezger, K. (1989). Origin of granulite terranes and the formation of the lowermost continental crust. *Science*, 244(4902), 326–329.
- Field, D., & Clough, P. W. (1976). K/rb ratios and metasomatism in metabasites from a precambrian amphibolite–granulite transition zone. *Journal of the Geological Society*, 132(3), 277–288.
- Field, D., & Elliott, R. (1974). The chemistry of gabbro/amphibolite transitions in south norway. *Contributions to Mineralogy and Petrology*, 47(1), 63–76.
- Fowler, M. (1986). Large-ion lithophile element characteristics of an amphibolite facies to granulite facies transition at gruinard bay, north-west scotland. *Journal of Metamorphic Geology*, 4(3), 345–359.
- Greaney, A. T., Rudnick, R. L., Gaschnig, R. M., Whalen, J. B., Luais, B., & Clemens, J. D. (2018). Geochemistry of molybdenum in the continental crust. *Geochimica et Cosmochimica Acta*, 238, 36–54.
- Hartigan, J. A., & Hartigan, P. M. (1985). The dip test of unimodality. *The annals of*

*Statistics*, 13(1), 70–84.

Jenner, F. E. (2017). Cumulate causes for the low contents of sulfide-loving elements in the continental crust. *Nature Geoscience*, 10(7), 524–529.

Kusebauch, C., John, T., Barnes, J. D., Klügel, A., & Austrheim, H. O. (2015). Halogen element and stable chlorine isotope fractionation caused by fluid–rock interaction (bamble sector, se norway). *Journal of Petrology*, 56(2), 299–324.

Markl, G., Musashi, M., & Bucher, K. (1997). Chlorine stable isotope composition of granulites from lofoten, norway: Implications for the cl isotopic composition and for the source of cl enrichment in the lower crust. *Earth and Planetary Science Letters*, 150(1-2), 95–102.

Polat, A., Hofmann, A., & Rosing, M. T. (2002). Boninite-like volcanic rocks in the 3.7–3.8 ga isua greenstone belt, west greenland: geochemical evidence for intra-oceanic subduction zone processes in the early earth. *Chemical geology*, 184(3-4), 231–254.

Rudnick, R. L., Barth, M., Horn, I., & McDonough, W. F. (2000). Rutile-bearing refractory eclogites: missing link between continents and depleted mantle. *Science*, 287(5451), 278–281.

Rudnick, R. L., & Gao, S. (2014). Composition of the Continental Crust. In *Treatise on Geochemistry* (p. 1-51). Elsevier. doi: 10.1016/B978-0-08-095975-7.00301-6

Rudnick, R. L., & Jackson, I. (1995). Measured and calculated elastic wave speeds in partially equilibrated mafic granulite xenoliths: Implications for the properties of an underplated lower continental crust. *Journal of Geophysical Research: Solid Earth*, 100(B6), 10211–10218.

Rudnick, R. L., McLennan, S. M., & Taylor, S. R. (1985). Large ion lithophile elements

- in rocks from high-pressure granulite facies terrains. *Geochimica et Cosmochimica Acta*, 49(7), 1645–1655.
- Rudnick, R. L., & Presper, T. (1990). Geochemistry of intermediate/-to high-pressure granulites. In *Granulites and crustal evolution* (pp. 523–550). Springer.
- Rudnick, R. L., & Taylor, S. R. (1987, December). The composition and petrogenesis of the lower crust: A xenolith study. *Journal of Geophysical Research: Solid Earth*, 92(B13), 13981–14005. doi: 10.1029/JB092iB13p13981
- Sighinolfi, G. P. (1971). Investigations into deep crustal levels: fractionating effects and geochemical trends related to high-grade metamorphism. *Geochimica et Cosmochimica Acta*, 35(10), 1005–1021.
- Stosch, H.-G., Lugmair, G., & Seck, H. (1986). Geochemistry of granulite-facies lower crustal xenoliths: implications for the geological history of the lower continental crust below the eifel, west germany. *Geological Society, London, Special Publications*, 24(1), 309–317.
- Tang, M., McDonough, W. F., & Ash, R. D. (2017). Europium and strontium anomalies in the morb source mantle. *Geochimica et Cosmochimica Acta*, 197, 132–141.
- Taylor, S. R., & McLennan, S. M. (1985). *The continental crust: its composition and evolution*. Blackwell Scientific Pub., Palo Alto, CA.
- Van Calsteren, P., Harris, N., Hawkesworth, C., Menzies, M., & Rogers, N. (1986). Xenoliths from southern africa: a perspective on the lower crust. *Geological Society, London, Special Publications*, 24(1), 351–362.

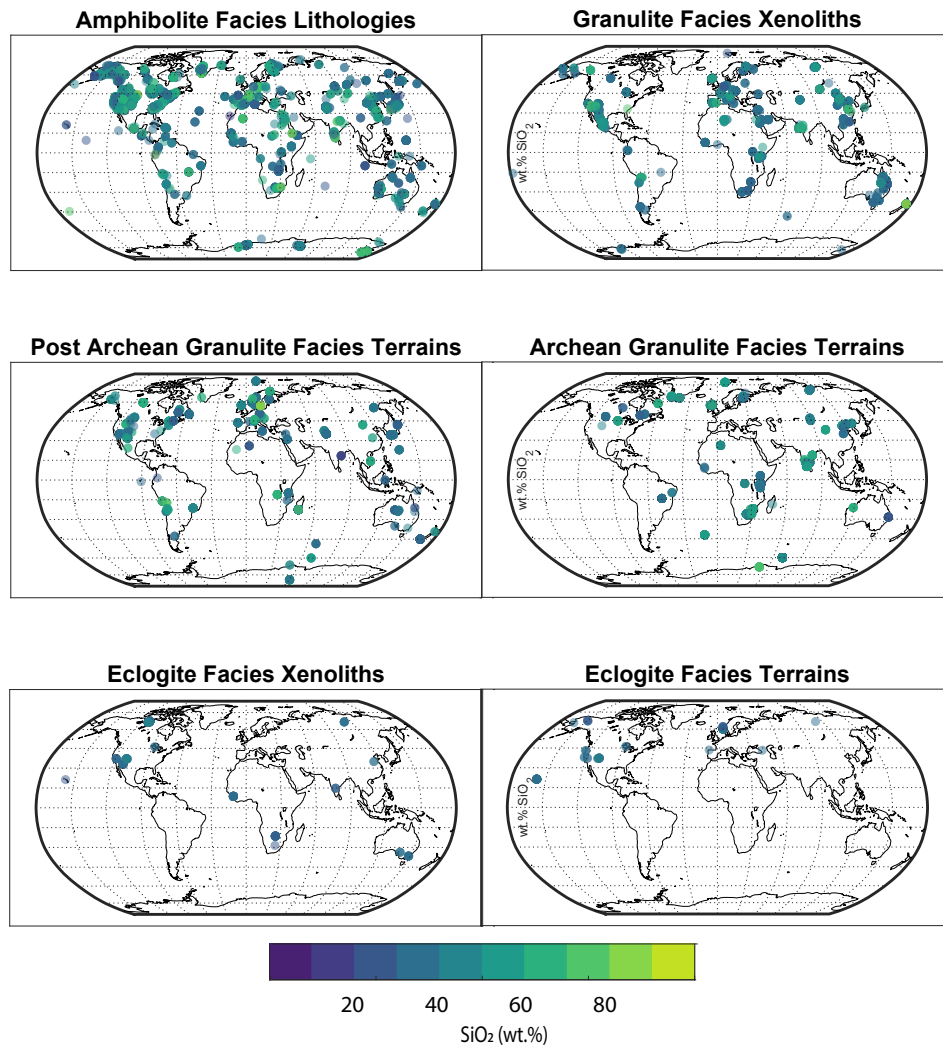


**Figure S1.** Maps of the metamorphic sample datasets that we have extensive sample coverage for amphibolite and granulite facies lithologies with more limited exposures of eclogite facies lithologies. Each circle is a single sample whose color is determined by weight percent  $\text{SiO}_2$ . Many circles overlap. There is little correlation between  $\text{SiO}_2$  and location.

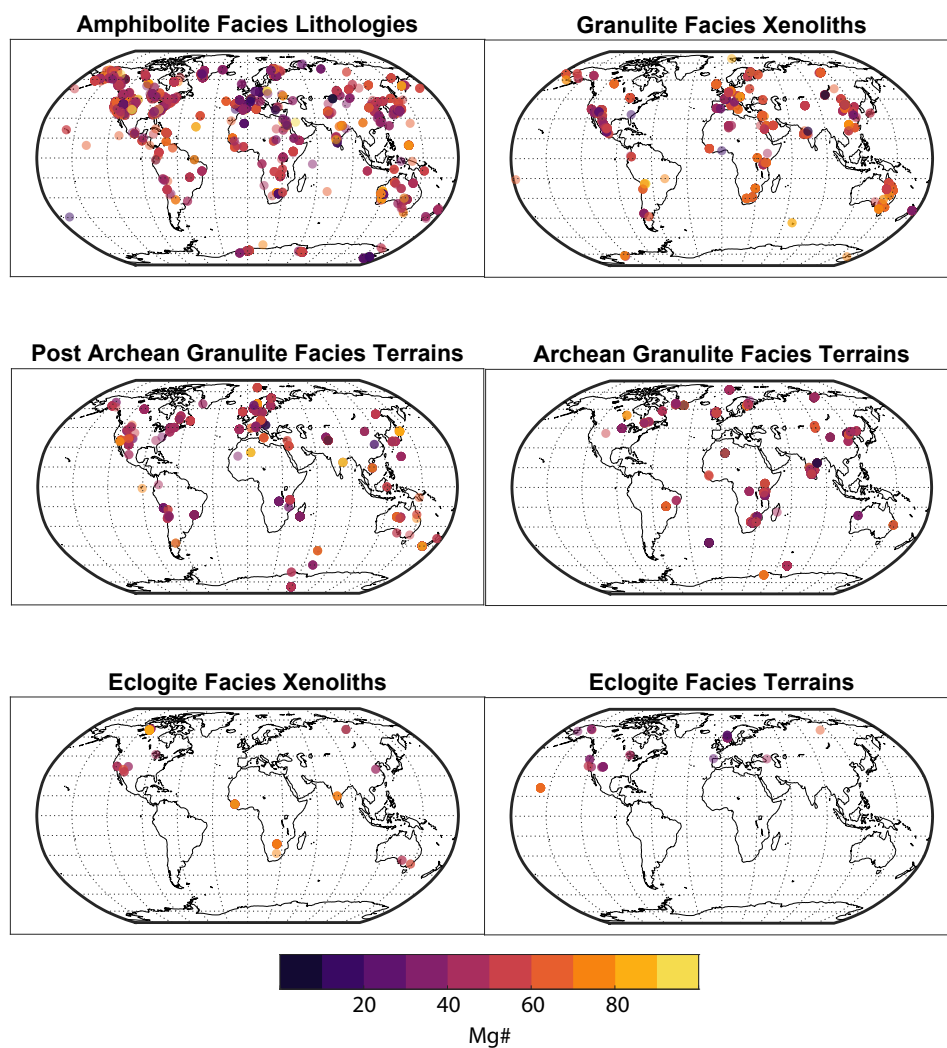


**Figure S2.** Maps of the metamorphic sample datasets that we have extensive sample coverage for amphibolite and granulite facies lithologies with more limited exposures of eclogite facies lithologies. Each circle is a single sample whose color is determined by weight percent  $\text{SiO}_2$ . Many circles overlap. There is no correlation between Mg# and location.

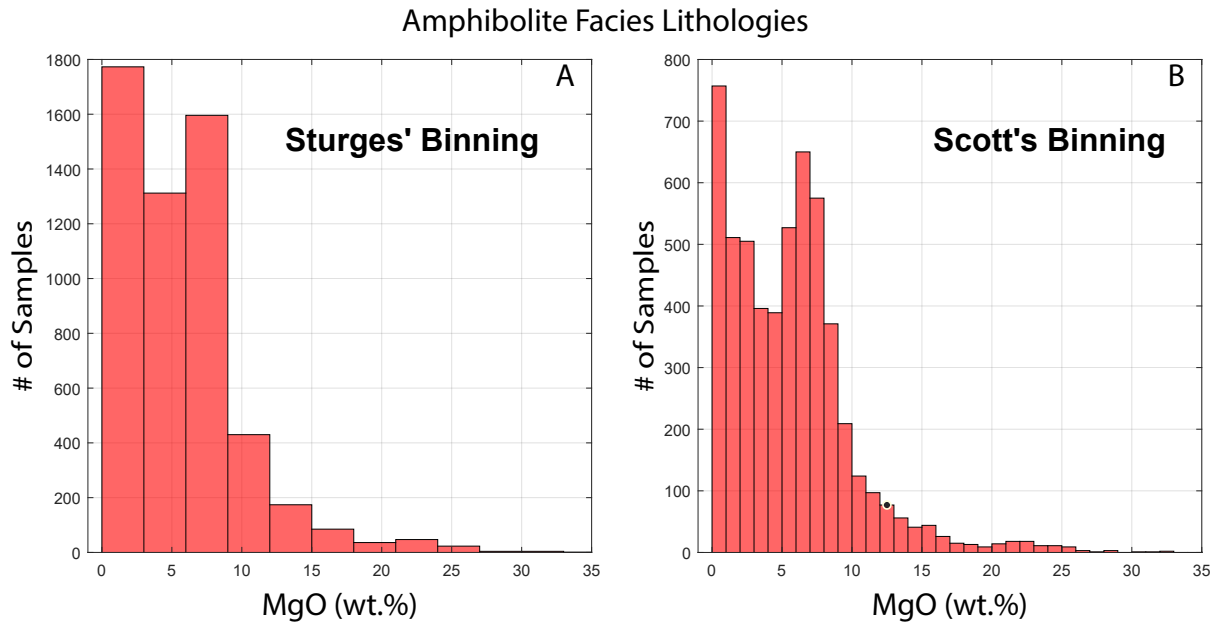


**Figure S3.** Amphibolite facies lithologies, when binned according to MgO, do not show obvious bimodality when binned according to Sturge's Law (fewer bins) but do show dual peaks when plotted with more bins. Such a phenomenon highlights the importance of binning and data visualization and need for more objective distribution rankings, such as the Hartigan's Dip Test.

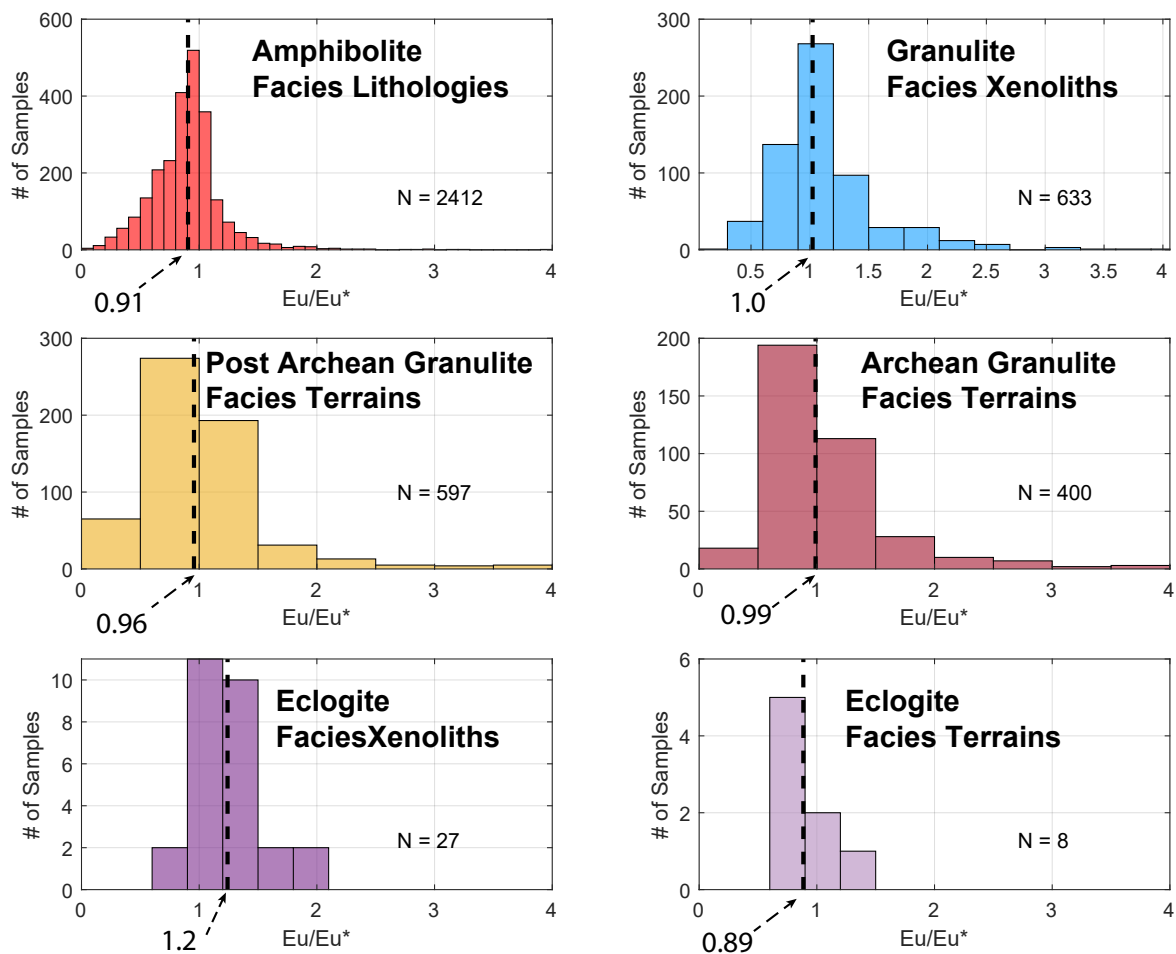


**Figure S4.** The right-skewed  $\text{Eu}/\text{Eu}^*$  distributions of our datasets all find a median value close to 1, which is 15 - 30% less than previous estimates. Because of the asymmetry in the distributions, both granulite facies xenoliths and terrains have similar values, though the more felsic Archean granulite facies lithologies have a higher percentage of  $\text{Eu}/\text{Eu}^*$  values  $>1$  than their more mafic Post Archean counterparts.

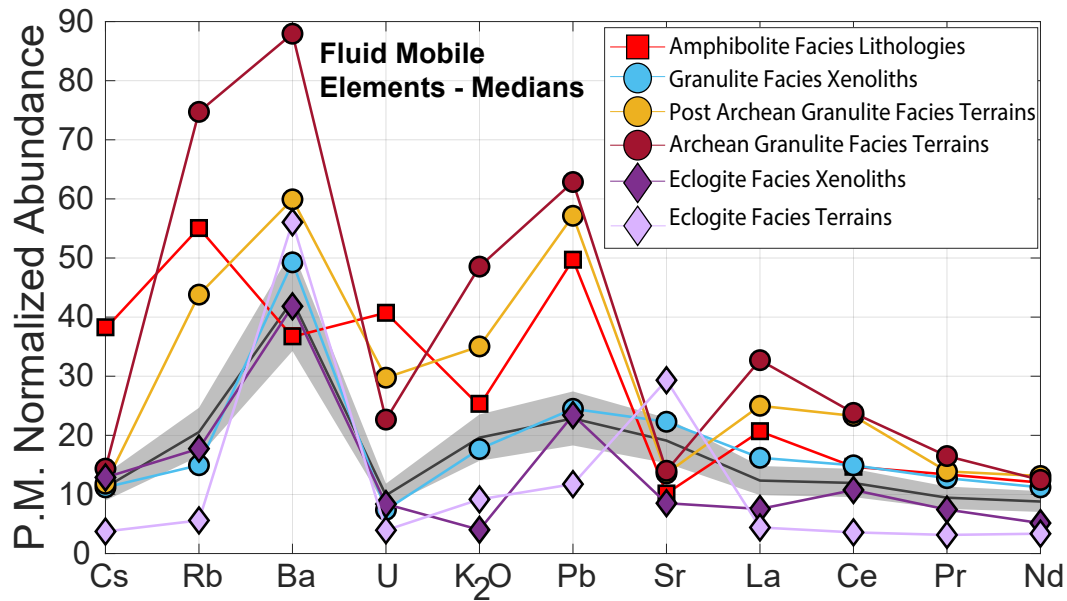


**Figure S5.** Fluid mobile element concentrations from amphibolite and granulite facies lithologies are comparable with previous estimates for the lower crust. Eclogite facies lithologies are up a half an order of magnitude more depleted. Variable labile element depletions cause the amphibolite facies lithologies to overlap with the granulite facies terrains, suggesting that either the amphibolite facies samples have experienced some fluid depletion or that the behavior of the labile elements is caused by an igneous process and not metamorphic dehydration. The black line and gray shaded region surrounding it is the Rudnick and Gao (2014) lower crustal composition  $\pm 15\%$ .

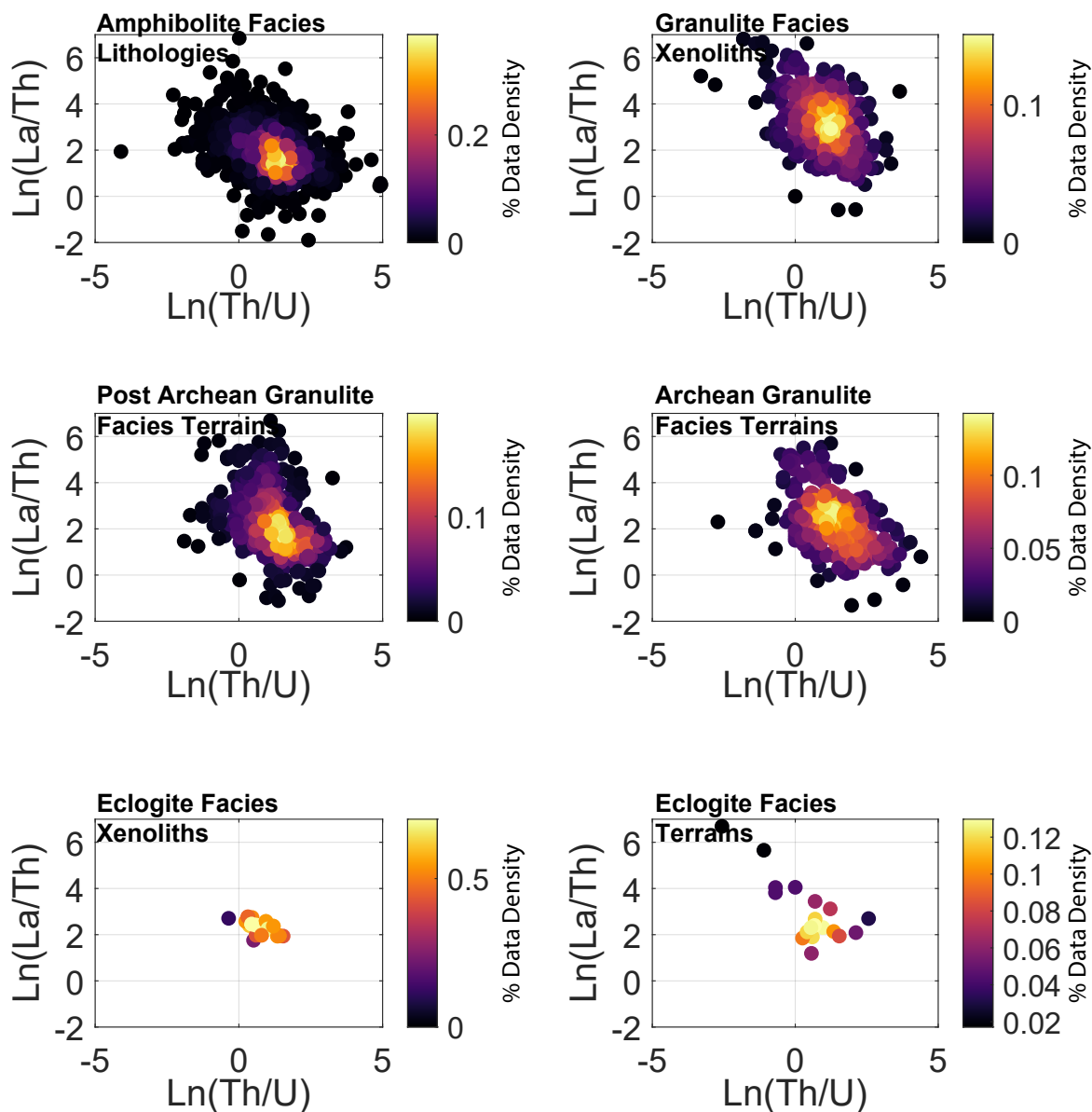


**Figure S6.**  $\text{La}/\text{Th}$  vs.  $\text{Th}/\text{U}$  in natural log space. Color indicates the data point density. High  $\text{La}/\text{Th}$  values correlate with low  $\text{Th}/\text{U}$  concentrations, indicating that low  $\text{La}/\text{Th}$  is due to depletions in  $\text{Th}$  instead of enrichments in  $\text{La}$ .

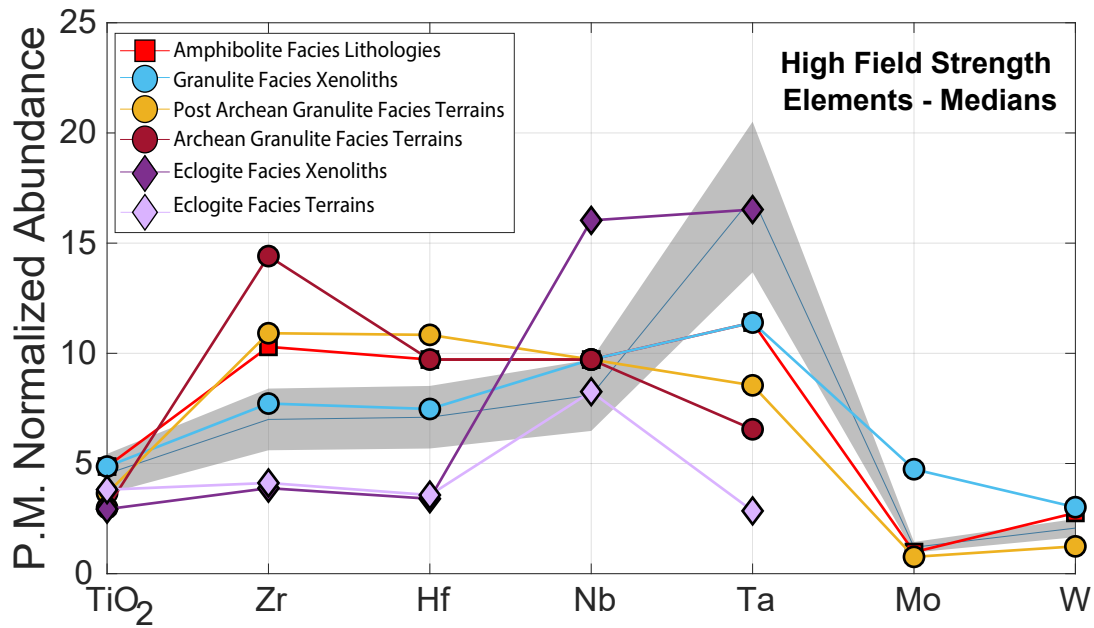


**Figure S7.** As with the fluid mobile elements, the high field strength element concentrations are broadly in agreement with previous estimates. Granulite facies xenoliths and eclogite facies lithologies show elevated concentrations of Mo, partly due to lack of data but also potentially because of the abundance of rutile, titanite, ilmenite, and magnetite in these predominantly mafic samples. Eclogite facies lithologies have negative Ta spikes, which are also potentially caused by the presence of rutile. The black line and gray shaded region surrounding it is the Rudnick and Gao (2014) lower crustal composition  $\pm 15\%$ .

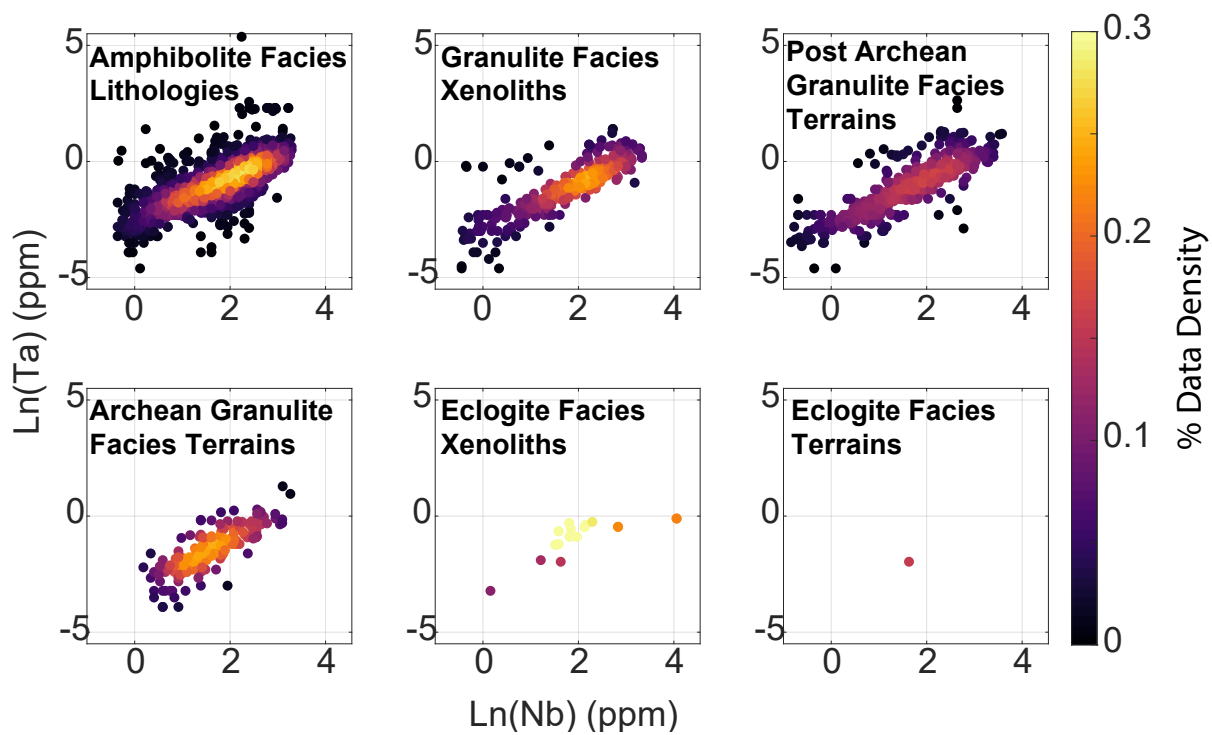


**Figure S8.** Nb vs. Ta forms a log-linear relationship with consistent Nb/Ta values for amphibolite and granulite facies lithologies. Color is relative data point density.

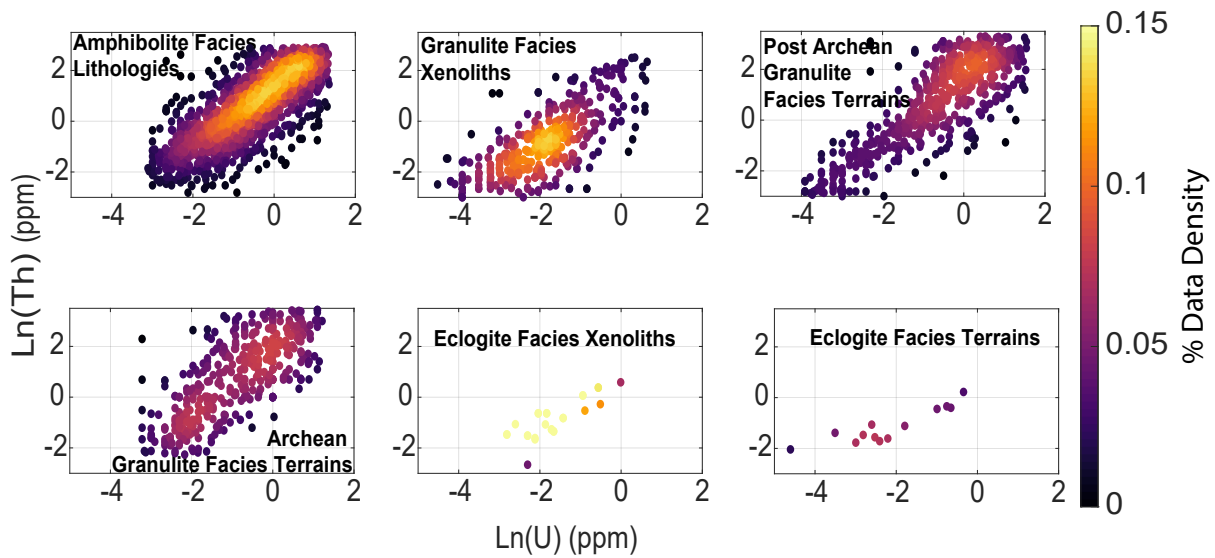


**Figure S9.**  $\text{Ln}[\text{Th}]$  vs.  $\text{Ln}[\text{U}]$  for amphibolite and granulite facies lithologies forms a linear trend. Color indicates relative data point density. The Th/U ratio for all lithologies forms a linear trend in log-log space. Scatter in U concentration could be caused by U's mobility in certain oxidation states since amphibolites can contain hydrous minerals.